

---

Masters Theses

Student Theses and Dissertations

---

1979

## Molybdenum stability in coal slags at 1400°C: Corrosion properties for MHD electrode applications.

Kenton Brian Wright

Follow this and additional works at: [https://scholarsmine.mst.edu/masters\\_theses](https://scholarsmine.mst.edu/masters_theses)



Part of the [Metallurgy Commons](#)

Department:

---

### Recommended Citation

Wright, Kenton Brian, "Molybdenum stability in coal slags at 1400°C: Corrosion properties for MHD electrode applications." (1979). *Masters Theses*. 3279.

[https://scholarsmine.mst.edu/masters\\_theses/3279](https://scholarsmine.mst.edu/masters_theses/3279)

This thesis is brought to you by Scholars' Mine, a service of the Missouri S&T Library and Learning Resources. This work is protected by U. S. Copyright Law. Unauthorized use including reproduction for redistribution requires the permission of the copyright holder. For more information, please contact [scholarsmine@mst.edu](mailto:scholarsmine@mst.edu).

MOLYBDENUM STABILITY IN COAL SLAGS AT 1400°C:  
CORROSION PROPERTIES FOR MHD ELECTRODE APPLICATIONS

BY

KENTON BRIAN WRIGHT, 1953-

A THESIS

Presented to the Faculty of the Graduate School of the



UNIVERSITY OF MISSOURI-ROLLA

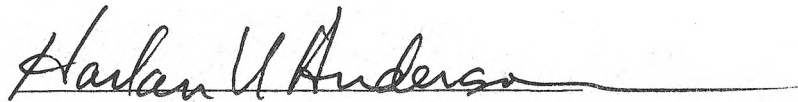
In Partial Fulfillment of the Requirements for the Degree

MASTER OF SCIENCE IN METALLURGICAL ENGINEERING

1979

Approved by

 (Advisor) 



## ABSTRACT

Molten coal slag corrosion studies conducted on molybdenum at 1400°C used static and stirred slag experiments and electrical current experiments to parallel electrode conditions of slagging duct MHD generators. Crucibles containing molybdenum and slag were exposed to combustion-type gases in a tube furnace. Carbon monoxide-carbon dioxide gas mixtures controlled oxygen partial pressures at selected values between  $10^{-11}$  and  $10^{-3}$  atm. Metallograph and microprobe examination of polished sample sections defined corrosion characteristics.

At 1400°C, molybdenum metal is stable below  $10^{-9}$  atm oxygen pressure. Molybdenum dioxide is stable at higher pressure, but volatile molybdenum trioxides prevent formation of stable oxide films in contact with gases. With a slag interlayer, molybdenum corrosion was lessened by slow diffusion processes (no gas-metal contact) and favorable thermodynamics. Still, iron alloyed with the molybdenum at low oxygen pressures and cathodic conditions, while molybdenum oxidation prevailed at higher oxygen pressures and anodic conditions. Dissolution into the slag of any molybdenum dioxide that formed was restricted by its solubility limit in the slag. Slag composition significantly affected corrosion. More iron oxide in the slag increased corrosion, as did the presence of potassium sulfate. Additions of carbon to the slag prevented molybdenum oxidation, but iron alloying and possible carburization occurred.

Under the test conditions, molybdenum electrodes undergo considerable attack as either the cathode or anode. However, the results cannot be applied to other conditions and molybdenum may be practical at lower temperatures or in refractory alloys. The test procedures developed can be used to screen electrode materials, identifying conditions of minimum attack. More elaborate tests are required to determine actual suitability of candidate materials.

## ACKNOWLEDGEMENTS

Sincere thanks go to Dr. Arthur E. Morris, whom as advisor gave much guidance and helpful discussion. His effort and concern made this work possible.

Microprobe analysis was made possible through cooperation of the Geology Department, University of Missouri-Columbia. The microprobe was purchased with assistance from the National Science Foundation, GA-18445. Special thanks go to Dr. Connie Barsky for her assistance.

The author also acknowledges the financial assistance provided by the United States Office of Education, through their Domestic Mining, Mineral, and Mineral Fuel Conservation Fellowship.

## TABLE OF CONTENTS

	Page
ABSTRACT.....	ii
ACKNOWLEDGEMENTS.....	iii
LIST OF ILLUSTRATIONS.....	viii
LIST OF TABLES.....	xii
I. INTRODUCTION.....	1
A. OPEN CYCLE, COAL-FIRED MAGNETOHYDRODYNAMIC GENERATORS.....	1
B. MHD ELECTRODES.....	3
C. MOLYBDENUM ELECTRODES.....	4
D. SCOPE OF EXPERIMENTAL STUDIES.....	5
II. LITERATURE REVIEW.....	7
A. MAGNETOHYDRODYNAMICS.....	7
1. Electrode Parameters.....	8
2. Slag Properties.....	9
3. Metallic and Ceramic Electrodes.....	10
4. Molybdenum Electrodes.....	10
B. MOLYBDENUM.....	11
1. Physical Properties.....	11
2. Molybdenum-Oxygen System.....	11
3. Molybdenum-Slag Reactions.....	12
4. Molybdenum-Iron System.....	16
III. EXPERIMENTAL METHOD.....	18
A. EQUIPMENT AND TECHNIQUE.....	18
1. Furnaces and Temperature Control.....	18
2. Atmosphere Control.....	18
3. Materials and Material Preparation.....	20
a. Molybdenum.....	20
b. Molybdenum Dioxide.....	20
c. Slags.....	21
d. Crucibles.....	23

## TABLE OF CONTENTS (Continued)

	Page
4. Methods of Analysis.....	24
a. Microscopic Examination.....	24
b. Microprobe Analysis.....	25
1) Calibration in Metallic Phases.....	27
2) Calibration in Slag Phases.....	28
3) Additional Corrections.....	28
B. EXPERIMENTS.....	29
1. Static Immersion Tests.....	29
2. Stirred Slag Tests.....	30
3. Electrical Current Studies.....	32
IV. RESULTS.....	35
A. STATIC IMMERSION TESTS.....	36
1. Static Immersion in Union Electric Slag.....	37
a. UE-1.....	37
b. UE-2.....	40
c. UE-3.....	40
d. UE-4.....	40
2. Static Immersion in Seeded Union Electric Slag...	42
a. UE <sub>S</sub> -1.....	44
b. UE <sub>S</sub> -2.....	47
c. UE <sub>S</sub> -3.....	47
3. Static Immersion in UMR Synthetic Slags.....	47
B. STIRRED SLAG TESTS.....	48
1. Molybdenum Dioxide Saturation of Union Electric Slag.....	48
a. Molybdenum Dioxide in Union Electric Slag....	48
b. Molybdenum Dioxide in Seeded Union Electric Slag.....	50
2. Rotated Molybdenum Wire.....	51
a. Mo <sub>r</sub> -1.....	51
b. Mo <sub>r</sub> -2.....	54
3. Rotated Carbon Rod in Union Electric Slag.....	54

## TABLE OF CONTENTS (Continued)

	Page
C. ELECTRICAL CURRENT STUDIES.....	57
1. Anode Pin/Cathode Ring: 1400°C.....	61
2. Cathode Pin/Anode Ring: 1400°C.....	65
3. Cathode Pin/Anode Ring: 1350°C.....	71
4. Direct Molybdenum-Iron Reactions.....	73
a. Molybdenum in Iron Powder.....	73
b. Molybdenum in Iron-Doped Slag.....	75
V. DISCUSSION OF RESULTS.....	77
A. STATIC IMMERSION TESTS.....	77
1. Static Immersion in Union Electric Slag.....	77
a. Molybdenum Oxidation and Corrosion.....	77
b. Molybdenum-Iron Alloying.....	79
2. Static Immersion in Seeded Union Electric Slag...	80
3. Static Immersion in UMR Synthetic Slags.....	81
B. STIRRED SLAG TESTS.....	82
1. Molybdenum Dioxide Saturation of Union Electric Slag.....	82
2. Rotated Molybdenum Wire.....	82
a. Mo <sub>r</sub> -1.....	83
b. Mo <sub>r</sub> -2.....	83
3. Rotated Carbon Rod.....	84
C. CORRELATION OF STATIC AND STIRRED TESTS.....	85
D. ELECTRICAL CURRENT STUDIES.....	85
1. Anode Reactions.....	88
2. Cathode Reactions.....	89
3. Direct Molybdenum-Iron Reactions.....	90
VI. SUMMARY AND CONCLUSIONS.....	91
BIBLIOGRAPHY.....	93
VITA.....	96
APPENDICES.....	97
A. MATERIAL PREPARATION.....	97
1. PREPARATION OF MOLYBDENUM DIOXIDE.....	97
2. TREATMENT OF UNION ELECTRIC SLAG.....	97

## TABLE OF CONTENTS (Continued)

	Page
B. TECHNIQUES OF ANALYSIS.....	99
1. MOLYBDENUM-SLAG SAMPLE PREPARATION.....	99
2. MICROPROBE CALIBRATIONS.....	99
a. Molybdenum-Iron Alloys.....	99
b. Slag Phase.....	101
3. CARBON DIOXIDE GAS ANALYSIS.....	104
4. CARBON ANALYSIS OF SLAGS.....	106
C. COMPILATION OF DATA TABLES.....	108
D. ADDITIONAL PHOTOMICROGRAPHS.....	114



## LIST OF ILLUSTRATIONS

Figure	Page
1. Schematic of a Magnetohydrodynamic Electrical Generator System, Including Some Design Parameters.....	2
2. Thermochemical Diagram for the Molybdenum-Oxygen System at 1400°C.....	13
3. Binary Phase Diagram of the Iron-Molybdenum System According to Hultgren.....	17
4. Vertical Furnace and Experimental Arrangement for Static Immersion Tests.....	19
5. Apparatus and Sample Arrangement for Rotated Molybdenum Rod Tests.....	31
6. Apparatus and Sample Arrangement for Rotated Carbon Rod Test.....	33
7. Apparatus and Sample Arrangement for Electrical Current Tests.....	34
8. Slag-Metal Interface, UE-1.....	39
9. Microprobe Concentration Profile for Iron and Molybdenum in the UE-2 Test.....	41
10. Molybdenum Surface, UE-3.....	39
11. Slag-Metal Interface, UE-4.....	43
12. Saturation Precipitation in UE Slag Near Molybdenum....	43
13. Slag-Metal Interface, UE <sub>S</sub> -1.....	45
14. Microprobe Concentration Profile of Iron and Molybdenum in the UE <sub>S</sub> -1 Test.....	46
15. Slag-Metal Interface, UE <sub>S</sub> -3.....	45
16. Molybdenum Dioxide in Slag, MoO <sub>2</sub> -1, Saturation Experiment in UE Slag.....	49
17. Molybdenum Dioxide in Slag, MoO <sub>2</sub> -4, Saturation Experiment in Seeded UE Slag.....	49
18. Slag-Metal Interface, Mo <sub>γ</sub> -1B.....	53

## LIST OF ILLUSTRATIONS (Continued)

Figure	Page
19. Slag-Metal Interface, Mo <sub>r</sub> -2T.....	53
20. Molybdenum Surface, Mo <sub>r</sub> -2T.....	55
21. Slag-Metal Interface, Mo <sub>r</sub> -2B.....	55
22. Microprobe Concentration Profile for Iron and Molybdenum in the Mo <sub>r</sub> -2 Test.....	56
23. Molybdenum Surface, UE + C.....	58
24. Dendrites Growing on Molybdenum in UE + C Test.....	58
25. Microprobe Concentration Profile of Iron and Molybdenum in the UE + C Test.....	59
26. Molybdenum Surface, Anode Pin, 1400°C, Electrical Cur- rent Test.....	62
27. Molybdenum Dioxide on the Anode Pin Surface.....	62
28. Microprobe Concentration Profile of Iron and Molybdenum in the Anode Pin/Cathode Ring Electrical Current Test...	63
29. Slag-Metal Interface, Cathode Ring, 1400°C, Electrical Current Test.....	64
30. Vertical Section of Cathode Pin/Anode Ring, 1400°C, Showing the Shape of Alloy Drop and Location of Sections Cut for Metallographic and Microprobe Analysis.	64
31. Molybdenum Surface, Cathode Pin, 1400°C, Electrical Current Test, (Top Section).....	66
32. Molybdenum Surface, Cathode Pin, 1400°C, Electrical Current Test, (Bottom Section).....	66
33. Microprobe Concentration Profile of Iron and Molybdenum in the Cathode Pin/Anode Ring Electrical Current Test, 1400°C.....	67
34. Alloy on Cathode Pin, Upper Section, 1400°C.....	68
35. Alloy Structure on Cathode Pin, Bottom Section Within Drop.....	69
36. Molybdenum Surface, Cathode Pin, 1350°C.....	69

## LIST OF ILLUSTRATIONS (Continued)

Figure	Page
37. Molybdenum-Iron Alloy on 1350°C Cathode Pin.....	72
38. Surface of the 1350°C Cathode Pin Alloy, Seen by Looking Through the Slag.....	72
39. Molybdenum Wire in Iron Pack, Sintered 12 Hours, High Heat Transfer Arrangement.....	74
40. Molybdenum-Iron Alloy, Iron Pack Experiment, High Heat Transfer Arrangement.....	74
41. Slag-Metal Interface, UMR-1 Slag with Added Iron Powder (300x).....	76
42. Molybdenum-Alloy Interface, UMR-1 Slag with Added Iron Powder (1300x).....	76
43. Summary of Microprobe Concentrations for Selected Points: Static Immersion, Rotated Wire, and Molybdenum Dioxide Saturation Tests in UE Slag.....	86
44. Summary of Microprobe Concentrations for Selected Points: Static Immersion and Molybdenum Dioxide Saturation Tests in Seeded UE Slag.....	87
45. Calculated Correction Curves for Molybdenum-Iron Alloys, Relating Relative Intensity with Composition for Microprobe Calibration.....	102
46. Carbon Dioxide Analyzer Used for Gas Analysis of Furnace Atmosphere.....	105
47. Apparatus Used to Analyze Coal Slags for Carbon.....	107
48. Molybdenum Surface, UE-1.....	115
49. Slag-Metal Interface, UE-2.....	115
50. Molybdenum Surface, UE-2.....	115
51. Slag-Metal Interface, UE-3.....	115
52. Slag-Metal Interface, UE-4, Under Polarized Light.....	117
53. Slag-Metal Interface, UE <sub>S</sub> -2.....	117
54. Molybdenum Section, UE <sub>S</sub> -2.....	117
55. Slag-Metal Interface, Mo <sub>γ</sub> -1T.....	117

## LIST OF ILLUSTRATIONS (Continued)

Figure	Page
56. Precipitate and Debris in Slag Between Electrodes, Electrical Current Tests.....	119
57. Slag-Metal Interface, Cathode Ring, 1400°C.....	119
58. Droplet Section, Cathode Pin, 1400°C.....	119
59. Mossy Deposit from Cathode Pin, Cathode Pin/Anode Ring, 1350°C.....	119
60. Slag-Metal Interface, Cathode Pin, 1350°C.....	121
61. Slag-Metal Interface, Cathode Pin, 1350°C.....	121
62. SEM Photomicrograph of Mossy Alloy Surface Seen as Removed From the Slag by LiH + LiOH Leach.....	121
63. Alloy Surface as Seen Looking Through the Slag, Cathode Pin, 1350°C.....	121
64. Molybdenum-Iron Interface, Iron Pack Experiment.....	123
65. Slag-Metal Interface Showing Pitting Corrosion, A Four Hour Test in UE Slag, $P_{O_2} = 10^{-7}$ atm.....	123
66. SEM Photomicrograph of Molybdenum-Slag Interface Showing Oxide Reaction Layer.....	123
67. SEM Photomicrograph of Interface Showing Oxide Layer and Texture of Underlying Molybdenum Surface.....	123

## LIST OF TABLES

Table	Page
I. Chemical Composition of Several Coal Slags.....	22
II. Summary of Molybdenum Static Immersion Tests.....	38
III. Summary of Molybdenum Dioxide Saturation Experiments....	50
IV. Summary of Rotation Tests in Union Electric Slag.....	52
V. Summary of Electrical Current Studies Using UE Bottom Slag, A 7 mm Electrode Separation, an Applied Voltage of 1.5 Volts, and an Applied $O_2$ Potential of $10^{-9}$ atm in 3 Hr Duration Tests.....	60
VI. Microprobe Concentration Data for Static Immersion Tests Using Union Electric Slag.....	109
VII. Microprobe Concentration Data for Static Immersion Tests Using Seeded Union Electric Slag.....	110
VIII. Microprobe Concentration Data for Stirred Slag Tests (Rotated Molybdenum Rod and Rotated Carbon Rod).....	111
IX. Microprobe Concentration Data for Electrical Current Tests in Union Electric Slag.....	112
X. Current Flow in Electrical Current Studies.....	113

## I. INTRODUCTION

### A. OPEN CYCLE, COAL-FIRED MAGNETOHYDRODYNAMIC GENERATORS

The development of MHD generators is being pursued principally as a supplement to conventional coal-fired electrical generators. The MHD process, when coupled to conventional steam generators, should give an overall efficiency of 50% or greater, compared to the 40% maximum for the steam cycle alone.<sup>1</sup> In addition, by its nature, the system removes much particulate and gaseous pollution from the waste gas without extensive treatment facilities. MHD uses the enthalpy of coal combustion gases to obtain electrical current directly. The process is termed open cycle since the hot gases pass only once through the generator. A schematic is shown in Figure 1.

The core of the MHD system operates with no moving parts. A combustion gas stream at about 2700°C, containing ionized particles, is forced through a channel surrounded by a powerful magnet. As the gas passes through the magnetic field, the ions are deflected across the flow. Two opposing channel walls are insulators, while the other two contain arrays of electrodes to collect the deflected charges. To enhance ionization at feasible temperatures, a seed material is added. Potassium carbonate is a promising possibility.

Coal contains up to 10% ash that fuses into a slag at high temperature. Most of the slag deposits on the combustor walls, but about 20% remains vaporized or entrained in the gas stream and is carried into the MHD channel.<sup>2</sup> Some of the remaining slag condenses in the channel if wall temperatures are below 1500°C. Seed material may also condense in the channel. The gas temperature and pressure decrease along the channel length and the progressive cooling is likely to cause a slag composition gradient along the channel. Differences in the composition may also develop through the slag thickness on the channel wall due to the temperature gradient through the wall. The slag and seed cause substantial corrosion/erosion problems wherever they are found in the system, making

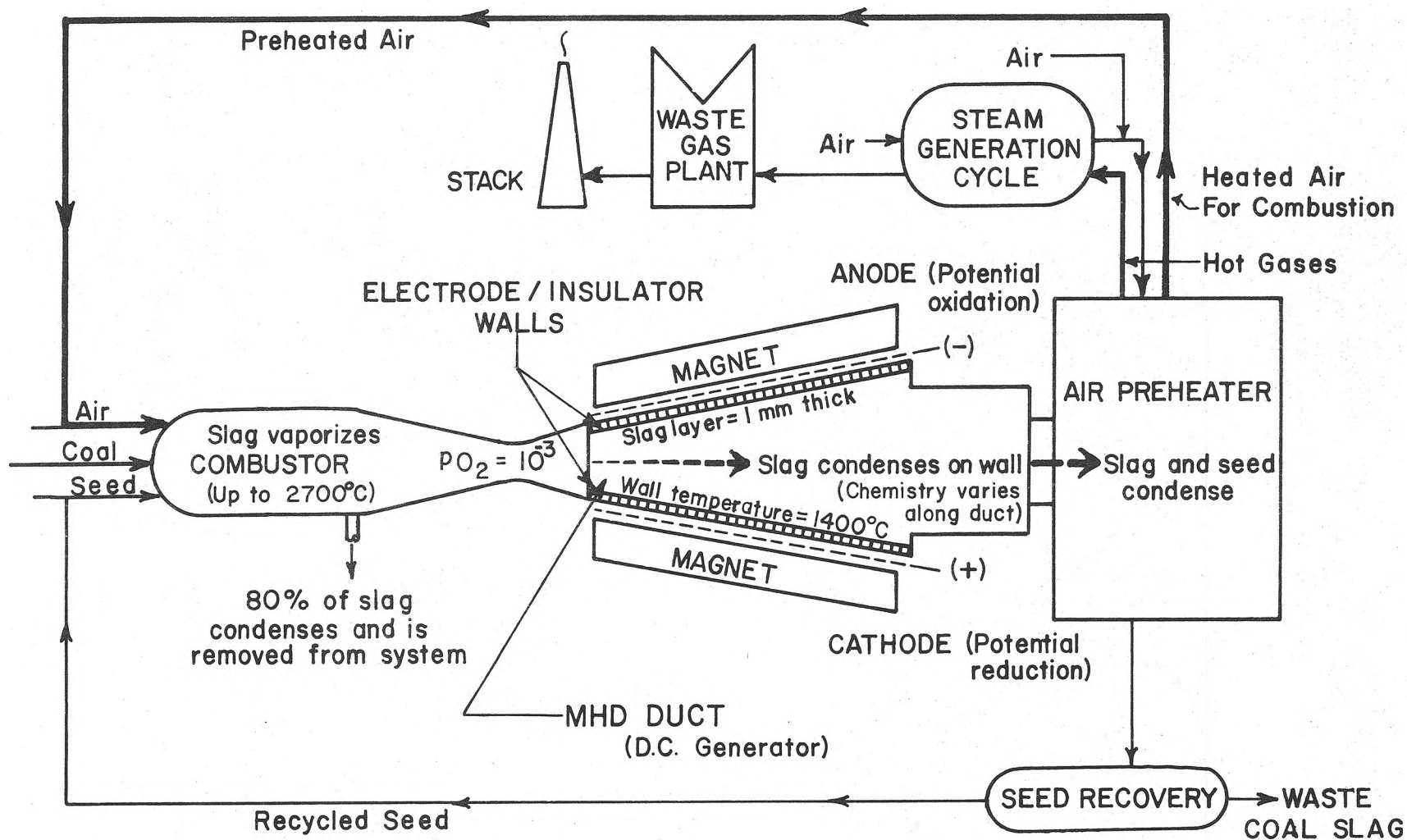


Figure 1. Schematic of a Magnetohydrodynamic Electrical Generator System, Including Some Design Parameters.

material design of the combustor, channel, and preheater sections critical to successful MHD development.

#### B. MHD ELECTRODES

The desired MHD channel life is 10,000 hours.<sup>2</sup> To achieve this, electrode components must withstand the harsh environment produced by combustion gases, slag, seed, and current flow. The most harmful constituents are oxygen at the anode and potassium, calcium, and iron at the cathode.<sup>1</sup> The oxygen pressure will be approximately  $10^{-3}$  atm in the gas. The condensed slag composition will vary greatly and the slag may be molten or solid, depending on the electrode temperature and composition of the slag. The current flow will average 1 amp/cm<sup>2</sup>, but may be much higher locally, due to uneven current distribution. If the wall temperature is low, current travels through the slag by an arcing mechanism, generating very high current densities.

A number of different electrode schemes have been investigated. Some use ceramic materials that are electronic conductors at high temperatures. Other systems use metallic electrodes, such as copper or Inconel, which must be cooled severely. Generally, ceramic electrodes can operate at higher wall temperatures, where the current travels in a diffuse mode. The use of ceramics may be limited by complicated current leadouts, degradation of electrical properties, or rapid erosion at the cathode.

Metallic electrodes have been designed for low to intermediate wall temperatures, 400° to 1300°C.<sup>1</sup> To hold these temperatures, much heat must be removed by cooling water. The resulting steep thermal gradient perpendicular to the wall complicates current flow and boundary conditions in the gas stream. A substantial solid slag layer develops over the electrode surface at the low temperatures. Current flow occurs in an arcing mode and the underlying electrode can be rapidly eroded if the arcs long remain stationary. Other metals are used at higher temperature, where the slag can be molten, but oxidation and corrosion becomes a serious concern at the anode.

Despite the obvious problems, metallic electrodes have many inherent advantages. Good electrical conductivities over wide



temperature ranges allow simple current leadout design. The metals are easily fabricated and have good thermal shock resistance. Their electrical properties do not deteriorate under current load and, when used as cathodes, the metals are protected by the surrounding reducing environment. The metallic electrodes are appealing if the temperature limitations can be eased by using higher melting metals, while at the same time maintaining resistance to oxidation and corrosion. A metallic cathode may be coupled with a ceramic anode to optimize conditions at both electrode walls.

### C. MOLYBDENUM ELECTRODES

Molybdenum has been mentioned as a possible electrode material, primarily on the basis of its good thermal and electrical properties.<sup>3</sup> It has been used extensively as resistance heating elements in molten glasses.<sup>4</sup> However, there are major differences between glass and coal slag; the latter contains substantial amounts of iron oxide. Iron, because of its two oxidation states, transfers oxygen through the slag. This becomes a potential source of molybdenum erosion, even at relatively low temperatures.

Molybdenum is noted for its poor oxidation resistance at elevated temperatures. In air, or in other high oxygen potential environments, the formation of volatile oxides prevent stable protective oxide layers from forming and so further oxidation is not inhibited. The oxidation thermodynamics cannot be changed, except by introducing alloying species, but the rate of oxidation can be slowed by lowering the rate at which oxygen reaches the metal. The presence of a slag layer alters the mechanism of oxidation, acting as a barrier against the transportation of oxygen towards the molybdenum surface and against the movement of reaction products or volatile oxides away from the surface.

This alone is not expected to make molybdenum a suitable candidate, but several other factors can be considered. The slag condensing on the channel wall will be in equilibrium with the combustion gas, having an oxygen potential of  $10^{-3}$  atm, but, on the cathode surface, the oxygen is driven away from the electrode

surface. Also, because of the high gas velocity and large amount of coal burned, significant amounts of carbon may be carried over with the slag; a condition found frequently with conventional low temperature coal combustion. The carbon lodged in the surface of molten slag would lower the oxygen potential of that slag. Carbon could be added to the channel specifically for this purpose.

#### D. SCOPE OF EXPERIMENTAL STUDIES

The evaluation of molybdenum reactions in coal slag is approached from a thermodynamic and kinetic viewpoint. Erosion and corrosion are studied in slag contact experiments, under conditions prevailing at an electrode wall. The experiments are aimed at basic understanding of the reactions involved, rather than towards gathering design engineering data for operating systems. Several different experiments are used to test molybdenum over a wide range of conditions, such that many different types of reactions can occur and the relative significance of each can be evaluated.

Despite the variation in experimental conditions, certain boundaries for the experiments can be translated into practical electrode and channel parameters to compare conditions for the channel and experiments. Slagging channel conditions are necessary to provide needed slag covering for the molybdenum, requiring temperatures in the range of 1400°C. Other test conditions assume a uniform slag composition, which is not likely to occur in an operating channel. The oxygen pressure is set at or lower than in combustion products at 1400°C and the gas pressure is fixed at one atmosphere, lower than in the channel.

Experiments examine effects of static and flowing slag conditions, the effect of seed and slag composition on molybdenum erosion, and the effect of current flow (the corrosion of molybdenum under induced cathodic and anodic conditions). Static and flowing slag tests are made over a range of different oxygen potentials applied to the slags. Two methods are used to modify the oxygen potential, either using direct control of the gas atmosphere, or addition of carbon to the slag. The surveyed conditions cover a broad range of

oxygen potentials, from very reducing to oxidizing values (in relation to molybdenum and slag stabilities at 1400°C).

The tests are simply constructed to give basic information rapidly. The feasibility of expanding the test procedures to other metal or alloy systems is discussed in analyzing the information gathered in the present study. In studying the molybdenum system, attention was directed to identifying the reactions that control the metal stability in the slag, to finding what steps could be taken to enhance stability, to showing where further study should be directed, and to exposing any obstacles to the suggested electrode application.

## II. LITERATURE REVIEW

A great deal of material has been written on theoretical and engineering aspects of magnetohydrodynamic systems. Fewer papers detail operating parameters important to materials selection, although the intensity of research in this area is increasing rapidly. A number of articles on electrode materials of both theoretical and experimental origin are available.

When molybdenum is mentioned as a candidate material, the discussion is often speculative. A few studies report testing of molybdenum for MHD applications.

Thermodynamic parameters of molybdenum systems have been studied to a limited extent. Parameters for the molybdenum-oxygen system are well documented. In the molybdenum-iron system, the phase diagram is generally established, but data on molybdenum and iron activities in the various phases is lacking, making useful thermodynamic calculations difficult.

Much recent effort has been directed towards defining the properties of coal slags at elevated temperatures. Much work also has been conducted on metal-slag systems. Information on the molybdenum-slag systems is limited and little work considers the molybdenum-coal slag system directly.

### A. MAGNETOHYDRODYNAMICS

The theory and engineering principles of the MHD system are discussed in depth in numerous publications. The most comprehensive description is Heywood and Womack's summary of the British MHD effort.<sup>5</sup> Short articles on the overall system operation and engineering criteria are also available.<sup>6-9</sup>

The MHD system is not thoroughly defined. The actual configuration and design of components depends heavily upon the outcome of current research. Many different directions are presently being pursued and the first generation of operating MHD units will likely be greatly different from those that follow. The variety

of topics under study has generated a tremendous volume of technical material and no review will be attempted here. Excellent reviews and bibliographies are available.<sup>2,10</sup>

A general concept of the MHD system is shown in Figure 1. Mixed coal and seed is burned with preheated, high pressure air in a separate combustor. The combustion products containing ionized seed are then allowed to expand through the channel. The direct current generated in the high density magnetic field is collected with complex arrays of electrodes. This current is put through an inverter to produce AC power. The effluent hot gases are used to preheat the air blast, seed is removed, and the cleaned gases pass on to a steam turbine generating plant.

1. Electrode Parameters. The criteria for MHD electrode stability have been much discussed in the literature, but the final choice of electrode material and configuration define, to a large extent, the conditions that must be created in the channel. Haywood and Womack<sup>5</sup> provide an excellent background on many electrode systems. There are criteria common to all the alternative systems. A fairly general description of these criteria is presented by Rossing and Bowen<sup>11</sup> and also by Bowen et al.<sup>12</sup>

These criteria require electrode-insulator systems capable of reliable and predictable life, as defined by acceptable electrical and mechanical properties. The efficiency of electrical and thermal conductivities is important since the electrode will be required to carry a current density of 1 amp/cm<sup>2</sup> or more. At cold electrode conditions, below 1000°C, the electrode must withstand the effects of current passing in an arcing mode that generate localized heat which must be rapidly dissipated to avoid electrode erosion and vaporization. High thermal conductivity becomes the major requisite. At higher temperature the electrode requires uniform current distribution to avoid rapid degradation. While high electrode temperatures favor uniform current transfer and increase efficiency, chemical and electrochemical reactions are accentuated.

The chemical stability of electrode materials is determined by the gaseous coal combustion products, the nature of slag present, the presence of condensed seed, temperature, and pressure. Except at high temperatures ( $>1500^{\circ}\text{C}$ ) the slag will form a layer over the electrode-insulator module and at temperatures over  $1100^{\circ}\text{C}$  the high slag conductivity will make the slag an integral part of the electrode system. The slag properties can be controlled to better protect the base material.

Other clearly fixed parameters are design limitations of the duct. The system must be compact to conserve valuable space within the magnet core, the current lead-outs must be practical, the material must be amenable to construction of the needed shapes, and in that configuration must resist thermal shock.

2. Slag Properties. The nature of the slag involved is critical to several sections of the MHD generator system; the combustor, the duct, and the air preheater. Substantial quantities of ash carry-over from the combustor into the channel is expected.<sup>7</sup> A comprehensive study of slag properties, the thermal diffusivities, electrical conductivities, viscosity, and effects of seed is reported by Bates.<sup>13,14</sup> The work is restricted to measurements of slags in equilibrium with air, rather than combustion product gases, but it provides a benchmark. Extensive work has also been conducted at the National Bureau of Standards, the work of Capps.<sup>15,16</sup> A useful background for thermodynamic and kinetic considerations with slags is available in The Making, Shaping and Treating of Steels.<sup>17</sup>

The properties of coal slag are shown dependent upon the slag composition and temperature. This becomes particularly important in the MHD channel, where temperature gradients along the channel will cause composition variations down the length, with the lowest volatility constituents condensing first. The slag carried over into the channel may be damaging in some ways; inducing corrosion, current leakage between electrodes, thermal diffusion barriers, and fouling. In other ways it may be beneficial, providing a protective covering for the electrode, yet allowing excellent current

flow into the electrode wall.

From a molybdenum corrosion standpoint, one of the most significant ingredients of the slag is iron, present both in ferric and ferrous states. The electrical conductivity and oxygen transfer properties of the slag are greatly influenced by the amount and oxidation state of iron in the slag. The amount of iron, the oxygen partial pressure in the combustion products, the temperature, and the acid/base ratio of the slag are the most important factors which influence the ferric/ferrous ratio in the slag.<sup>18</sup> Increasing the concentration of silica, for example, forces virtually all iron oxide into the ferrous state. The ratio can also be modified by reducing agents such as carbon. Several references cite the occurrence of carbon in coal slags.<sup>5,13</sup>

3. Metallic and Ceramic Electrodes. Numerous discussions of various electrode materials are available. Discussions by Raring<sup>1</sup> on many electrode systems, by Rossing and Bowen<sup>11</sup> on high temperature electrode systems, by Petty et al.<sup>19</sup> on the cold electrodes, and the thorough background of Haywood and Womack,<sup>5</sup> together cover the common electrode systems.

The development of workable electrodes is at the center of MHD development and much attention has been directed towards the topic. The suggested materials range from cold copper (400°C), stainless steel, Inconel, and molybdenum on the metallic end, to stabilized zirconia, lanthanum chromite, silicon carbide, and other spinel oxides or ceramic materials at the other extreme. Each satisfies certain requirements and each imposes restrictions on the operating system.

Cadoff et al.<sup>20</sup> have evaluated several ceramic electrode materials in tests similar to those of this study. A number of direct comparisons between the studies are made in the discussion of results of the present work.

4. Molybdenum Electrodes. The use of molybdenum as an electrode has not been discussed extensively in the literature. The principal reference is given by Bowen et al.<sup>12</sup> They discuss the

thermodynamic properties of molybdenum in oxygen and sulfur environments and conclude molybdenum may be an alternative if, by proper arrangement, kinetic stability is established. The rate of oxygen transfer from gases, through the slag layer, is suggested to be the rate determining step defining useful stability. They propose the recession rate can be controlled by electrode temperature, gas composition, slag-seed composition, and electrode microstructure composition.

Experimental testing has included a short duration exposure test in a slagging MHD channel (without current flow).<sup>21</sup> Less than 0.1 mm of corrosion occurred in 30 minutes at a temperature of at least 1200°C.

## B. MOLYBDENUM

A background of properties relevant to electrode usage is presented. The physical properties are briefly described while coverage of the molybdenum chemical properties will be limited to interactions with oxygen and iron.

1. Physical Properties. General properties are well reviewed in the Metals Handbook, 8th Edition.<sup>22</sup> Of interest in this study is the high melting point (2610°C), thermal conductivity (at 1400°C, 23% that of copper at 500°C), electrical resistivity (78 microhm at 1400°C), and the modulus of elasticity (at 1400°C approximately equal to that of copper at 20°C). The properties all appear adequate for electrode application.

With very slight impurities of oxygen and nitrogen (1 ppm), molybdenum fractures in a brittle mode at room temperature, while pure molybdenum in a cold worked state will not. The brittle-ductile transition temperature is affected by purity, degree of cold work, and grain size. These effects are summarized by Savitskii and Burkhanov.<sup>23</sup> The brittle nature was a secondary effect noted in this study.

2. Molybdenum-Oxygen System. Gulbransen has discussed in detail the oxidation of molybdenum.<sup>24</sup> A thermochemical diagram of

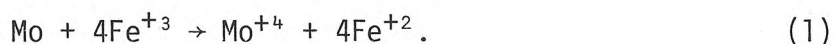


the molybdenum-oxygen system at 1400°C, calculated from Gulbransen's data, is shown in Figure 2. The results show that at 1400°C, molybdenum dioxide is the only stable solid oxide up to a partial pressure of about  $10^{-3}$  atm. However, the sum of the partial pressures of the volatile monomer and trimer trioxides reaches about 1 atm when the oxygen pressure is only  $10^{-5}$  atm. The molybdenum will oxidize above  $10^{-9.2}$  atm oxygen partial pressure and the oxide will tend to volatilize.

3. Molybdenum-Slag Reactions. The presence of coal slag in contact with molybdenum alters molybdenum-oxygen equilibrium as metal-slag reactions occur. The combination of iron and oxygen in the coal slag complicates the corrosion of molybdenum. It is apparent that in a dynamic MHD system, no material can be thermodynamically stable in the coal slag, but thermodynamic considerations are still useful in identifying relative stabilities with the objective of minimizing any reaction tendencies between system phases.

A treatment of molybdenum reactions with slag is presented by Thorne et al.<sup>25</sup> The slag may be considered to consist of a solvent of stable oxides (such as alumina, silica, and lime) and a solute of less stable iron oxides. Of course, the criteria for stability are arbitrary, but for present purposes, slag constituents are considered to form stable oxides if they do not tend to change oxidation state at 1400°C when the partial pressure of oxygen varies in the range from  $10^{-3}$  to  $10^{-12}$  atm. Iron oxide is the only constituent that is not stable by these criteria. This range was selected since either metallic molybdenum, its dioxide, or its trioxide are stable within it.

When molybdenum contacts molten coal slag, the reaction that tends to predominate depends greatly on the initial oxidation state of iron in the slag. For coal slags melted in a gas having an oxygen pressure of  $10^{-3}$  atm, for example, molybdenum reacts principally with the ferric iron:



Since the activities of the ions are difficult to estimate, it is more convenient to write the above reaction in terms of dissolved oxides,

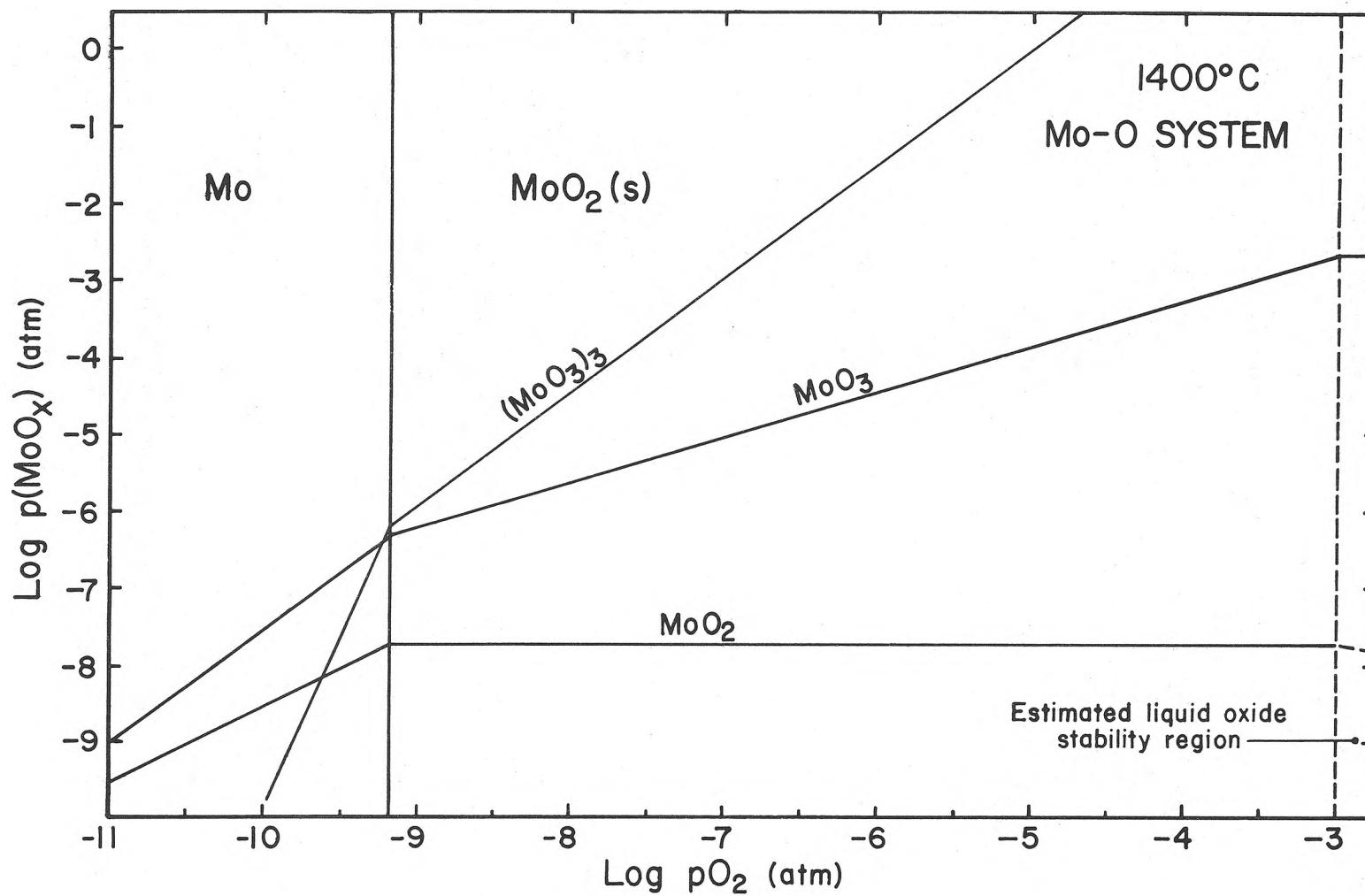
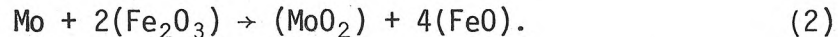


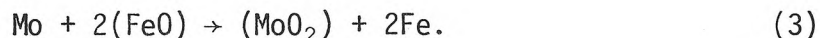
Figure 2. Thermochemical Diagram for the Molybdenum-Oxygen System at 1400°C.

where parentheses denote hypothetical dissolved species:

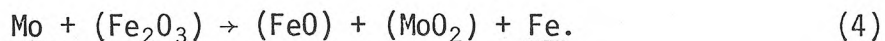


In absence of additional oxygen from the gas, the above reaction will proceed until equilibrium with the slag is reached. The amount of slag, the temperature, and the oxygen activity of the slag (as expressed in the iron oxides) determine the amount of metal dissolved by the reaction. Under certain circumstances, the equilibrium will not be reached directly. If the reaction between molybdenum and slag causes dissolved molybdenum dioxide concentrations in the slag approaching the solubility limit, a film of dioxide forms at the reaction interface.

For coal slags melted in contact with a much lower oxygen pressure, such as  $10^{-12}$  atm, molybdenum reacts principally with ferrous iron:



The iron alloys with molybdenum to form an alloy solid solution, denoted by underlining. Under suitable circumstances, such as in the presence of a carbonaceous reducing agent or a cathodic environment, the iron content of the solid solution might reach the solubility limit and intermetallic compounds of iron and molybdenum form. A third equation describes reactions showing iron can be reduced to alloy with molybdenum when the ferric iron is involved:



The equilibrium constants for reactions (2), (3), and (4) require a finite value for the activities of each component, regardless of the oxygen pressure. Thus even at the highest oxygen pressures studied in this investigation, some iron dissolves in the molybdenum, and at the lowest oxygen pressures, some molybdenum dioxide will form and dissolve in the slag. The equilibrium concentrations of dissolved species cannot be calculated because of a lack of activity data.

The work of Thorne et al.<sup>25</sup> indicates high silica slags in equilibrium with molybdenum contain less molybdenum dioxide than do lower silica slags. In the Mo-Fe-Si-O system, the amount of molybdenum dioxide dissolved into the slag ( $\text{Fe}_x\text{O} + \text{SiO}_2$ ) was highly dependent upon the silica content of the slag phase. Much more dioxide dissolved in iron-rich slag than in silica saturated slag. The dissolved dioxide concentration increased with temperature, but the increase was smaller with high silica slag. They also summarize the work of Rusakov et al.,<sup>26</sup> stating that molybdenum dissolves into the slag in the form of molybdenum dioxide and other lower oxides. These are found to crystallize as complex dioxides upon cooling ( $\text{FeO}\cdot\text{MoO}_2$  and  $\text{MgO}\cdot\text{MoO}_2$ ), or to decompose to molybdenum metal and molybdenum dioxide.

Kinetic factors complicate the picture. Diffusion of oxygen through the slag and reaction with a molybdenum dioxide layer (if present), diffusion of dissolved molybdenum dioxide away from the reaction site, and the dissolution rate of a dioxide layer are involved in establishing the rate of approach to the various equilibria.

In the absence of any mitigating factors, Reaction (2) would be expected to predominate in the MHD type combustion environment. The ferric and ferrous iron ions act as transfer media for oxygen moving from the gas to the metal.<sup>12</sup> The formation of a molybdenum dioxide reaction layer may impede further oxidation, if the layer is adherent. A steady state could prevail, with dissolution of molybdenum dioxide into the flowing slag balanced by the rate of molybdenum oxidation.

Useful experimental background for metal-slag reactions are available from several sources.<sup>27-29</sup> Borom and Pask<sup>27</sup> studied interface reactions between iron and glass (approximately 40%  $\text{SiO}_2$ , 20%  $\text{B}_2\text{O}_3$ , 20%  $\text{Na}_2\text{O}$ , 10%  $\text{CaO}$ , and the rest other oxides) using techniques similar to those of the present study. Their work is considered in later discussions.

4. Molybdenum-Iron System. Because of reactions between molybdenum and coal slag, there can be a sizable tendency for iron to alloy into the molybdenum, especially in cathodic environments, as discussed in previous sections. The alloying occurs according to the phase diagram of the iron-molybdenum system, shown in Figure 3 as given in Hultgren et al.<sup>30</sup> At 1400°C (1673 K), no liquid phases are present at any binary composition. Sizable solid solution regions exist for both iron and molybdenum-rich alloys, and two intermetallic compounds are stable. The diagram shows several other stable phases at lower temperatures, which tend to complicate interpretation of non-equilibrium cooled samples.

Activity and activity coefficient data for molybdenum and iron in the various phases would be very helpful for thermodynamic calculations in the molybdenum-slag systems. Unfortunately, the information is not available.

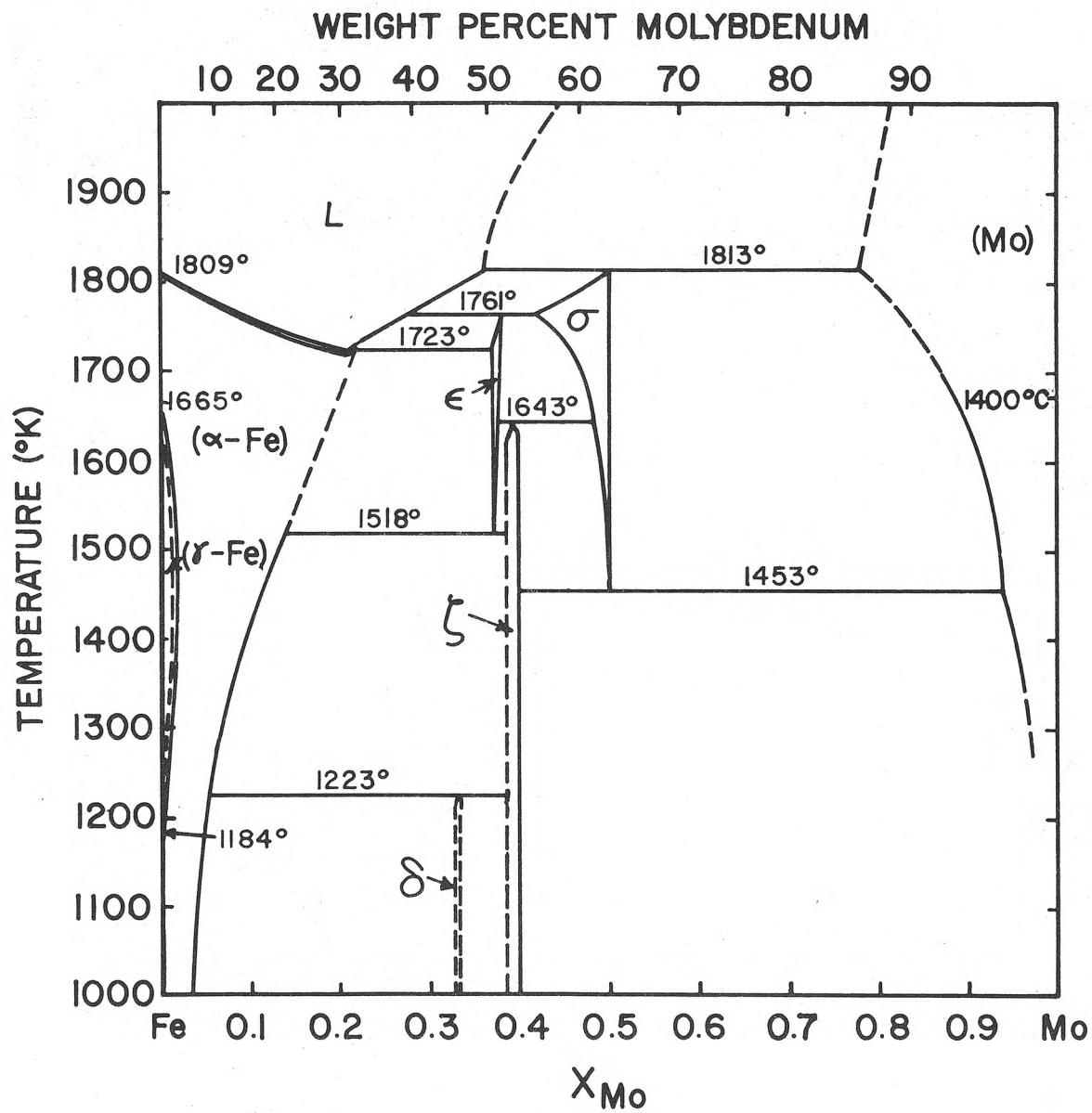


Figure 3. Binary Phase Diagram of the Iron-Molybdenum System According to Hultgren et al.<sup>30</sup>

### III. EXPERIMENTAL METHOD

#### A. EQUIPMENT AND TECHNIQUE

Molybdenum and coal slags were reacted at 1400°C in a controlled atmosphere furnace. Data were obtained by examination of the sample after cooling and sectioning. The primary analysis technique was microprobe analysis, supported with physical measurement, metallography, and wet or gravimetric chemistry.

1. Furnaces and Temperature Control. The experimental work was conducted in two different types of furnaces. Work at 1400°C used a silicon carbide heated vertical tube furnace. Analysis and sample preparation work below 1000°C used a horizontal wire wound furnace.

A schematic of the vertical tube furnace is shown in Figure 4. The furnace contained a mullite tube of 4.4 cm diameter and 112 cm length. Rubber stoppers faced with ceramic radiation shields formed gas tight, heat resistant seals at both ends. The tube rested on its lower end to minimize tensile stresses in the refractory. A gear driven lead screw lowered samples into the tube at 13 mm/min. A platform in the tube positioned all samples at an identical location.

Temperature control for the vertical tube furnace was provided by a Pt/Pt-13%Rh thermocouple connected to a suppressed range millivolt controller. The controller was checked regularly with a Pt/Pt-10%Rh thermocouple calibrated against an identical thermocouple standardized by the National Bureau of Standards. The temperature was regulated to within 2°C of 1400°C. The temperature at a height 5 cm above the sample position was no more than 6°C below 1400°C.

The horizontal tube furnace contained tubes of approximately 3 cm diameter, made of either Vycor or mullite, as required by the particular experiment. Chromel-Alumel thermocouples, one connected to a millivolt potentiometer and another connected to a controller, provided temperature measurement and regulation.

2. Atmosphere Control. All experiments were conducted under controlled atmospheres. A bubbler on the exit side of the furnace maintained a slight positive pressure in the furnace and also

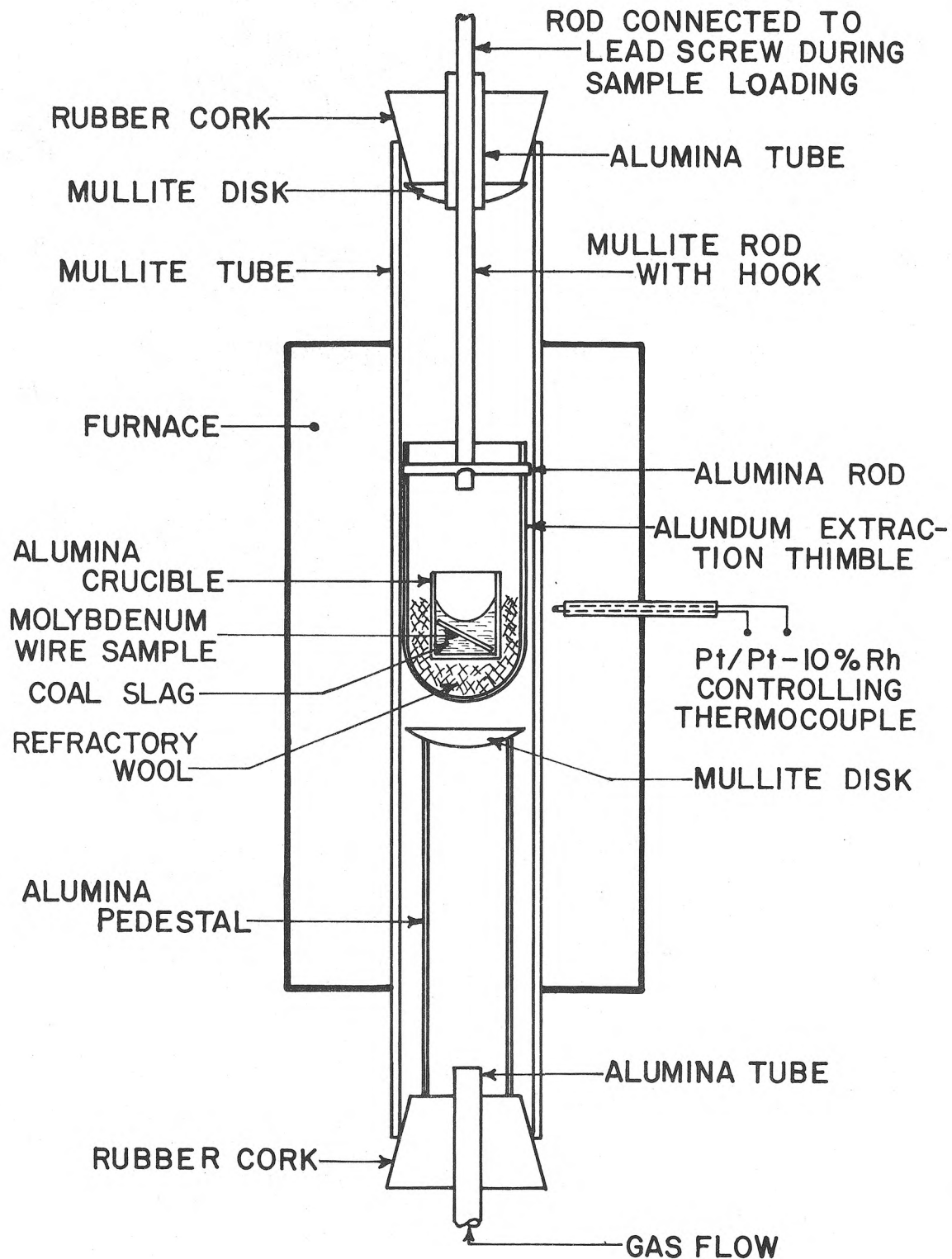


Figure 4. Vertical Furnace and Experimental Arrangement for Static Immersion Tests.



indicated the approximate flow rate. Hydrogen, oxygen, nitrogen, and argon were used directly from the cylinders. The use of tank regulators and needle valves provided sufficient flow control. Nitrogen and argon sometimes received a gettering treatment to remove traces of oxygen.

Carbon monoxide-carbon dioxide mixtures were regulated with a dual tube flowmeter proportioner. A caustic absorption technique measured the exact composition of the mixture by the methods described in Appendix B. The oxygen partial pressure of the gas within the furnace was calculated from the measured carbon monoxide/carbon dioxide ratio. Because in most cases the oxygen activity of the slag could not be assumed to be in equilibrium with the gas, the oxygen partial pressure over the slag is called an applied oxygen potential, implying that the system was shifting in response to this value. The reader should remember, throughout this study, that the system was dynamic, so concentrations of reactants at the interface shifted continuously during all the experiments.

3. Materials and Material Preparation. The various chemicals, atomic absorption standards, and other test, analysis, or preparation materials were of reagent qualities usually available. Some of the more important materials are described more fully.

a. Molybdenum. Molybdenum wire of 1.3 mm diameter was used for most tests. A supplier analysis could not be obtained, but atomic absorption flame analysis indicated impurities of 0.015% iron and less than 0.01% aluminum. In addition to the wire, the electrical current studies used 0.38 mm thick molybdenum sheet, which contained 0.007% iron and less than 0.01% aluminum.

b. Molybdenum Dioxide. Microprobe calibration and slag saturation experiments required molybdenum dioxide. Molybdenum trioxide (Fisher Reagent grade) and molybdenum powder (99.8%) were mixed in suitable proportions and then reacted in a tube furnace to form the needed molybdenum dioxide. The process consisted of sealing the well blended powders in an evacuated silica capsule and then heating the mixture at 900°C for 24 hours. The product was checked by gravimetric

and x-ray diffraction techniques and was found to be molybdenum dioxide with about 0.3% molybdenum metal remaining. Appendix A contains details of preparation and testing.

As a check on experimental equipment and reference information, the oxygen partial pressure marking the division between molybdenum and molybdenum dioxide stability regions at 1400°C was determined and compared to that shown in Figure 2. Molybdenum was exposed for short time periods to carbon monoxide-carbon dioxide gas mixtures containing increasingly more oxygen (lower carbon monoxide/carbon dioxide ratios) until molybdenum dioxide formed. The value found was  $10^{-9.3}$  atm oxygen, quite close to the  $10^{-9.2}$  atm pressure calculated from Gulbransen's data.<sup>24</sup>

c. Slags. Although experiments were conducted with several different slags, the majority used a high silica, eastern-type slag provided by the Union Electric Company. The slag was a water quenched bottom ash from a cyclone burner at their Sioux Power Station. The composition of the as-received slag is shown in Table I. A sample of the flyash generated from this same burner was also supplied by Union Electric and its composition is very similar to that of the bottom slag. The flyash was not used in any corrosion experiments.

A uniform slag for all experiments was prepared by remelting 10 kg of the as-received bottom slag in an iron crucible, as described in Appendix B. The use of an iron crucible, plus the high silica content of the slag, assured practically all of the iron would be in the ferrous state.<sup>17</sup> For this reason, the bottom slag was then reanalyzed and the iron oxide content of the remelted slag, also shown in Table I, is expressed as ferrous oxide, instead of the normally reported ferric oxide. The slag viscosity at 1400°C was calculated to be 88 poise according to the method of Watt and Fereday reported by Capps.<sup>16</sup> As mentioned in the introduction, conventional slags often contain carbon. The amount present in the UE bottom slag was of interest because of the strong effect carbon asserts at high temperature in reducing iron oxide. Both the as-received UE bottom slag and flyash were analyzed selectively for carbon by a dry train carbon dioxide absorption technique. The test did not rely on ignition loss data,

TABLE I. CHEMICAL COMPOSITION OF SEVERAL COAL SLAGS

Type of Slag	SiO <sub>2</sub>	Al <sub>2</sub> O <sub>3</sub>	Fe <sub>2</sub> O <sub>3</sub>	MgO	CaO	Na <sub>2</sub> O	K <sub>2</sub> O	SO <sub>3</sub>	Carbon	TiO <sub>2</sub>	P <sub>2</sub> O <sub>5</sub>
Union Electric Bottom Ash (as received)	50.6	24.0	18.2	0.9	5.1	0.7	1.9	0.8	0.06	-	-
Union Electric Bottom Ash (remelted)	50.4	20.4	17.4#	-	7.3	-	-	0.6	-	-	-
Union Electric Flyash	50.4	22.0	20.7	0.8	4.0	1.0	2.6	0.3	1.0	-	-
UMR-1, Low Iron Synthetic Slag	39.1	13.0	23.5	7.0	17.4	*	*	*	*	*	*
UMR-2, High Iron Synthetic Slag	21.8	13.0	41.7	6.1	17.4	*	*	*	*	*	*
National Bureau of Standards #385**	39.7	14.9	20.5	7.9	16.9	*	*	*	*	*	*
Flyash-Illinois #6 Peabody-Pawnee Mine**	46.99	18.35	21.16	1.02	4.80	2.01	2.42	1.92	-	0.90	0.25
Hanford Power Plant Bottom Slag, Utah Coal**	59.18	18.31	6.90	0.94	10.81	2.11	0.94	-	-	0.96	0.37
MHD Combustor, Pittsburgh Energy Center, MHD 12 A**	59.81	22.14	14.92	4.41	2.14	0.24	1.34	-	-	0.72	0.35

- indicates analysis unknown

\* indicates no additions of these compounds were made

# present and reported as FeO (see explanation in text)

\*\* data from J. Lambert Bates<sup>13</sup>

eliminating the complications of weight loss data. The results are included in Table I, showing virtually no carbon in the as-received bottom slag, but significant amounts in the flyash. The technique is described in detail in Appendix B.

Slag composition was not one of the factors chosen as a variable in this work. Therefore, the choice of the UE bottom slag for most corrosion experiments was based on such factors as availability, ease of containment in alumina crucibles, and a liquidus temperature below 1350°C. The combustion of coal from different mines produces ash of a wide composition range, as shown in Table I. Of the slags listed, the one closest to the UE slag composition is the Illinois #6 flyash.

Two other slags were used in a few experiments to get a general idea of the effects of slag composition on molybdenum stability. These were slags produced synthetically by mixing oxide and carbonate compounds in desired proportions and then fusing the mixtures in air. Denoted UMR-1 and UMR-2, their compositions are reported in Table I.

For other composition tests, a seeded slag was desired. This was prepared from the UE slag. Initially 10% potassium sulfate, as powder, was mixed with the ground slag. When melted, the potassium sulfate reacted with the slag to form potassium oxide dissolved in the slag, sulfur oxides, free or ionic sulfur, and residual potassium sulfate. The sulfur compounds reacted with the slag, dissolving to saturation, and the remainder escaped as gas. The resulting froth forced some slag from the crucibles, which disrupted the tests. After release of the gas, the slag continued to climb from the crucible due to the crucible being wetted with slag. Another sample of the seeded slag was prepared by pre-melting the mixture in air at 1300°C until all foaming had ceased.

d. Crucibles. High purity (99.8%), dense alumina crucibles with a 1.0 mm wall thickness adequately withstood the corrosive effects of the molten slags. Static UE slag, in the tests of under 10 hours duration, formed a reaction layer with the crucible, but

did not decrease the wall thickness by more than 0.1 mm. Beyond that duration, discoloration of the alumina occurred because slag constituents soaked into the crucible structure. After 20 hours of exposure, contamination of the slag became significant as reaction layers spalled from the inside surface. The crucible also blistered on the outside surface as the alumina was attacked. Stirring the slags caused much more rapid erosion, occasionally creating a hole in the wall within 4 hours. Both UMR synthetic slags eroded the crucibles more rapidly than the UE slag, their attack being greatest at the gas-slag interface.

4. Methods of Analysis. The bulk of data obtained for the corrosion experiments were obtained by metallographic inspection and electron microprobe analysis. Gas analysis and carbon analysis methods for coal slag were also developed during this study and details of all these are discussed in Appendix B. The first two techniques are considered critical to this study and are discussed more fully here.

a. Microscopic Examination. Investigations with a Bausch & Lomb Research Metallograph helped identify the visible reaction products in the molybdenum-slag corrosion samples. Quantitative information on reaction layer thickness and molybdenum erosion came from filar eyepiece and micrometer stage measurements. Preparation of samples followed usual metallographic procedure, using diamond polishing compound to give maximum flatness for subsequent microprobe analysis. Details of sample preparation are included in Appendix B.

The distance the surface of the molybdenum sample receded was the main measurement of the extent of corrosion. Surface recession data are reported as the distances from the existing molybdenum surfaces to the original surfaces. Experimentally, this was calculated simply as one-half the difference between initial and final wire diameters as measured with the filar eyepiece. Any oxide reaction layers found on the molybdenum surfaces were not considered part of the remaining molybdenum, but alloyed regions were considered integral parts of the molybdenum.

Oxide reaction layers were most effectively studied using polished, unetched surfaces. Polarized light greatly facilitated phase identification, since metallic phases remained bright in all analyzer orientations, while the oxides appeared strongly colored.

Etchants were necessary, however, to reveal the microstructure of unreacted or alloyed molybdenum. Nital was the preferred etchant for iron-rich phases, while Murakami's reagent (a potassium ferri-cyanide solution) was used for molybdenum-rich phases. Since Murakami's reagent had negligible effect on nital etched iron-rich phases, the two etchants were often used on the same surface, one after the other.

The glassy UE slag was somewhat transparent and some features beneath polished surfaces could be seen through the slag. This was especially true with a concentrated source of illumination, as provided by oil immersion optics. Crystal morphology of precipitates in the slag and the shape or texture of surfaces could be seen. This proved valuable when studying the molybdenum dioxide saturation of the slag or studying structures and changes on the molybdenum surface.

When it was found necessary to remove the molybdenum from the slag without disturbing any reaction layers, a caustic leach made of lithium hydroxide and lithium hydride, heated above the mixture's melting point, worked quite well.<sup>31</sup> Oxide reaction layers were removed, but alloy phases were not affected.

b. Microprobe Analysis. The electron microprobe analysis of corrosion samples was a most important data collection technique, as most reactions between molybdenum and slag occurred only over a few micrometers on each side of the interface. Reaction layer composition and concentration gradient profiles both resulted from microprobe studies. The writings of Birks,<sup>32</sup> Reed,<sup>33</sup> and Andersen<sup>34</sup> were the basis for all analytical techniques used. The study employed an Applied Research Laboratory triple spectrometer unit.

Accurate measurement depended upon minimum disruption of the electron beam passing into the sample and of the emitted x-rays

passing from the surface. Surface irregularities which affect intensity by absorption of x-rays were minimized with highly polished surfaces. Electron beam distortion caused by charging of the non-conductive slag surfaces necessitated use of a conductive surface film. A vacuum-deposited carbon film provided a conductive layer essentially transparent to the electron beam. Standards were recoated with each batch of samples to minimize differences in absorption due to varying carbon film thickness.

The unit was operated with a 15 KeV electron beam energy. The analyzed spot was approximately  $2\mu\text{m}$  in diameter. A counting interval of 20 seconds was used. For all standards, accuracy was obtained by counting through 10 sets of 20 second intervals. The specimens were moved between each interval and excessive variations were used as an indication of inhomogeneity.

Point counting with three spectrometers gave simultaneous quantitative data on molybdenum, iron, and aluminum. The Mo  $L_{\alpha}$  and the Fe  $K_{\alpha}$  wavelengths were selected for quantitative measurements, while Al  $K_{\alpha}$  wavelength measurements located the slag interface quite accurately. Concentration profiles were generated using a mechanical advance to shift the sample a known distance between 20 second counting sequences.

As just mentioned, a sharp change in the detected aluminum counts identified the location of the slag interface, so the slag interface is used as the reference in constructing microprobe concentration profiles. This interface does not always correspond to the molybdenum surface, as oxide layers sometimes exist in between. Therefore the tabulated molybdenum surface recessions (measured from the molybdenum interfaces) do not always match the surfaces recession values (to the slag interfaces) reported on the microprobe plots. The two references could be easily reconciled when oxide layers were uniform in thickness, but since this is not always true, the two different bases are maintained throughout.

Ideally, concentration (weight fraction) is derived by simple ratio comparison of intensities (number of counts detected) at

characteristic wavelengths of the species measured. The intensities are generated by counting on a sample and on a standard of known composition. Then simply:

$$C_a = \frac{I_a}{I_{(a)}} C_{(a)} \quad (5)$$

where  $C_a$  is the unknown concentration in the sample,  $I_a$  is the measured sample intensity, and  $C_{(a)}$  and  $I_{(a)}$  are the known concentration and measured intensity for the reference standard. However, interfering matrix effects, fluorescence, background, and other variables usually complicate the relation between concentration and intensity.

For the systems analyzed in this study, two different correction methods were used. For the metallic phases calculated corrections were suitable, while for the slag phases experimental standards were necessary.

1) Calibration in Metallic Phases. Corrections can be made by calculation in simple alloy systems, although significant error sometimes remains. Nevertheless, Birks estimates his corrections will result in accuracies with  $\pm 2\%$  of the true concentrations.<sup>32</sup> His methods were used in this study. In all cases, summation of corrected weight percentages gave  $100\% \pm 1.8\%$ , thereby justifying the use of Birks' calculations.

Molybdenum concentration in areas of high molybdenum content, such as in the molybdenum wire and in some molybdenum-iron alloy phases, was calculated using matrix absorption, fluorescence, and atomic number corrections. Examples of these calculations and the resultant calibration curves are presented in Appendix B. The relation between molybdenum content and measured intensity was observed to be nearly linear above 70% molybdenum content.

Iron concentrations in the metallic phases were calculated using corrections for matrix absorption only. Corrections for atomic number were insignificant, while fluorescence did not occur. The 15 KeV energy of the electron beam was below that necessary



to excite the Mo  $K_{\alpha}$  wavelength, which is the only molybdenum wavelength short enough to cause fluorescence in iron. The calculated correction curve remained nearly linear up to 10% iron.

2) Calibration in Slag Phases. In complex systems of compounds, such as the multi-component slag, calculated corrections are not practical. A more suitable method is calibration using homogeneous standards with compositions similar to those of the samples. Such comparison standards must be homogeneous, so that microprobe readings are consistent and so the standard composition can be analyzed by other methods. With careful preparation and checking, good standards can be used to calculate the composition of samples through the use of Equation (5) using only corrections for background, as long as the two compositions do not differ greatly.

For analysis of molybdenum in the slag phase, homogeneous comparison standards were prepared by doping slag with molybdenum dioxide. The standards were analyzed by atomic absorption techniques. Three standards were used, one containing no molybdenum and two doped slags holding 1.06% and 3.23% of molybdenum in solution. Preparation and analysis of these standards is discussed fully in Appendix B.

The concentration of iron in the slag was not considered an important variable, and no rigorous calibration was used. The approximation used is discussed in Appendix B.

3) Additional Corrections. Birks' corrections are based upon relative intensity measurements already freed of all background (stray counts detected by the microprobe). A common method used to determine the background involves shifting the crystal analyzer slightly off peak on either side of the detected wavelength. To avoid any difficulties in returning the analyzer exactly to the same counting position after each check, an alternative method was used.

The background for iron was taken to be the number of iron counts collected by the iron detector when counting on pure

molybdenum. The residual molybdenum count likewise detected on pure iron represented the molybdenum background. So counting on an iron standard simultaneously gave the iron calibration count and the molybdenum background. This method agreed with the off-peak method within about 10% of the background. The background counts were deducted from the total count in all calculations before relative intensity was computed.

## B. EXPERIMENTS

Molybdenum-slag corrosion was studied using UE slag in three types of experiments. Static immersion tests identified the reactions occurring when reaction products accumulated in the reaction zone. Static conditions may occur in some parts of the channel during operation. In other static immersion experiments, potassium sulfate was added to the UE slag to study changes in reactions caused by seeded slag.

Stirred slag tests accelerated the corrosion process by dispersing reaction products and increasing mass transport through the slag, a condition expected in most of the MHD channel. Molybdenum was rotated to simulate slag flow. Stirred slag tests were also used to obtain saturation data for molybdenum oxides in the slag, and to determine the effects of carbon on the molybdenum-slag reactions.

Electrical current tests in static UE slag studied reactions at anode and cathode surfaces. All electrical tests were at constant voltage.

The effect of slag composition was briefly examined using synthetic slags containing greater amounts of iron oxides, and larger ferric/ferrous ratios than found in the UE slag. Only qualitative data were taken in the composition tests.

1. Static Immersion Tests. The test series studied oxygen pressure effects (and to a limited degree, slag composition) on the nature of reaction products formed at the molybdenum-slag interface and on the extent of erosion. Tests were conducted at

1400°C in atmospheres that varied oxygen partial pressure from  $10^{-11.6}$  to  $10^{-2.8}$  atm. The tests generally ran for 16 hours. A diagram of the sample arrangement is shown in Figure 4.

Molybdenum wires 18 mm long and 1.3 mm in diameter were placed diagonally into alumina crucibles 16 mm in diameter and 25 mm deep. About 4 g of powdered slag filled the crucible, but when melted that amount only just covered the wire. Because of the surface meniscus shape, a 5 mm length of the wire near the slag surface was a constant 3 mm below the surface. To be consistent, all sections studied were cut from this portion. At the lower end of the molybdenum wire, about 8 mm of slag covered the wire. The configuration is shown in Figure 4.

With the crucible packed into the sample holder, the arrangement was lowered mechanically into the furnace hot zone while the furnace was continuously purged with nitrogen. When the sample was well into the hot zone, the appropriate carbon monoxide-carbon dioxide gas mixture was admitted.

2. Stirred Slag Tests. Three different types of stirred tests were conducted. One stirred molybdenum dioxide into slag for solubility measurements, while a second type rotated molybdenum rods in slag to study the effect of slag movement on reactions at the corrosion interface. Both test series used oxygen partial pressures fixed at  $10^{-9.1}$  or  $10^{-2.8}$  atm. The third type rotated a carbon rod in slag containing stationary molybdenum to study the strong reducing effects of carbon and resultant changes in the nature and formation rate of molybdenum corrosion products. Flowing argon blanketed the sample in this test.

In molybdenum dioxide saturation experiments, the objective of stirring was to insure contact between the entire slag charge and the dioxide. To achieve saturation, the charge was first homogenized by intimately mixing -200 mesh slag with -400 mesh molybdenum dioxide in an ether slurry and was then dried. In the furnace, the slag melt was stirred for 20 hours at 12 rpm with a platinum loop attached to the same equipment used to rotate molybdenum wires, as shown in Figure 5.

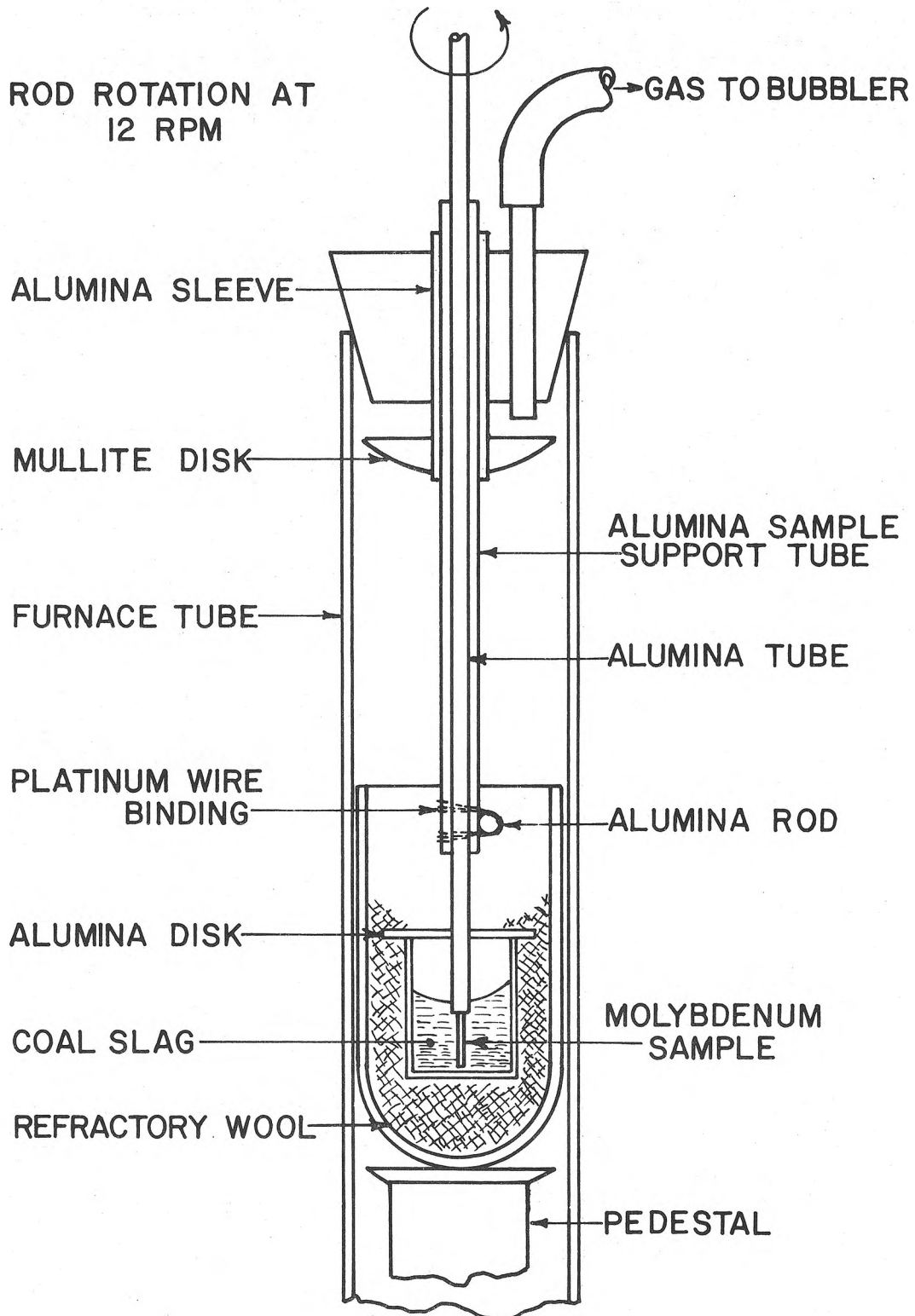


Figure 5. Apparatus and Sample Arrangement for Rotated Molybdenum Rod Tests. Modified Arrangement also used for Stirred Molybdenum Dioxide Saturation Tests.

The rotated molybdenum rod tests used 1.3 mm diameter wires held vertically in the melt and rotated about their axis at 12 rpm. Tests lasted 16 hours. The surface speed was initially fixed at 45 mm/min, but it changed as erosion progressed. The molybdenum oscillated slightly about its axis because of clearances between the support rod and rod guides. The sample lowering and gas flow procedures were similar to static test procedures. The test arrangement is shown in Figure 5.

In the rotating carbon rod test, a 6.4 mm diameter graphite rod was rotated at 12 rpm in the center of a slag bath containing a stationary molybdenum wire. The wire was placed in a ring at the bottom of the crucible. The 26 mm carbon rod was completely immersed in 40 g of slag contained in a 30 mm diameter crucible. The sample arrangement is shown in Figure 6.

3. Electrical Current Studies. Anode and cathode reactions occurring in the molybdenum-slag system at 1350°C and 1400°C were studied with constant voltage tests. The potential was fixed at 1.5 volts, while current was allowed to vary during the course of the 3 hour tests. The current was monitored throughout the test and was recorded at intervals. A carbon monoxide-carbon dioxide mixture controlled the oxygen pressure at  $10^{-9.6}$  atm at 1350°C and at  $10^{-9.1}$  atm at 1400°C.

The experimental arrangement is shown in Figure 7. The electrodes consisted of a vertical center wire of molybdenum and a surrounding circular band of molybdenum sheet. The crucible was 16 mm in diameter and contained about 4 g of slag. In one set of experiments at 1400°C the center pin was the cathode and in another it was the anode. The current density at each electrode was then fixed by the relative electrode surface area. Initially the center pin had a current density eleven times that of the ring.

The 1350°C test was conducted to check the results obtained at 1400°C and to obtain some information on the temperature dependence of the reactions found. The center pin was cathodic in this test.

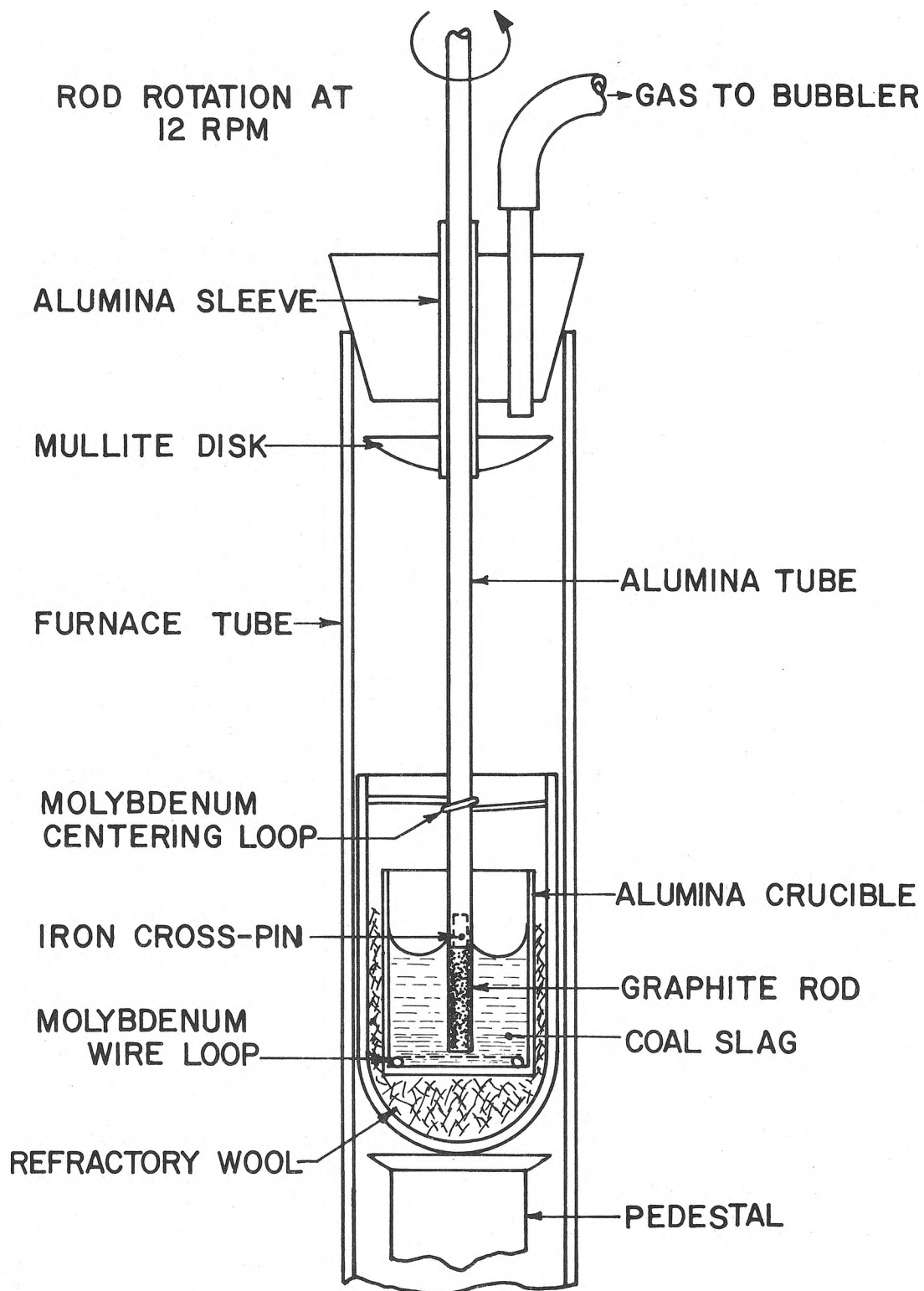


Figure 6. Apparatus and Sample Arrangement for Rotated Carbon Rod Test.

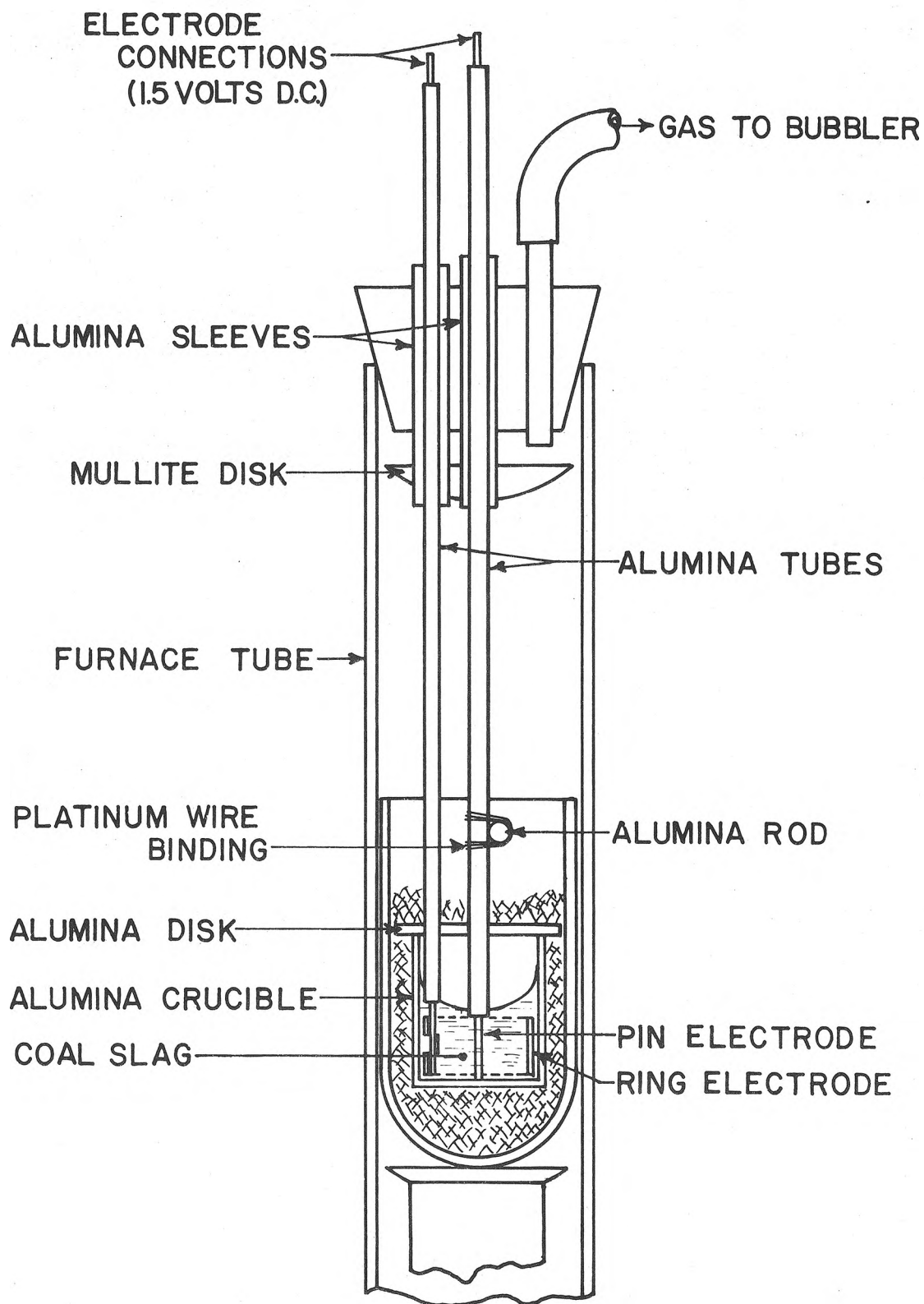


Figure 7. Apparatus and Sample Arrangement for Electrical Current Tests.

#### IV. RESULTS

Most results of this investigation are of three types: concentration data obtained by microprobe analysis, size measurements, and metallographic examination of the specimens. Results are presented in the form of tables correlating test conditions and measurements of selected concentration and corrosion data, graphs of microprobe concentration profiles, and photomicrographs of selected samples in order to facilitate comparisons between test conditions. Numerical data used to construct microprobe concentration profiles are listed in Appendix C. Supplementary photomicrographs are shown in Appendix D and these are keyed to related text by references in parenthesis.

The extent of reaction between molybdenum and coal slag is determined by the concentration of iron in the molybdenum and the concentration of molybdenum in the slag. The two concentrations cannot be measured at the metal-slag interface, because the microprobe always detects nearby phases as the interface is approached, due to beam scattering and secondary emissions. So, concentrations at specified distances from the interfaces (usually 10  $\mu\text{m}$ ) are chosen for tabulation, with the understanding the reported values are useful for comparisons, but not for accurate property calculations.

A special abbreviation is used to designate the location and type of concentration being reported. For example:

$$C_{\text{Fe} \rightarrow \text{Mo}}^{10 \text{ Mo/Ox}} = 0.1\% \text{ iron} \quad (6)$$

reads the concentration of iron in molybdenum solid solution 10  $\mu\text{m}$  back from the molybdenum-molybdenum dioxide interface is 0.1% iron.

Other symbols used are S, representing the slag phase, and A, for molybdenum-iron alloys other than molybdenum-rich solid solution. In the slag phase, values of molybdenum oxide and approximate iron oxide content are reported instead as the atomic species molybdenum and iron for convenience in plotting the concentration curves.



#### A. STATIC IMMERSION TESTS

In static tests, the movement of reaction products away from the reaction zone was restricted. Small temperature gradients certainly existed, causing some slag movement, but the relatively high slag viscosity and the small crucible size kept motion to a minimum. The samples clearly show where reaction products formed and indicate how the reactions were affected by increasing product concentrations and reaction layer thicknesses.

In the static tests, the oxygen activity of the slag near the molybdenum surface depends upon the amount of oxygen transported through the slag, relative to the amount reacted with the molybdenum. A test was devised to quickly check the oxygen diffusion through the slag under various conditions. A suitable arrangement substituted iron for the molybdenum and measured the amount of oxidation occurring. Iron was chosen since at 1400°C both metals oxidize at about the same oxygen pressure,  $10^{-9.8}$  atm for iron ( $a_{\text{FeO}} = 1$ ) and  $10^{-9.2}$  atm for molybdenum. Like molybdenum, iron reacts readily with oxygen, but any iron oxide formed dissolves rapidly in the coal slag. The quantity of oxygen transported by the slag is estimated by simply noting the amount of iron corrosion.

Iron sheet was held under UE slag layers of various thickness, for different lengths of time, and with different applied oxygen potentials. With lower potentials ( $10^{-9.1}$  atm), little weight loss occurred and extending the test duration only slightly increased the corrosion effect. With higher oxygen potentials ( $10^{-2.8}$  atm), oxidation was greater, but did not begin immediately, the actual lag time being dependent on the thickness of the covering slag layer. The lag was roughly one-half hour for 2 mm layers and two hours for 10 mm layers. Once corrosion began, 0.12 g of iron (20% of the iron sheet thickness) dissolved in a 2 hour period. Based on this observation, any lag induced by the 3 mm slag layers covering molybdenum wires in the static tests caused minimal effect on results of the 10 to 16 hour tests.

The results of static immersion tests are divided into sections on UE slag and on seeded UE slag. Both sets used the same experimental approach and the same test parameters where possible. The data collected from both sets are summarized in Table II.

1. Static Immersion in Union Electric Slag. Tests of 16 hour duration were conducted at four different applied oxygen potentials. Two distinct reactions predominated at different oxygen pressures, as suggested in discussion of Reactions (2), (3), and (4) in the Literature Review. At low oxygen potentials ( $10^{-11.6}$  atm), alloying reactions occurred according to the equilibrium described in Reaction (3) or (4), while at higher oxygen potentials (to  $10^{-2.8}$  atm), oxidation dominated according to Reaction (2).

a. UE-1. At the lowest oxygen potential tested,  $10^{-11.6}$  atm, small amounts of molybdenum oxides formed in dimples on the molybdenum surface, as visible in Figure 8. The upper, dark area is the slag, the lower, light portion is the molybdenum and the particles along the interface between the two are molybdenum dioxide.

At this low oxygen pressure, iron reduced from the slag as molybdenum oxidized. The iron alloyed with molybdenum and the  $C_{Fe \rightarrow Mo}^{10 \text{ Mo/S}} = 2.7\%$  iron, as measured by microprobe. Around 5% iron was measured at the interface, but as mentioned before, this value is uncertain, because iron from the slag begins to be detected near the interface. In any event, the iron concentration in the molybdenum rises sharply as the molybdenum-slag interface is approached. Away from the interface, an iron concentration plateau exists, as evident by  $C_{Fe \rightarrow Mo}^{20 \text{ Mo/S}} = 2.3\%$ . The diffused iron caused no visible changes in the molybdenum microstructure, as seen on sections etched with Murakami's reagent (Appendix D-48). Slight surface grain growth is visible, and it is thought due to causes incidental to this study, as discussed later.

Although the molybdenum surface recession was undetectably small, the  $C_{Mo \rightarrow S}^{5 \text{ Mo/S}}$  was 0.56%. The small volume loss caused by

TABLE II. SUMMARY OF MOLYBDENUM STATIC IMMERSION TESTS

Sample Identification	In Union Electric Slag				In Seeded Union Electric Slag		
	UE-1	UE-2*	UE-3	UE-4	UE <sub>S</sub> -1	UE <sub>S</sub> -2†	UE <sub>S</sub> -3
Applied pO <sub>2</sub> , Log (atm) <sup>2</sup>	-11.6	-10.9	-9.1	-2.8	-10.9	-9.1	-2.8
Duration, (hr)	16	16	16	16	10	16	10
Corrosion Products	Beads of MoO <sub>2</sub>	Beads of MoO <sub>2</sub>	Broken MoO <sub>2</sub> Layer	MoO <sub>2</sub> Layer	MoO <sub>2</sub> , Fe Drops	Loose MoO <sub>2</sub>	Flaky MoO <sub>2</sub> Layer
Reaction Layer Thickness, (μm)	2	4	3	6	No Layer	2	5
C <sub>Mo → S</sub> <sup>10 Mo/S</sup>	0.55%	1.3%	0.96%**	3.5%**	1.3%***	1.4%	3.9%
C <sub>Fe → Mo</sub> <sup>10 Mo/S</sup>	2.6%	0.90%	1.1%	0.26%	5.0%	0.10%	0.09%
Recession of Surface, (μm)	0	1	12	38	11	51	38

\* Results from this test do not correlate with other tests.

\*\* C<sub>Mo → S</sub><sup>10 O<sub>x</sub>/S</sup>

\*\*\* C<sub>Mo → S</sub><sup>20 Mo/S</sup>

† Slag premelted with K<sub>2</sub>SO<sub>4</sub> seed in air.

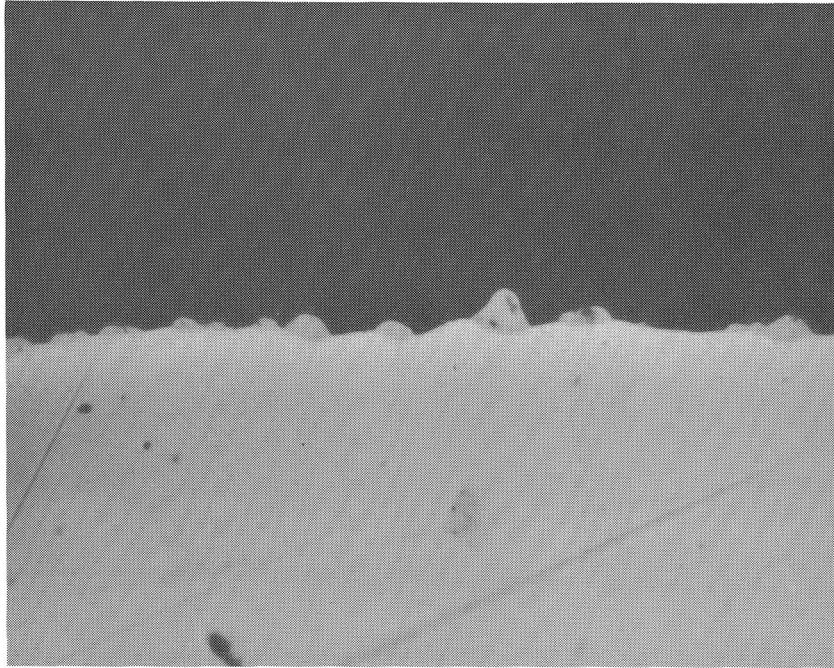


Figure 8. Slag-Metal Interface, UE-1. (1300x), unetched.

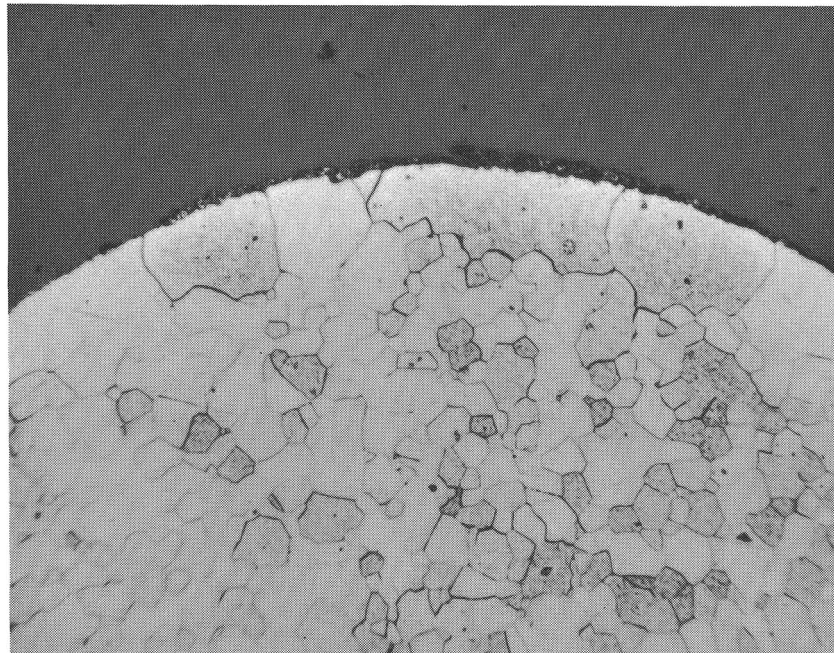


Figure 10. Molybdenum Surface, UE-3. (140x), etched in Murakami's Reagent.

dissolution of molybdenum into the slag was apparently offset by swelling of the surface as iron diffused into the wire. The molybdenum dioxide content of the slag was uniform near the wire.

b. UE-2. In the second test, the applied oxygen pressure was raised to  $10^{-10.9}$  atm. The amount of molybdenum dioxide on the molybdenum increased, taking the form of loosely grouped, rounded particles (Appendix D-49,50). The microprobe profile for this test (typical in appearance to other low oxygen tests) is shown in Figure 9. Referring to Table II, the  $C_{Fe \rightarrow Mo}^{10 Mo/S}$  is substantially lower than for UE-1, while the  $C_{Mo \rightarrow S}^{10 Mo/S}$  is more than doubled. Only slight surface recession occurred.

c. UE-3. A third test was conducted at  $10^{-9.1}$  atm oxygen pressure, just above the  $10^{-9.2}$  atm limit for molybdenum stability (see Figure 2). More molybdenum dioxide formed at the interface than for UE-2, but molybdenum and slag were still in contact in some areas. Surface recession reached 12  $\mu\text{m}$ . Figure 10 shows a photomicrograph of this sample. The faintly visible dark areas between the wire and slag are etched oxides. The oxide formed an irregular layer about 3  $\mu\text{m}$  thick and the molybdenum dioxide particles appear more as distinct crystals than in the first two tests (Appendix D-51 is a higher magnification of the interface). Large grains within the molybdenum, near the wire surface, are also evident in Figure 10.

In this test, a decreased amount of iron diffused into the molybdenum when compared to UE-1, but the amount increased from that of UE-2. In a like manner, the  $C_{Mo \rightarrow S}^{10 Ox/S} = 0.96\%$  fell between data from the first two tests. The iron content in the molybdenum was nearly constant from 4 to 12  $\mu\text{m}$  below the surface. The molybdenum dioxide content of the slag was constant in the region measured near the wire, but none was detected at distances far from the surface (greater than 2000  $\mu\text{m}$ ).

d. UE-4. At the highest applied oxygen pressure tested,  $10^{-2.8}$  atm, oxidation of the molybdenum was the dominant reaction. The molybdenum surface receded 38  $\mu\text{m}$  and a 6  $\mu\text{m}$  molybdenum dioxide

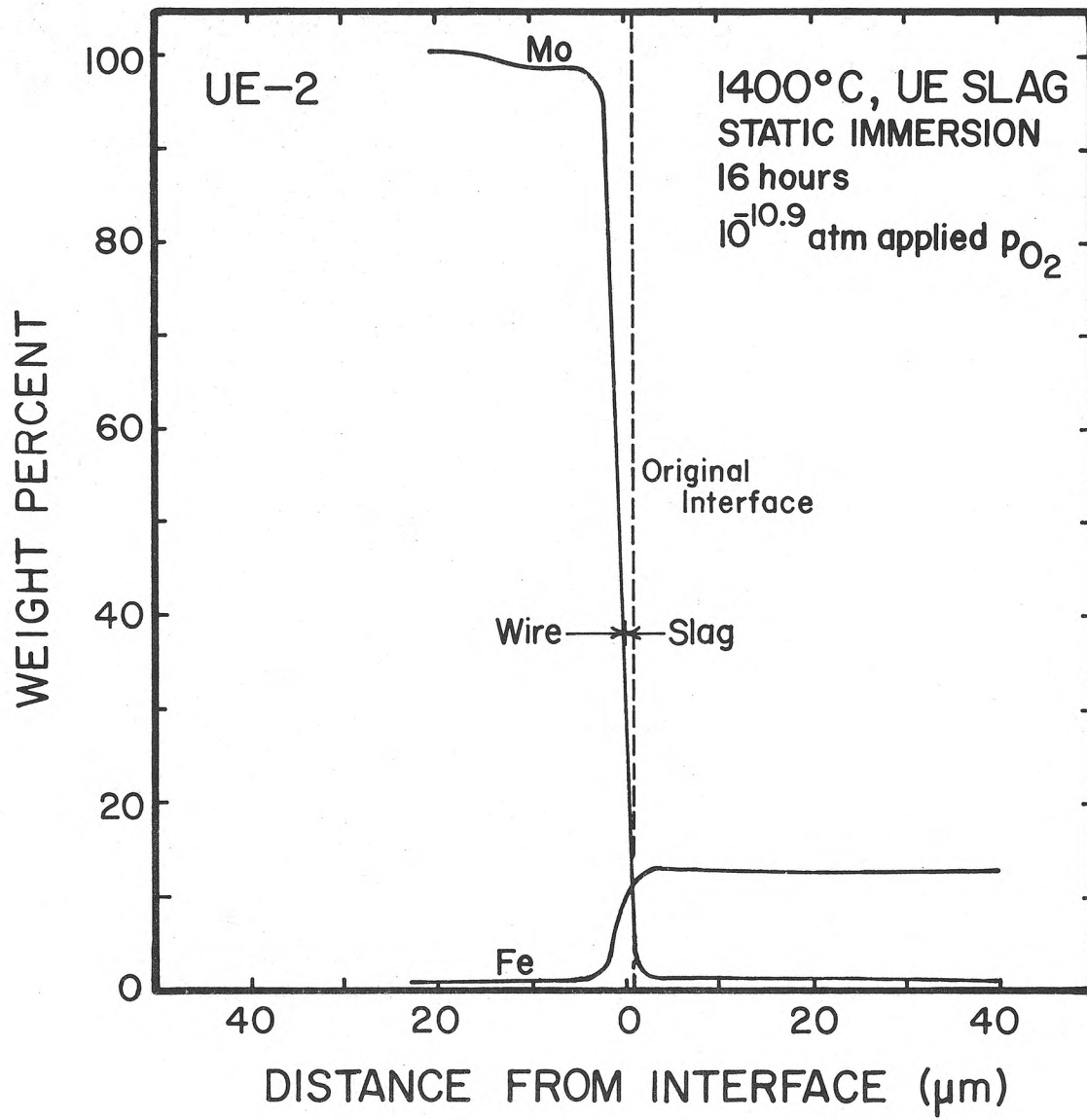


Figure 9. Microprobe Concentration Profile for Iron and Molybdenum in the UE-2 Test.

layer remained on the metal surface. The oxide formed an unbroken layer, apparently consisting of two different structures. The structures are not fully understood. Only molybdenum dioxide was identified within the layer using the microprobe, but the analysis is not considered conclusive. A typical section of the structure is shown in Figure 11 (See also Figure 19). The two different regions are clearly visible, one appearing as a network of stubby projections (lighter colored) extending from the molybdenum surface, and the other forming a matrix around the first. Together, they form a uniformly thick layer on the wire.

Examination of the section using polarized light show the matrix oxide to be large crystals, roughly 4  $\mu\text{m}$  wide, that extend completely through the oxide layer. Several of the smaller projecting oxide clusters are contained in each matrix crystal. With certain analyzer orientations, the contrast between the two regions nearly vanishes (Appendix D-52).

The molybdenum contained the lowest concentration of iron of all the UE static tests; the  $C_{\text{Fe} \rightarrow \text{Mo}}^{10 \text{ Mo/Ox}} = 0.26\%$ . The oxide layer contained similar amounts of iron,  $\approx 0.3\%$ , though greater uncertainty exists, as no microprobe standards were established for iron in the molybdenum dioxide phase.

The concentration of molybdenum dioxide in the slag was the highest in this test series, with  $C_{\text{Mo} \rightarrow \text{S}}^{10 \text{ Ox/S}} = 3.5\%$ . As before, the slag remained quite inhomogeneous. Only background count levels of molybdenum were detected 3000  $\mu\text{m}$  from the wire. Near the wire, where the slag appears saturated with molybdenum dioxide, some of the oxide precipitated from the melt upon cooling. The zone of saturation and precipitation is seen as a fogged region in Figure 12, taken from a similar test at  $10^{-1.8}$  atm applied oxygen pressure. Macroscopically, the saturated zone appears as a red colored band around the wire. The band extends 180  $\mu\text{m}$  from the wire surface.

2. Static Immersion in Seeded Union Electric Slag. Three experiments, conducted like the static tests just presented, used

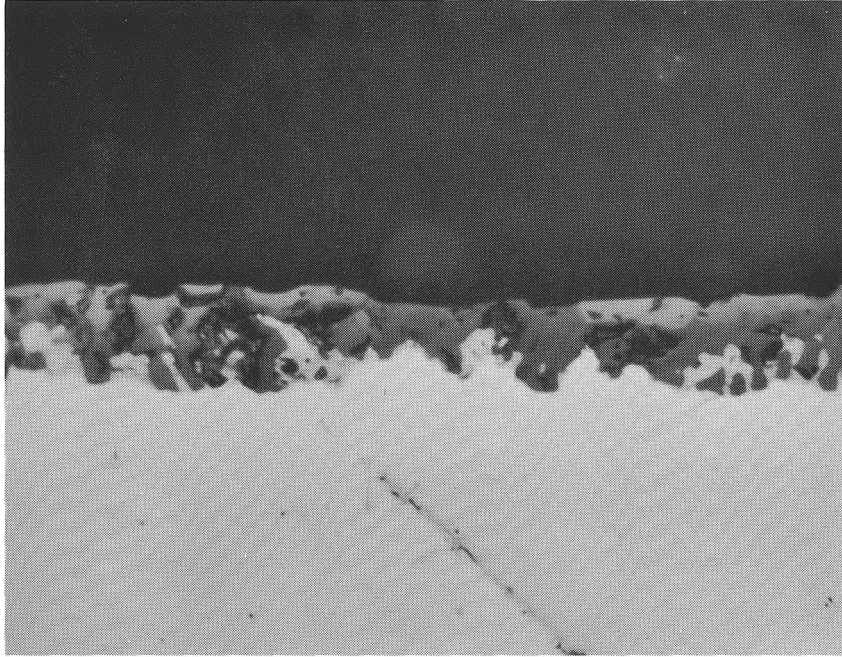


Figure 11. Slag-Metal Interface, UE-4. (1300x), unetched.

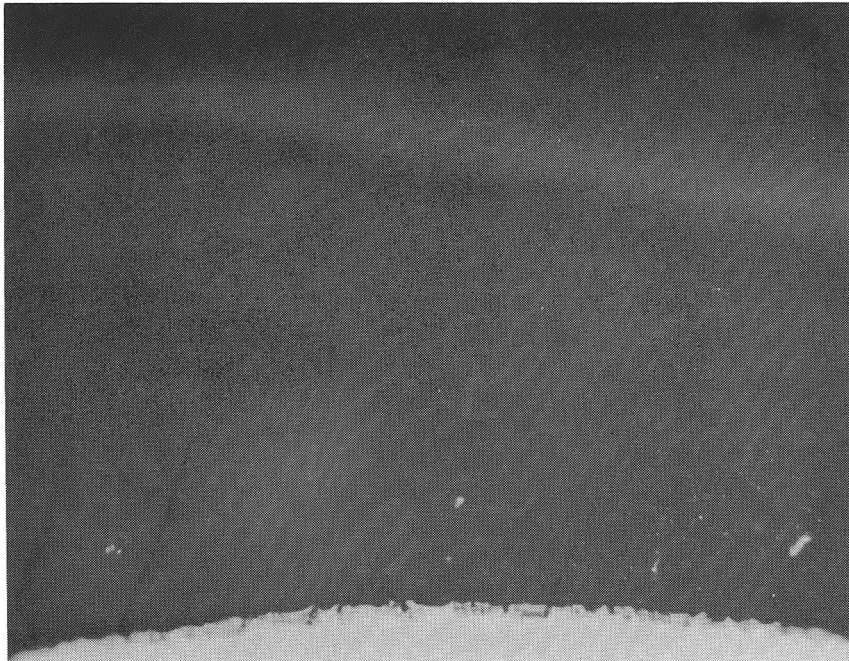


Figure 12. Saturation Precipitation in UE Slag Near Molybdenum. (400x), unetched.



the same UE slag with additions of 10% potassium sulfate as seed material. Two experiments started with unreacted mixtures of slag and seed and ran at applied oxygen pressures of  $10^{-10.9}$  and  $10^{-2.8}$  atm. These were limited to 10 hour durations due to slag loss, as discussed in the Experimental Methods. For another test, at  $10^{-9.1}$  atm, previously reacted seeded slag was used and the experiment was run 16 hours successfully. The volatilization of potassium and sulfur compounds made resulting species concentrations different from the original, but the resulting slag compositions were not determined.

The addition of seed had a marked effect on results, as indicated in Table II. Compared to results under equivalent conditions in plain UE slag, more iron alloyed with molybdenum in low oxygen partial pressures and more molybdenum oxidation occurred at high oxygen partial pressures. Surface erosion increased and the nature of reaction layers changed.

a. UE<sub>S</sub>-1. The microstructure in the 10 hour test at  $10^{-10.9}$  atm consisted of metal and oxide droplets in the slag near the molybdenum-slag interface, as shown in Figure 13. Metallic particles were found dispersed throughout the slag. The molybdenum section, duplex etched in nital and Murakami's reagent, showed no significant microstructure changes. There were no visible iron-rich phases at the surface and no unusual molybdenum grain changes.

Microprobe analysis partly identified the nature of the drops in the slag and Figure 14 shows the microprobe profile. The two sets of sharp peaks in the slag phase resulted as the beam crossed over small beads of material. The beads were 1-3  $\mu\text{m}$  in diameter, so measurements free of interference from surrounding slag were not possible. The exact compositions remain unknown, but from the peaks, one bead was apparently an iron-molybdenum alloy and the other was probably molybdenum dioxide. In the first bead, significant amounts of both iron and molybdenum were detected, while in the second high concentrations of molybdenum but no iron were found.

Within the molybdenum, the  $C_{\text{Fe} \rightarrow \text{Mo}}^{10 \text{ Mo/S}} = 5.0\%$  and the value tapered off deeper in the wire. The molybdenum dioxide content

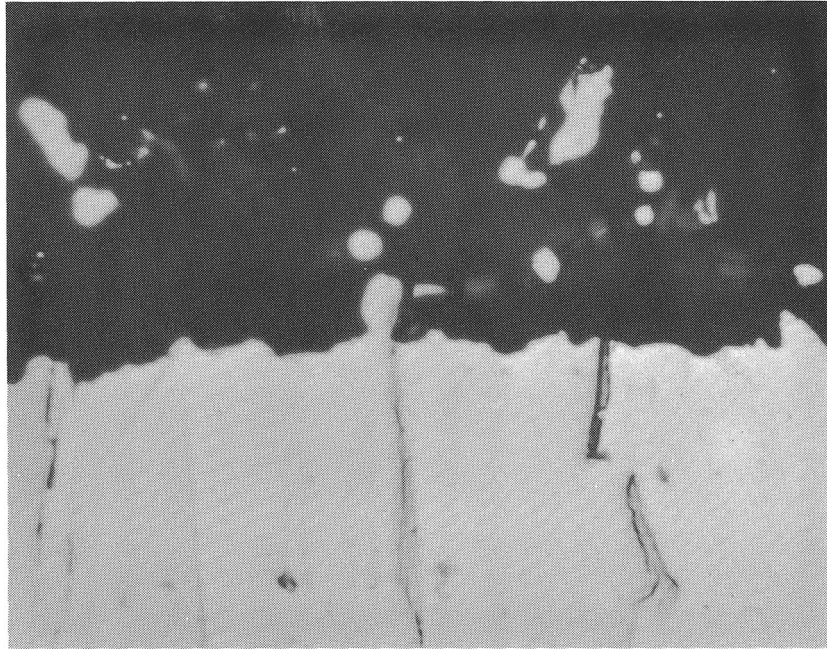


Figure 13. Slag-Metal Interface,  $UE_S-1$ . (1300x), unetched.

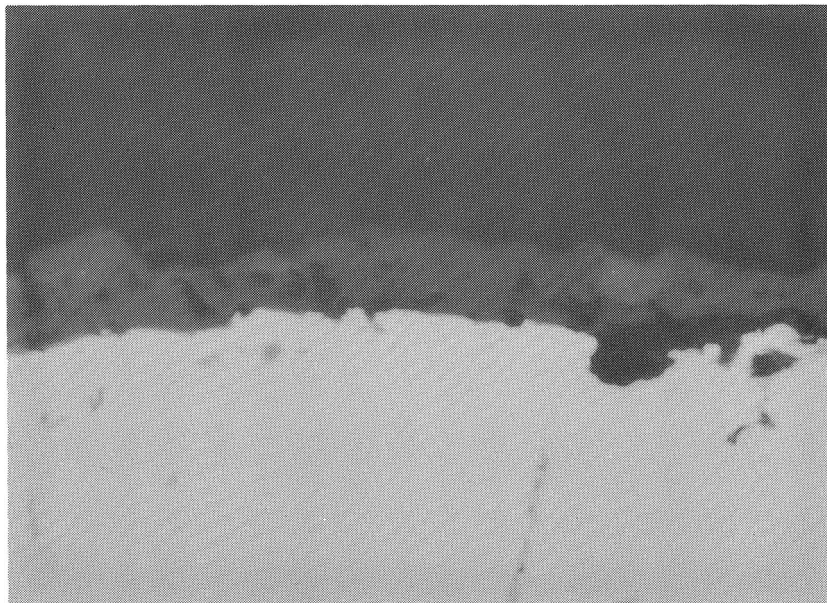


Figure 15. Slag-Metal Interface,  $UE_S-3$ . (1300x), unetched.

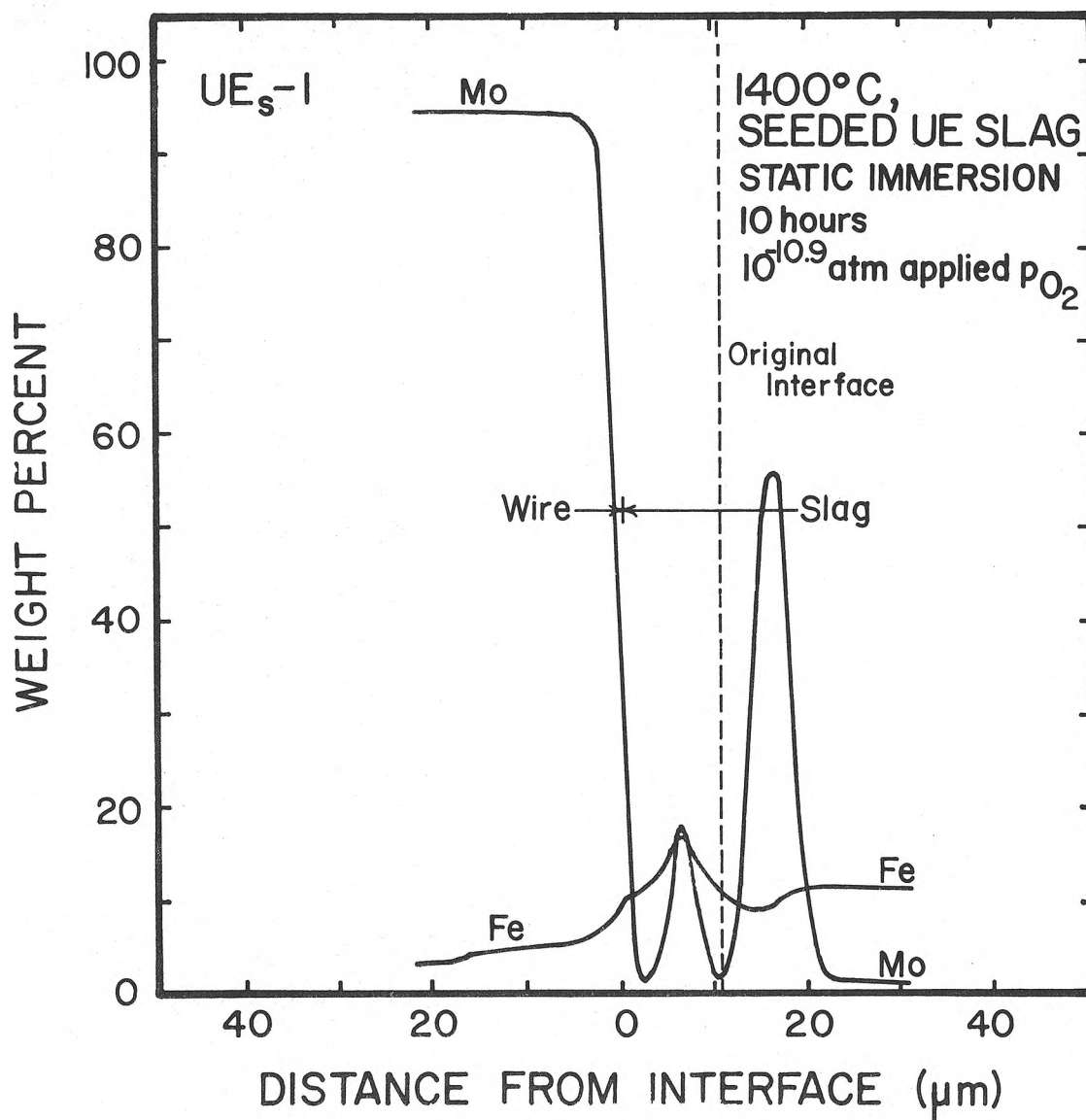


Figure 14. Microprobe Concentration Profile of Iron and Molybdenum in the UE<sub>s</sub>-1 Test.

of the slag was little different than in the UE-2 test at the same applied oxygen potential.

The molybdenum surface receded 11  $\mu\text{m}$ , about 10 times that found in the UE-2 test, despite the 25% shorter duration of the seeded test.

b. UE<sub>S</sub>-2. In the 16 hour test at  $10^{-9.1}$  atm oxygen pressure, using air-melted seeded slag, some surface oxide was present on the molybdenum (Appendix D-53,54). Molybdenum dioxide particles were also found loose in the slag, but no metallic beads were found. The erosion of the molybdenum surface was 51  $\mu\text{m}$ , the largest of any static immersion test. Very little difference is found in the  $C_{\text{Mo} \rightarrow \text{S}}^{10 \text{ Mo/S}}$ , comparing the results of the first and second seeded tests, as seen in Table II, while the  $C_{\text{Fe} \rightarrow \text{Mo}}^{10 \text{ Mo/S}}$  dropped fifty-fold.

The  $C_{\text{Fe} \rightarrow \text{Mo}}^{10 \text{ Mo/S}}$  is much lower than in previous tests, being ten times smaller than in UE-3, the other test at  $10^{-9.1}$  atm oxygen potential. The  $C_{\text{Mo} \rightarrow \text{S}}^{10 \text{ Mo/S}}$  changed less dramatically, increasing to 1.4% molybdenum from 0.96% in the UE-3 test.

c. UE<sub>S</sub>-3. In the 10 hour test at  $10^{-2.8}$  atm oxygen pressure, the oxide layer on the molybdenum surface formed nearly to the thickness found in the plain slag test, UE-4. The appearance was much different, as seen in Figure 15. No mixed oxide structures are present and the layer cracked away from the metal surface upon cooling. The dark band adjacent to the molybdenum is the crack. The surface recession of 38  $\mu\text{m}$  is equal that found in the longer UE-4 test. The highest  $C_{\text{Mo} \rightarrow \text{S}}^{10 \text{ Ox/S}}$  and the lowest  $C_{\text{Fe} \rightarrow \text{Mo}}^{10 \text{ Mo/Ox}}$  of all the static immersion tests occur in UE<sub>S</sub>-3.

3. Static Immersion in UMR Synthetic Slags. Tests using different slags briefly examined some effects of slag composition. The UE slag was compared with two synthetic slags, UMR-1 and UMR-2, whose compositions are included in Table I. The UMR slags were higher in iron, having iron/silica ratios of 0.42 and 1.34 respectively, while the UE slag had a ratio of 0.27. The UMR slags were prepared by melting constituent mixtures in air, while the UE slag was melted in contact with iron.

Tests of four hour duration compared reaction of molybdenum in each slag using a carbon dioxide-hydrogen atmosphere of  $10^{-6.8}$  atm oxygen potential. The UMR-1 slag caused a  $64 \mu\text{m}$  surface recession, while the high iron UMR-2 slag caused a  $400 \mu\text{m}$  loss. Only about  $7 \mu\text{m}$  of erosion occurred in UE slag.

## B. STIRRED SLAG TESTS

Several different experiments are grouped under the stirred slag tests. Static and stirred slag saturation by molybdenum dioxide was measured under several oxygen potentials to determine its solubility. Both static and stirred data are combined in this section for convenience. Molybdenum wires were rotated in UE slag under two different applied oxygen potentials. The resulting dispersion of reaction products produced more uniform slag compositions. The rotating rod format was also used to expose UE slag to a carbon-bearing environment. This arrangement held graphite below the slag surface, causing continuous carbon reduction of the slag.

### 1. Molybdenum Dioxide Saturation of Union Electric Slag.

Molybdenum dioxide saturation data was collected for both plain and seeded UE slag. The results are reported in Table III. These values provide checks on data collected in the UE-3 and UE-4 tests in the presence of molybdenum, and provide additional information in seeded UE slag at  $10^{-8.8}$  atm oxygen pressure. Comparisons of the data show that a uniform slag composition did not occur in static plain UE slag and occurred only after long periods in stirred plain UE slag. Uniform saturation was easily reached in static seeded slag.

a. Molybdenum Dioxide in Union Electric Slag. Three tests used molybdenum dioxide powder mixed with plain UE slag. The first, MoO<sub>2</sub>-1, was a static test and showed very limited reaction with the dioxide. The dissolved molybdenum dioxide was not uniformly distributed in the slag; even near dioxide particles, much variation in the concentration was found. Figure 16 shows a vertical section through the top of MoO<sub>2</sub>-1. The slag was saturated near the dioxide

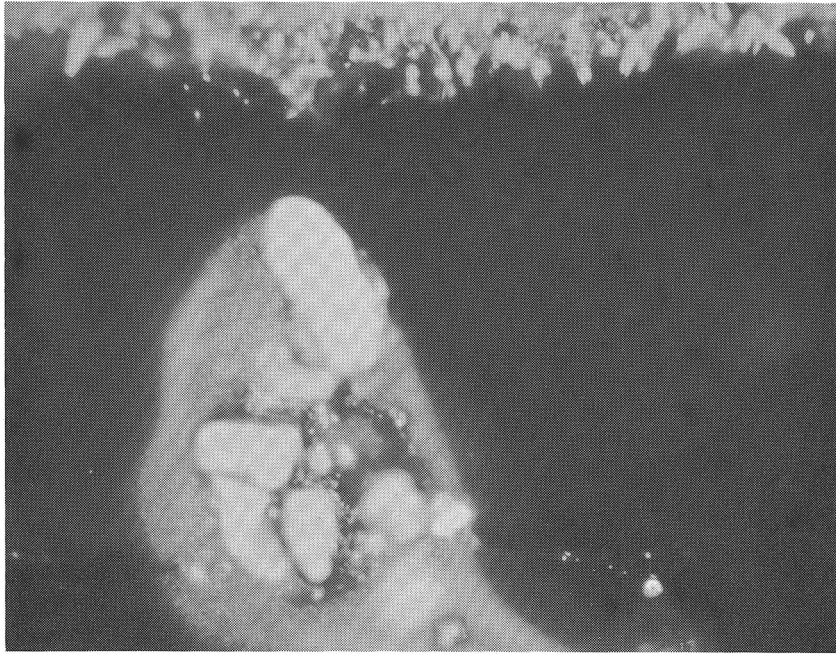


Figure 16. Molybdenum Dioxide in Slag, MoO<sub>2</sub>-1.  
Saturation Experiment in UE Slag.  
(1300x), focused into slag.

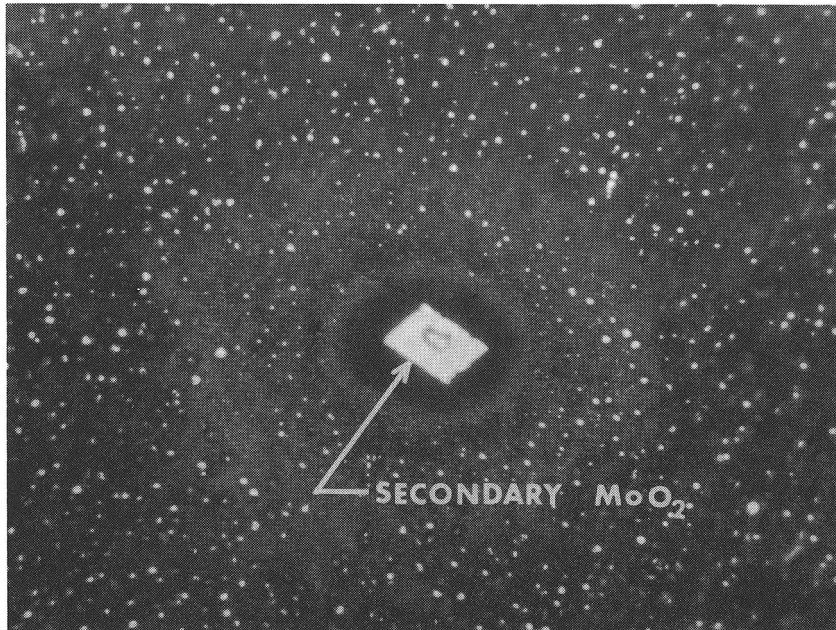


Figure 17. Molybdenum Dioxide in Slag, MoO<sub>2</sub>-4.  
Saturation Experiment in Seeded UE Slag.  
(1300x), focused into slag.

particles, as evidenced by the cloud of precipitate around them. Other crystals of molybdenum dioxide are found at the slag surface, seen as the flaky, dendritic structure at the top of Figure 16. These appear substantially different than the added molybdenum dioxide particles, which also tended to stay at the slag surface.

TABLE III. SUMMARY OF MOLYBDENUM DIOXIDE SATURATION EXPERIMENTS

	In Union Electric Slag			In Seeded UE Slag
	MoO <sub>2</sub> -1*	MoO <sub>2</sub> -2	MoO <sub>2</sub> -3**	MoO <sub>2</sub> -4
Sample Identification	MoO <sub>2</sub> -1*	MoO <sub>2</sub> -2	MoO <sub>2</sub> -3**	MoO <sub>2</sub> -4
Test Condition	Static	Stirred	Stirred	Static
Applied p <sub>O<sub>2</sub></sub> , Log (atm)	-8.6	-9.1	-2.8	-8.8
Duration, (hr)	20	20	20	12
Molybdenum in Slag, (Wt%)	0.7%	0.76%	3.23%	3.4%

\*Saturation occurred only near molybdenum dioxide particles.

\*\*No excess molybdenum dioxide remained after the test.

In the other two tests, excess molybdenum dioxide was stirred within UE slag using a platinum loop attached to a spinning rod. All undissolved molybdenum dioxide settled to the bottom of the melt. At  $10^{-9.1}$  atm pressure, MoO<sub>2</sub>-2, the slag absorbed 0.76% molybdenum. The molybdenum dioxide concentration was uniform throughout the slag. In the MoO<sub>2</sub>-3 test at  $10^{-2.8}$  atm, no excess molybdenum dioxide was observed after the test. A layer of yellow to light violet powder coated the upper cool region of the furnace tube, indicating evolution of volatile molybdenum trioxide. The slag was homogeneous and this sample was subsequently used as a microprobe standard, as no molybdenum dioxide precipitated upon cooling.

b. Molybdenum Dioxide in Seeded Union Electric Slag. The seeded slag test used molybdenum dioxide added to a mixture of 10% potassium sulfate and UE slag. The dioxide reacted to a greater extent than in the plain UE slag and upon cooling an oxide cloud

precipitated throughout the slag. In addition, secondary crystals of molybdenum dioxide were observed, as shown in Figure 17. These were possibly caused by the effect of alternate decrease and increase in solubility with the small thermal cycling of the furnace. This was taken as a strong indication the slag was thoroughly saturated at 1400°C. Microprobe analysis of areas away from the secondary crystals gave a value of 3.4% molybdenum. The excess molybdenum dioxide particles originally added moved to the top half of the crucible. Small bubbles, almost a foam, were also found towards the slag surface.

2. Rotated Molybdenum Wire. Two experiments were conducted, using oxygen pressures of  $10^{-9.1}$  and  $10^{-2.8}$  atm. Molybdenum wires of 1.3 mm diameter were rotated at 12 rpm for 16 hours. The samples were sectioned at two depths, once just below the slag-gas interface, and a second time near the bottom of the crucible, about 6 mm from the slag surface. At the lower oxygen pressure, the results did not vary much from that found in static immersion, but a substantial difference was found between static and stirred tests at the higher oxygen pressure. Some difference was found between the top and bottom wire sections in both tests. The data are collected in Table IV.

a. Mo<sub>r</sub>-1. At an oxygen pressure of  $10^{-9.1}$  atm, the microstructure of the interface at the top section showed no reaction layer whatever (Appendix D-55). At the bottom section, a slight oxide layer was present, as shown in Figure 18. The surface recession was identical for both Mo<sub>r</sub>-1T and Mo<sub>r</sub>-1B, at 12 μm, which matched that from the static UE-3 test at the same oxygen potential.

The microprobe analysis shows the  $C_{Fe \rightarrow Mo}^{10 Mo/S}$  for the top section is slightly lower than the  $C_{Fe \rightarrow Mo}^{10 Mo/Ox}$  for the bottom section. These concentrations are not much different than for UE-3. The iron concentrations at the top section did decrease more rapidly deeper in the molybdenum. The molybdenum dioxide content of the slag is slightly higher at Mo<sub>r</sub>-1T than at Mo<sub>r</sub>-1B, and both are lower than found in the UE-3 static test.



TABLE IV. SUMMARY OF ROTATION TESTS IN UNION ELECTRIC SLAG

	Rotated Molybdenum Wire				Rotated Carbon Rod
Sample Identification	Mo <sub>r</sub> -1		Mo <sub>r</sub> -2		UE + C
Applied p <sub>O<sub>2</sub></sub> , Log (atm) <sup>2</sup>	-9.1		-2.8		Argon
Duration, (hr)	16		16		12
Section Identification	Mo <sub>r</sub> -1T (Top)	Mo <sub>r</sub> -1B (Bottom)	Mo <sub>r</sub> -2T (Top)	Mo <sub>r</sub> -2B (Bottom)	-
Corrosion Products	None	MoO <sub>2</sub> Particles	MoO <sub>2</sub> Layer	MoO <sub>2</sub> Layer	Iron-Molybdenum Alloy in Slag and Wire
Reaction Layer Thickness, (μm)	0	2	4	8-18	56
<sup>10</sup> C <sub>Mo → S</sub> O <sub>x</sub> /S	0.8%*	0.6%	3.3%	3.6%	0.07%*
<sup>10</sup> C <sub>Fe → Mo</sub> Mo/O <sub>x</sub>	1.12%**	1.21%	0.23%	0.42%	5.0%**
Recession of Surface, (μm)	-12	-12	-270	-25	+6
- = loss + = gain					

\* <sup>10</sup>C<sub>Mo → S</sub> Mo/S

\*\* <sup>10</sup>C<sub>Fe → Mo</sub> Mo/S

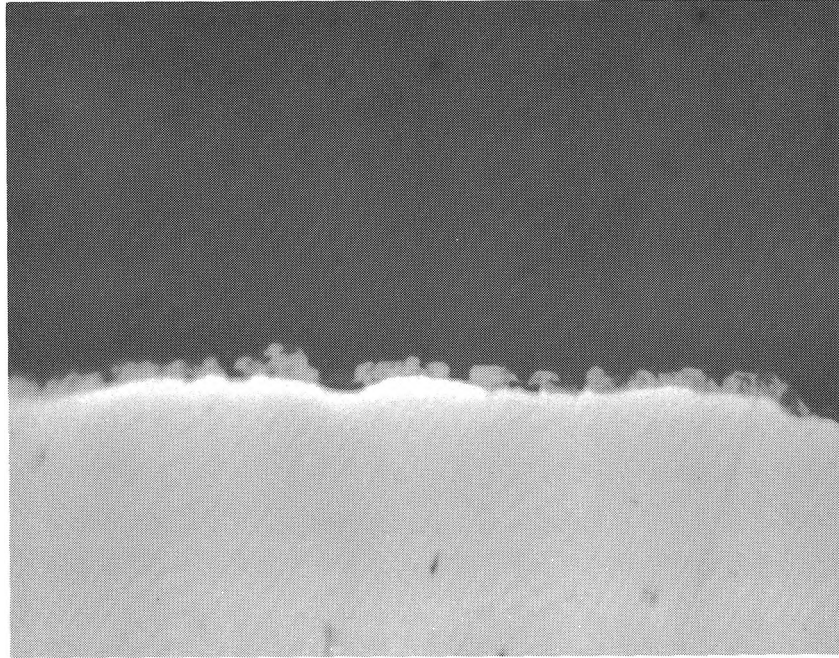


Figure 18. Slag-Metal Interface, Mo $\gamma$ -1B. (1300x), unetched.



Figure 19. Slag-Metal Interface, Mo $\gamma$ -2T. (1300x), unetched.

b. Mo<sub>r</sub>-2. At an applied oxygen pressure of  $10^{-2.8}$  atm, the effect of rotation was more pronounced. At Mo<sub>r</sub>-2T, the surface receded 270  $\mu\text{m}$ , and developed a 4  $\mu\text{m}$  thick oxide film, shown in Figure 19. The wire surface eroded uniformly, reducing the wire diameter by over 40%, as seen in Figure 20. No changes in molybdenum grain structure occurred. At the lower section, Mo<sub>r</sub>-2B, the erosion was much less severe, but the oxide film was two to four times thicker. The molybdenum surface receded 25  $\mu\text{m}$ . The remaining oxide layer had the duplex oxide structure shown in Figure 21.

A microprobe plot of Mo<sub>r</sub>-2T is shown in Figure 22. An examination of the values for both sections in Table IV shows that substantial differences exist. The  $C_{\text{Fe} \rightarrow \text{Mo}}^{10} \text{ Mo/Ox}$  was about twice as great at the bottom section than at the top, while the  $C_{\text{Mo} \rightarrow \text{S}}^{10} \text{ Ox/S}$  was nearly the same at both sections. However, it is interesting to note the molybdenum dioxide concentration was a little lower at the top, just opposite the case for Mo<sub>r</sub>-1.

At the applied oxygen pressure of  $10^{-2.8}$  atm, the alumina tube used to hold the molybdenum was severely eroded. The 0.5 mm thick tube wall was completely dissolved, from the slag-gas interface down, a loss of 500  $\mu\text{m}$  of alumina. No such erosion was noted at the lower oxygen potential tested.

3. Rotated Carbon Rod in Union Electric Slag. Carbon in contact with slag created oxygen potentials much lower than in controlled atmosphere tests. The slag was continuously mixed by the completely immersed, rotating carbon rod. Reaction of the slag with carbon produced carbon monoxide and any gas escaping from the slag was swept from the furnace by flowing argon. Metallic iron was reduced from the slag during the 12 hour test. When the carbon rod was withdrawn from the sample at the end of the experiment, small beads of iron-carbon alloy adhered to the rod. The carbon surface was somewhat pitted. No slag adhered to the carbon.

The slag contained beads of metal, up to 50  $\mu\text{m}$  in diameter. On selected beads, the composition ranged from 1.5% molybdenum and

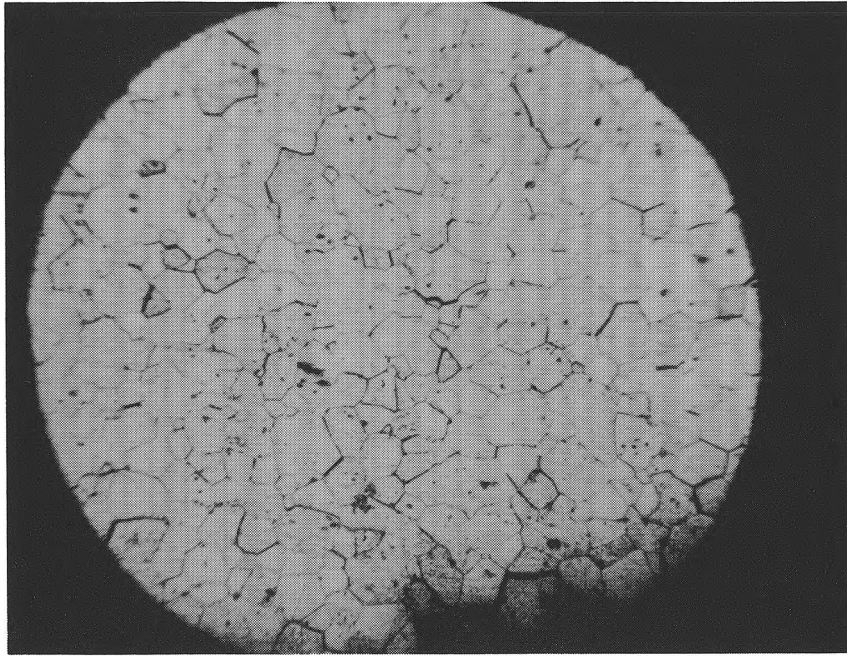


Figure 20. Molybdenum Surface, Mo<sub>r</sub>-2T. (120x), etched in Murakami's Reagent.



Figure 21. Slag-Metal Interface, Mo<sub>r</sub>-2B. (1300x), unetched.

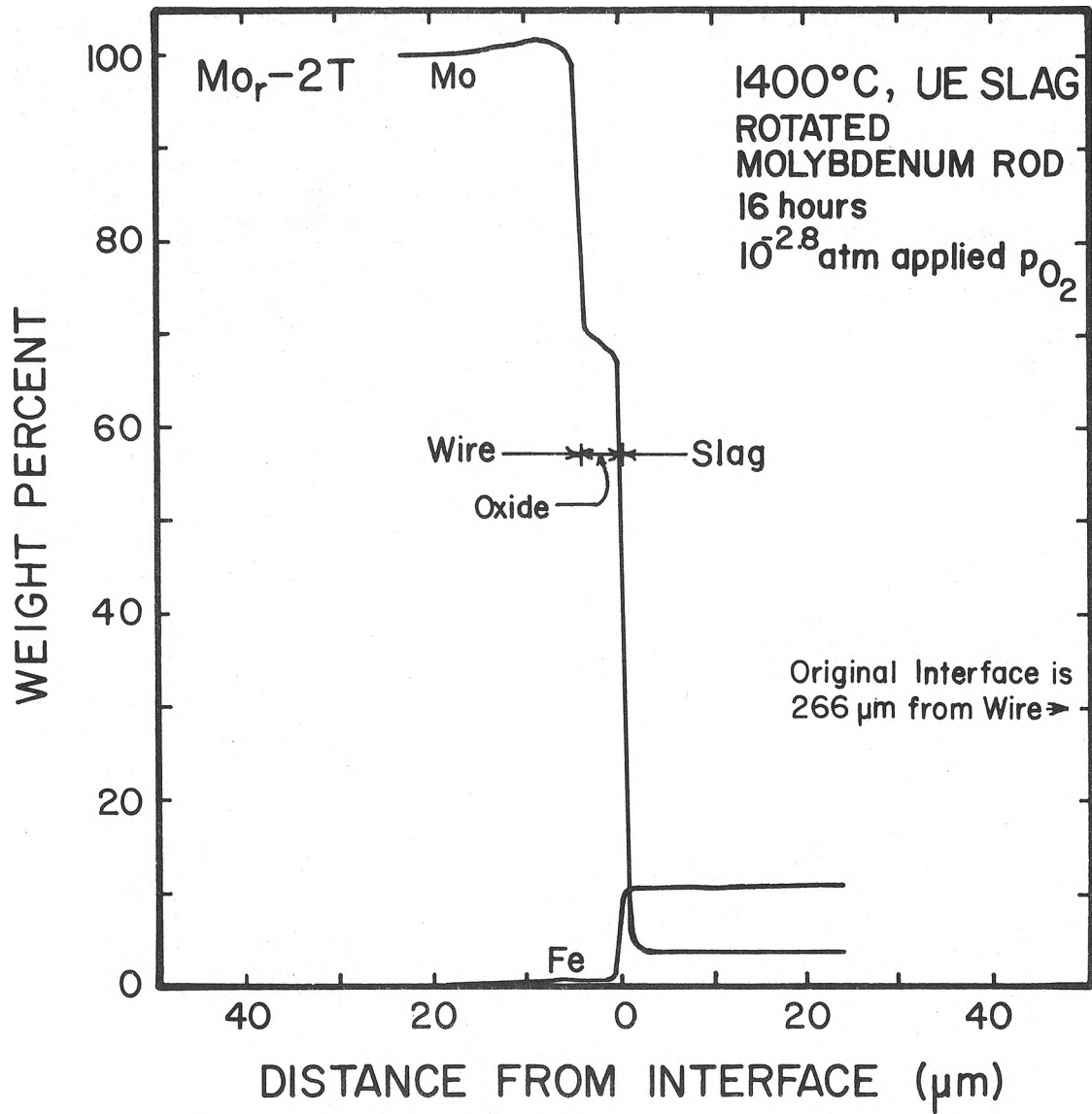


Figure 22. Microprobe Concentration Profile for Iron and Molybdenum in the Mo<sub>r</sub>-2 Test.

93.4% iron to an alloy of 3.3% molybdenum and 88.1% iron. The remaining 5.1 to 8.6% was not identified.

Measurement of the molybdenum wire showed surface swelling of 6  $\mu\text{m}$ . The molybdenum underwent a definite change in microstructure, as seen in Figure 23. Two distinct layers are revealed on the etched section. The light-colored outer band is about 30  $\mu\text{m}$  thick. The second zone appears to be the same type of enlarged grains found in some of the static and stirred immersion tests. At higher magnification, small dendrites are visible along the edge of the molybdenum, as shown in Figure 24.

Figure 25 shows the microprobe profile for the metal-slag interface. The  $C_{\text{Fe} \rightarrow \text{Mo}}^{5-25 \text{ Mo/S}}$  was very consistent at about 5.0% iron. This corresponds well to the outer band in Figure 23. Summation of microprobe measured fractions of iron and molybdenum appeared to account for all of the alloy material, though the data are considered too sketchy for high confidence levels. No analysis for other constituents was attempted. In the slag, the concentration of molybdenum dioxide was very low.

### C. ELECTRICAL CURRENT STUDIES

The passage of current is an extremely important characteristic affecting electrode stability. As mentioned earlier, the voltage drop across electrodes in the slag will create reducing and oxidizing conditions at the cathode and anode, respectively. Electrochemical reactions occurring in the molybdenum-slag system were studied under both the cathodic and anodic conditions.

The current tests were run at a constant voltage of 1.5 V. With a pin electrode surrounded by a second ring electrode, both submerged in slag, the inter-electrode distance was 7 mm and the initial ring/pin area ratio was 11:1. Three experiments were conducted; two at 1400°C, one using the center pin as the anode and the other using it as the cathode, and one at 1350°C, using the center pin as the cathode. The results are summarized in Table V. Data on current flow are included in Appendix C, Table X.

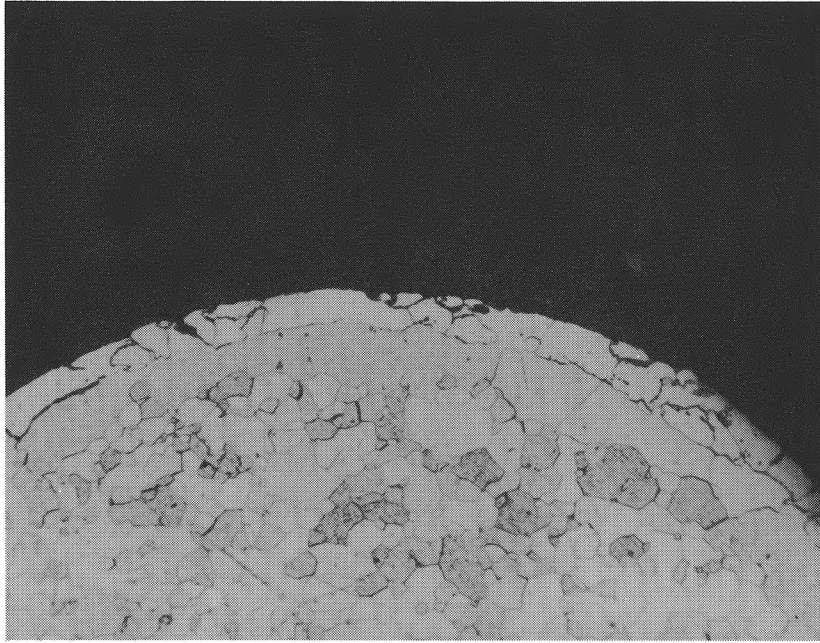


Figure 23. Molybdenum Surface, UE + C. (140x), etched in Murakami's Reagent.

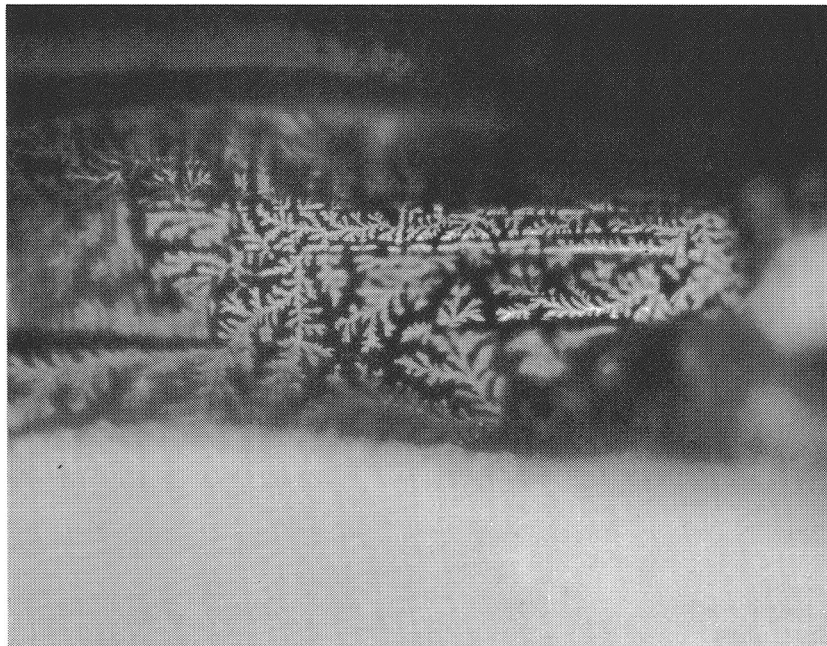


Figure 24. Dendrites Growing on Molybdenum in UE + C Test. (1100x), focused into slag.

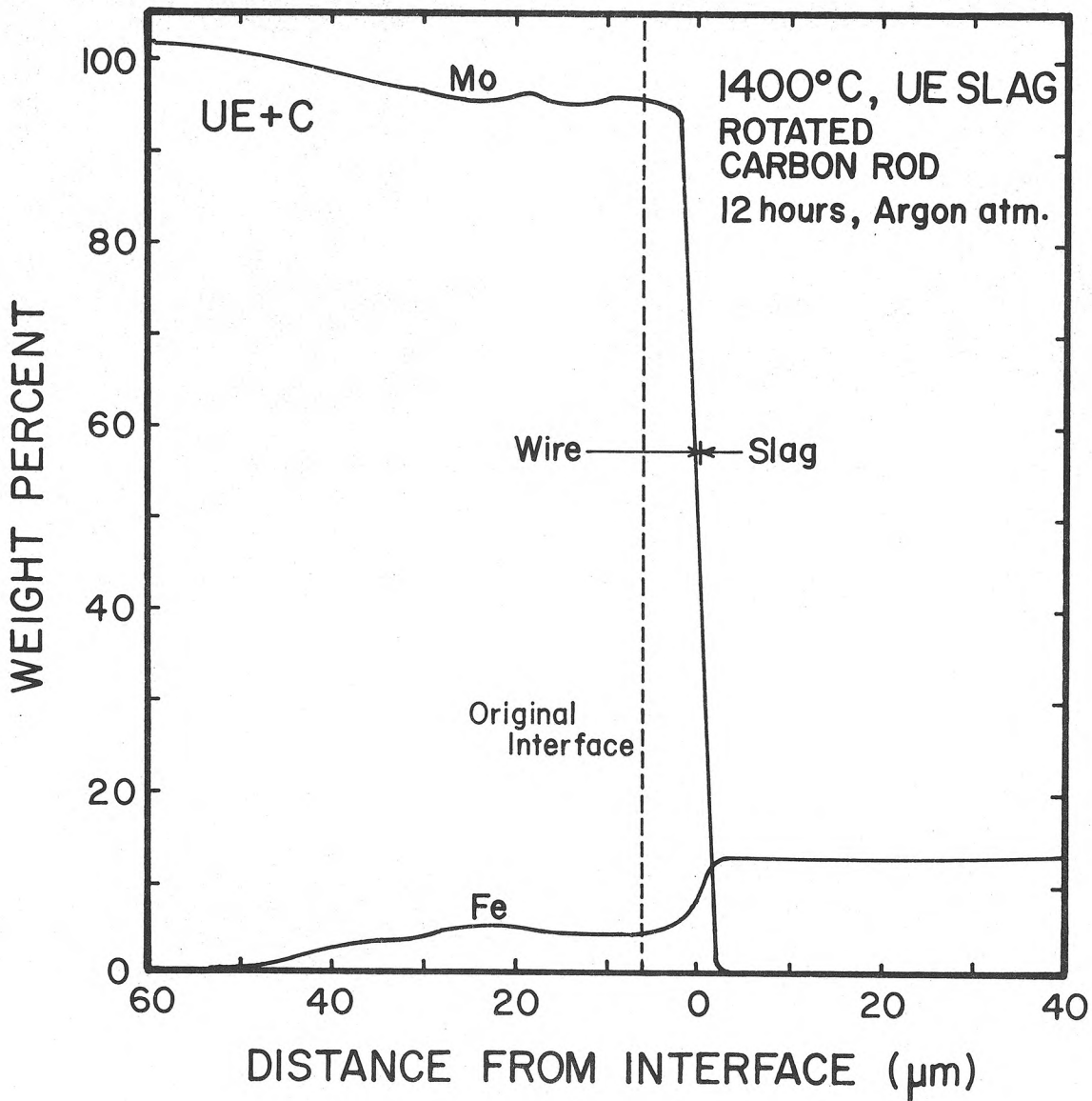


Figure 25. Microprobe Concentration Profile of Iron and Molybdenum in the UE+C Test.



TABLE V. SUMMARY OF ELECTRICAL CURRENT STUDIES USING UE BOTTOM SLAG, A 7 mm ELECTRODE SEPARATION, AN APPLIED VOLTAGE OF 1.5 VOLTS, AND AN APPLIED O<sub>2</sub> POTENTIAL OF 10<sup>-9.1</sup> ATM IN 3 HR DURATION TESTS.

Configuration	Anode Pin/ Cathode Ring	Cathode Pin/ Anode Ring	Cathode Pin/ Anode Ring
Temperature, °C	1400°	1400°	1350°
Current Flow	60 mA initially, dropped to 16-18 mA in 15 min; then constant for remainder of test	73 mA initially, dropped to 70 mA for 2 hrs. Current then increased and periodic excursions between 100-300 mA followed	48 mA initially, increased to 70 mA in 1 hr, then sporadic fluctuations between 180-340 mA
Approximate* Current Density at the noted current, A/cm <sup>2</sup>	16 mA Anode: 0.05 Cathode: 0.0045	60 mA Anode: 0.017 Cathode: 0.19	70 mA Anode: 0.020 Cathode: 0.22
Reaction Layer	Anode: Mo oxides with MoO <sub>2</sub> Spikes Cathode: Fe-Mo alloy	Anode: Mo oxides Cathode: Fe-Mo alloy	Anode and cathode similar to 1400° appearance
Reaction Layer Thickness, μm	Anode layer: 2 Anode spikes: 50 Cathode: 13	Anode: 3 Cathode: 255	
Molybdenum in Slag, Wt%	By anode: 4.8% By cathode: 0.3%	By anode: 3.3% By cathode: 0.3%	
Iron in Molybdenum, Wt%	Anode: 0.10% Cathode: 33%	Anode: 0.7% Cathode: 50-70%	
Recession (-) or Swelling (+) of Surface, μm	Anode: -140 Cathode: +9	Anode: -98 Cathode: 0	

\*Electrode surface area assumed unchanged.

1. Anode Pin/Cathode Ring: 1400°C. When the center pin was an anode, the pin reaction was oxidation. The surface recession of the molybdenum pin was 140  $\mu\text{m}$ . The surface was covered with a 2  $\mu\text{m}$  oxide layer similar to that in other tests, but containing additional oxide crystals projecting from the surface. Figure 26 shows the sectioned and etched pin. The surface eroded somewhat irregularly and no changes in the molybdenum grains are visible. Figure 27 shows the interface at higher magnification, where the oxide projections are clearly visible. The nearby slag contained numerous small oxide particles, present as distinct crystals.

The microprobe concentration profile is shown in Figure 28, with the anode on the left. As expected for oxidizing conditions, iron concentration in the pin is low,  $C_{\text{Fe} \rightarrow \text{Mo}}^{10 \text{ Mo/Ox}} = 0.10\%$ . Several oxide projections in the slag were crossed by the microprobe during analysis and these areas appear as sharp peaks in the molybdenum concentration curve. The thin, continuous oxide film was not detected by the microprobe.

The slag between anode and cathode contained much particulate, both oxide and metal. These were distributed unevenly, in streaks and swirls radiating from the pin to the ring (Appendix D-56 shows one typical area). The  $C_{\text{Mo} \rightarrow \text{S}}^{60 \text{ Ox/S}} = 4.8\%$ , well above the molybdenum dioxide concentration in any other test.

At the cathode ring surface, iron alloying reactions occurred. A section of the cathode is shown in Figure 29 (Appendix D-57). The etched surface layer is an iron-molybdenum alloy containing 33% iron. The areas in the underlying molybdenum that appear to contain pores are thought to be molybdenum solid solution regions rich in iron. The concentration of iron was measured at 7.5% in this region. The  $C_{\text{Mo} \rightarrow \text{S}}^{10 \text{ A/S}} = 0.3\%$  is lower than in the UE-3 and Mo<sub>r</sub>-1 tests at the same oxygen potential.

The use of constant voltage produced current densities much less than the 1 amp/cm<sup>2</sup> criteria suggested for MHD applications.<sup>1</sup> In the anode pin/cathode ring test, steady current flow was established at 16 mA after 15 min of testing, but the initial current

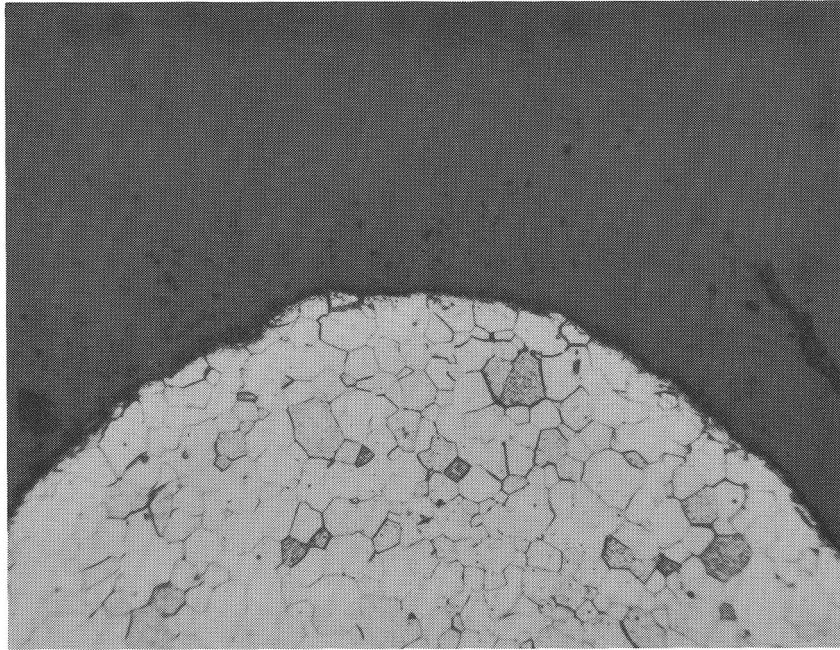


Figure 26. Molybdenum Surface, Anode Pin, 1400°C, Electrical Current Test. (140x), etched in Murakami's Reagent.

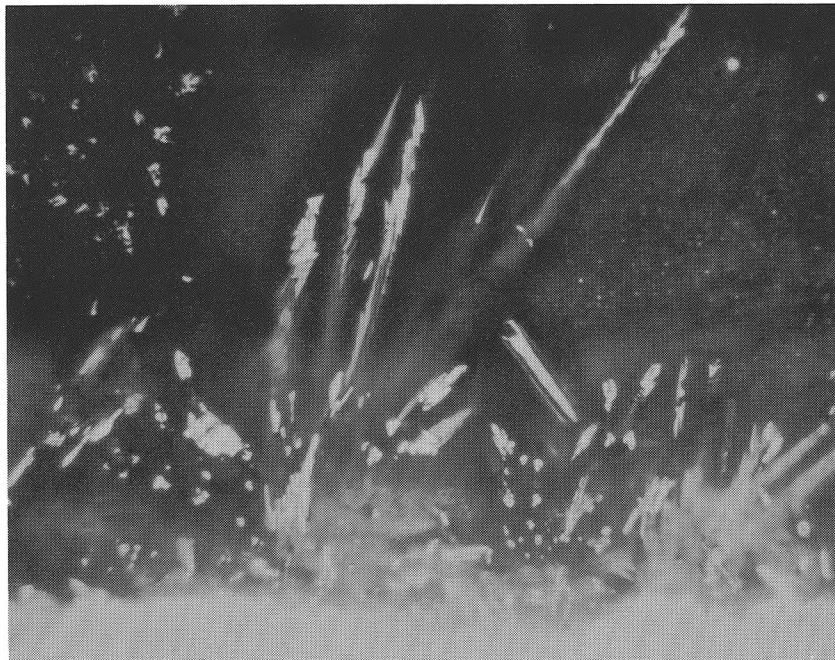


Figure 27. Molybdenum Dioxide on the Anode Pin Surface. (1300x), focused into the slag.

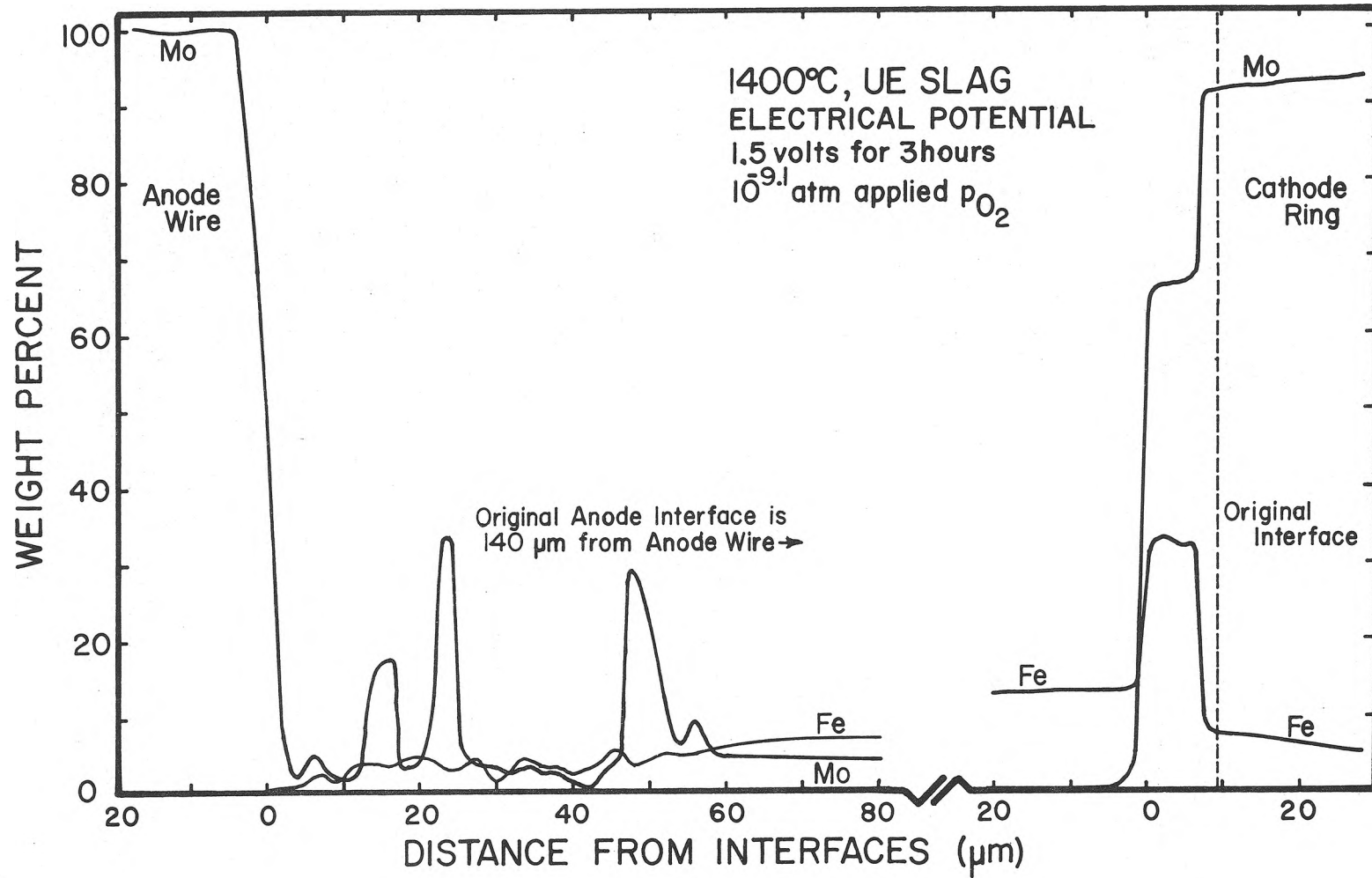


Figure 28. Microprobe Concentration Profile of Iron and Molybdenum in the Anode Pin/Cathode Ring Electrical Current Test.

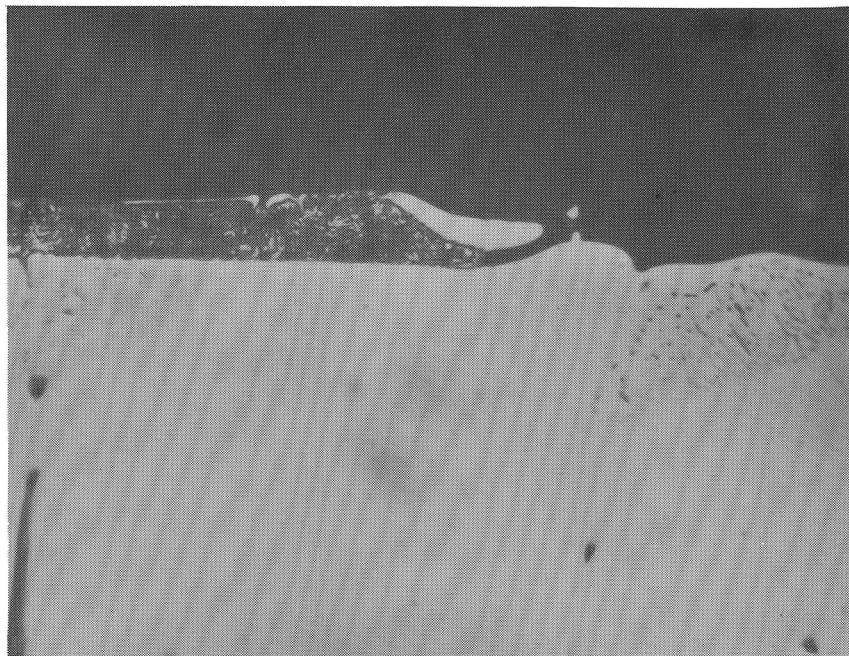


Figure 29. Slag-Metal Interface, Cathode Ring, 1400°C, Electrical Current Test. (700x), nital etch.

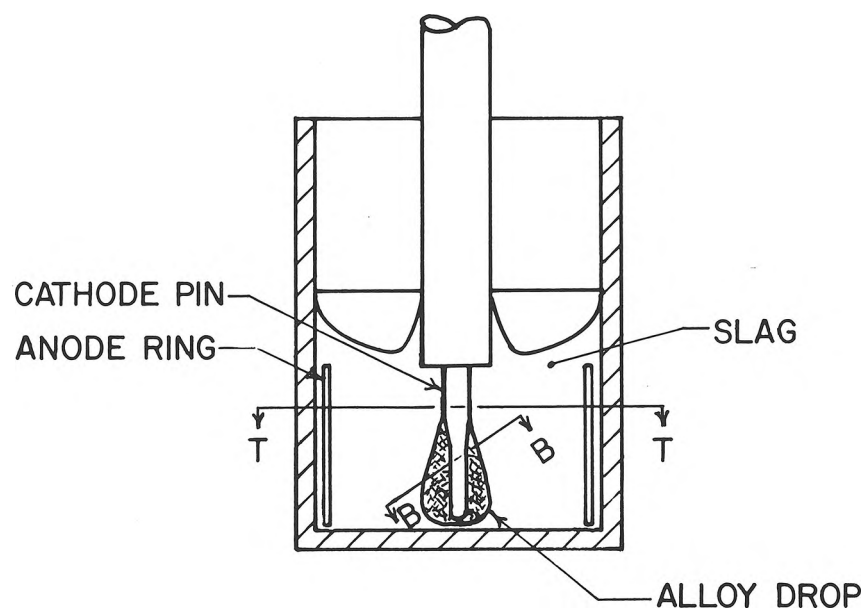


Figure 30. Vertical Section of Cathode Pin/Anode Ring, 1400°C, Showing the Shape of Alloy Drop and Location of Sections Cut for Metallographic and Microprobe Analysis. (3x).

flow was much greater, around 60 mA. The approximate current densities (calculated from the original surface area and the plateau current flow) are given in Table V.

2. Cathode Pin/Anode Ring: 1400°C. This test was conducted to compare the effects of high current density versus low current density on electrode reactions by exchanging the electrode polarities of the previous test. The anode reactions (oxidizing conditions) were now carried out at lower current density, while the cathode reactions (reducing conditions) were carried out at higher density. As before, the potential was kept constant at 1.5V.

Massive amounts of iron reduced from the slag at the cathode pin. The iron alloyed heavily with the molybdenum and the alloy took the shape of a teardrop around the bottom of the pin. The drop has a maximum cross section of 3.5 mm. A sketch of this drop is shown in Figure 30. Included in the figure are section lines indicating where samples were taken.

Figures 31 and 32 show the structure at the two sections. Figure 31 is the upper cut across the pin, taken 3 mm below the bottom of the insulating alumina tubing, and Figure 32 is the bottom section through the drop. At the top section, the outer dimension across the alloyed pin equals the original wire diameter. The drop microstructure obviously differs in the shape of various phase structures from that at the upper section, although the same molybdenum-iron alloy phases are apparently present in both sections (Appendix D-58).

The microprobe profile for the upper section of the pin is shown toward the left of Figure 33. The slag near the cathode pin has a concentration of molybdenum dioxide equal that near the cathode ring in the previous test. Figure 34 shows a more detailed photomicrograph of the upper cathode pin section and Figure 35 shows a section of the cathode drop.

Figure 34 is oriented with the slag/metal interface toward the top. The acicular structure in the top half is similar to that extending beyond the field of view to the interface. The

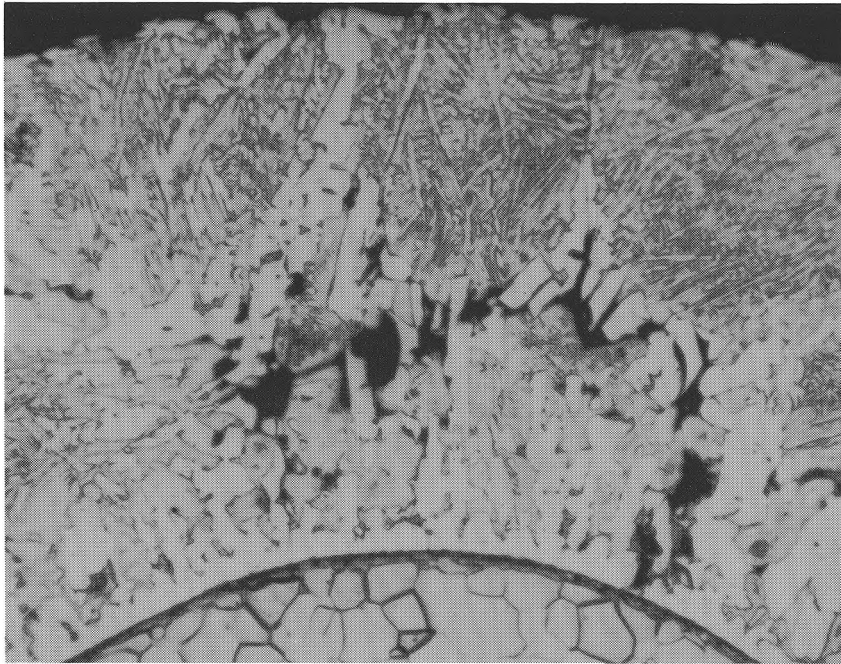


Figure 31. Molybdenum Surface, Cathode Pin, 1400°C, Electrical Current Test, (Top Section). (290x), nital and Murakami's Reagent etch.

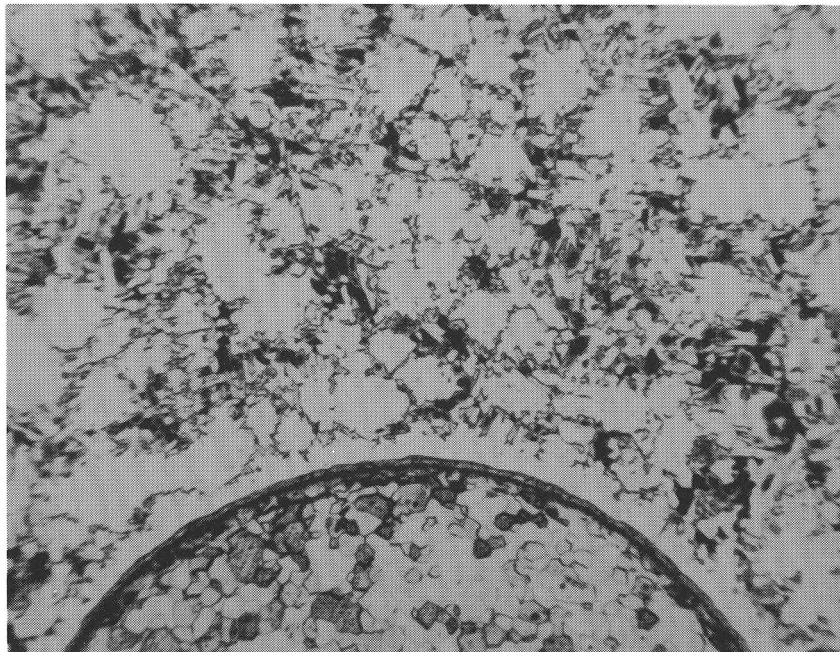


Figure 32. Molybdenum Surface, Cathode Pin, 1400°C, Electrical Current Test, (Bottom Section). (70x), nital and Murakami's Reagent etch.

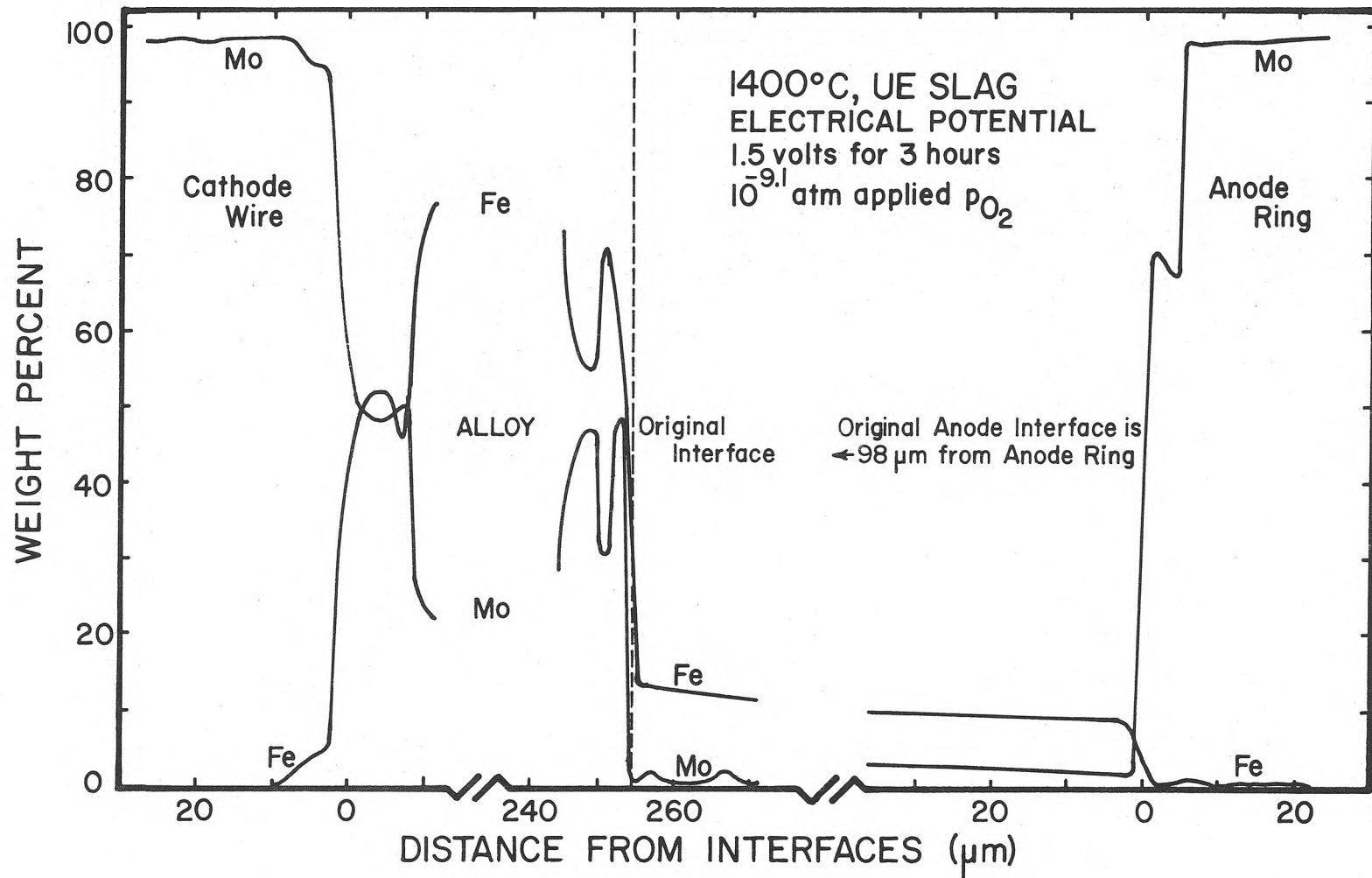


Figure 33. Microprobe Concentration Profile of Iron and Molybdenum in the Cathode Pin/Anode Ring Electrical Current Test, 1400°C.





Figure 34. Alloy on Cathode Pin, Upper Section, 1400°C.  
(1300x), nital etch.

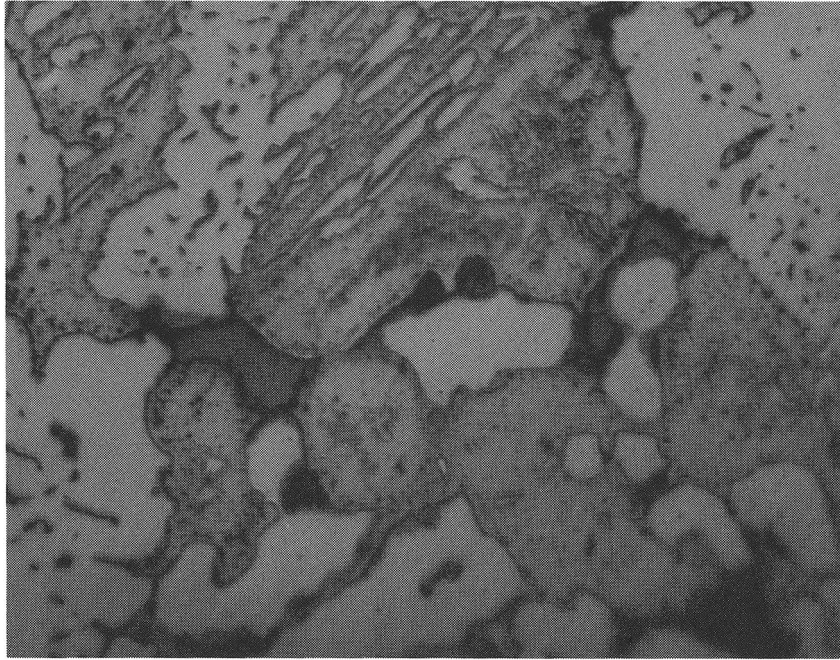


Figure 35. Alloy Structure on Cathode Pin, Bottom Section, Within Drop. (1300x), nital etch.

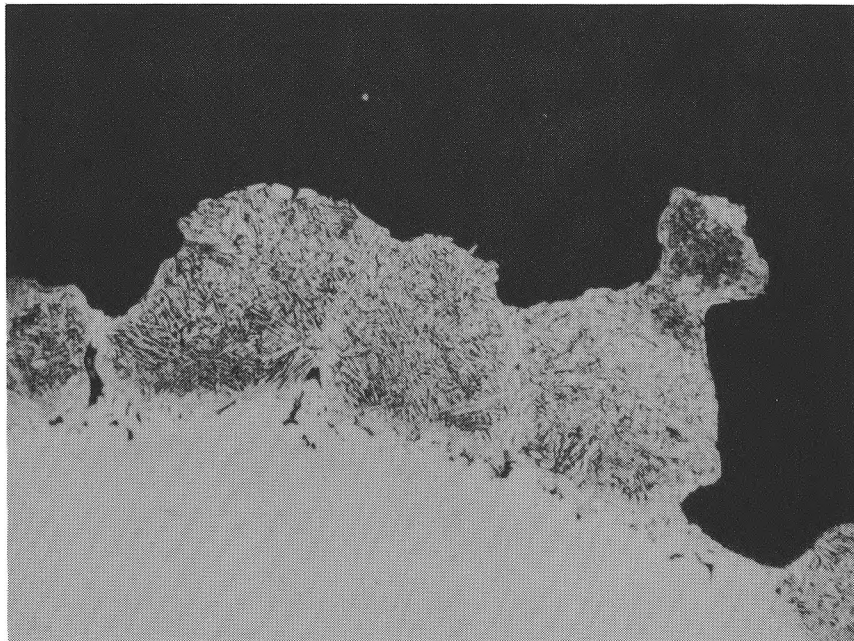


Figure 36. Molybdenum Surface, Cathode Pin, 1350°C. (280x), nital etch.

microprobe measured 49% molybdenum and 51% iron in the lighter acicular structure and 29% molybdenum with the remainder iron in the darker matrix. In the lower half of the figure, nearer the molybdenum, the acicular structure gives way to a clumpy configuration. The light phase still contains 49% molybdenum, but the darker matrix has a variable composition, being 29% molybdenum near the light phase, but dropping to 24% in the center of the larger iron-rich areas. These correspond to the speckled regions visible in the lower half of Figure 34.

Near the molybdenum, just visible at the bottom of Figure 34, the 49% molybdenum phase formed a thin, continuous layer over the surface, also visible in Figures 31 and 32. The concentration of iron fell sharply over 6  $\mu\text{m}$  in the molybdenum itself, as seen in Figure 33, much more sharply than found for the cathode ring.

At the anode ring, surface recession was 98  $\mu\text{m}$ , about two-thirds that found at the anode pin. From Table V, the  $C_{\text{Mo} \rightarrow \text{S}}^{10 \text{ Ox/S}}$  is also about two-thirds that near the anode pin. Large numbers of small particles are found in the slag, just as before. The iron concentration,  $C_{\text{Fe} \rightarrow \text{Mo}}^{10 \text{ Mo/Ox}} = 0.7\%$ , found in the ring is seven times that at the anode pin.

The current flow also differs between the two tests. The center electrode carries about four times the current when it is the cathode. Current densities are thus higher at both electrodes. The initial current flow is very nearly the same in both tests. In the cathode pin/anode ring test, a steady current of 60 mA was reached after about five minutes of current flow. The value remained constant for nearly two hours, then began to climb and finally oscillated randomly between 100 and 300 mA. A repeat test gave similar behavior, but this time the outer band was moved around whenever the current began to jump. This returned the current to the 60 mA level. The agitation disturbed the sample, so no other data was collected.

The hanging drop on the cathode pin gave every indication of having been molten. As shown in the iron-molybdenum phase diagram,

Figure 3, the lowest solidus temperature is 40°C above the 1400°C test temperature. Non-dispersive x-ray analysis was used to scan the drop for elements other than iron and molybdenum that might lower the solidus temperature. No other elements were found.

3. Cathode Pin/Anode Ring: 1350°C. One hypothesis for the drop formation suggested the temperature at the cathode might increase to 1440°C as a result of combined factors: the heat of reaction between molybdenum and iron as they alloy, the rapid rate of reaction, the heating effects of current flow, and the insulating nature of the slag. To test this, the previous experiment was repeated at 1350°C. The 50°C temperature decrease was thought to be enough to eliminate any melting due to localized heating. The same carbon dioxide-carbon monoxide gas mixture was used, resulting in an oxygen potential of  $10^{-9.6}$  atm.

Less alloy formed on the wire, and the formation of the drop was not repeated. Figure 36 shows one section of the sample. Some structural differences are found when compared to Figures 31 and 32 from the higher temperature test. The light phase appears more squared off and the large, glomerate areas are lacking. A higher magnification view of the molybdenum-alloy interface is shown in Figure 37. A broken binding on the sample holder caused the crucible to be jostled as it was removed from the furnace. Some alloy was torn from the surface, showing the material had poor mechanical strength at 1350°C. The alloy formed dendrites in the slag (Appendix D-59 to 61).

The surface of the alloy was examined microscopically with oil immersion optics, looking through the slag onto the surface. The structure consists of small nodules, one upon another, blending into the alloy base, as shown in Figure 38. The surfaces appear perfectly smooth. The alloy was removed from the slag using a caustic leach and reexamined by scanning electron microscope. The same structure was noted (Appendix D-62). The mechanism causing this morphology is unknown.

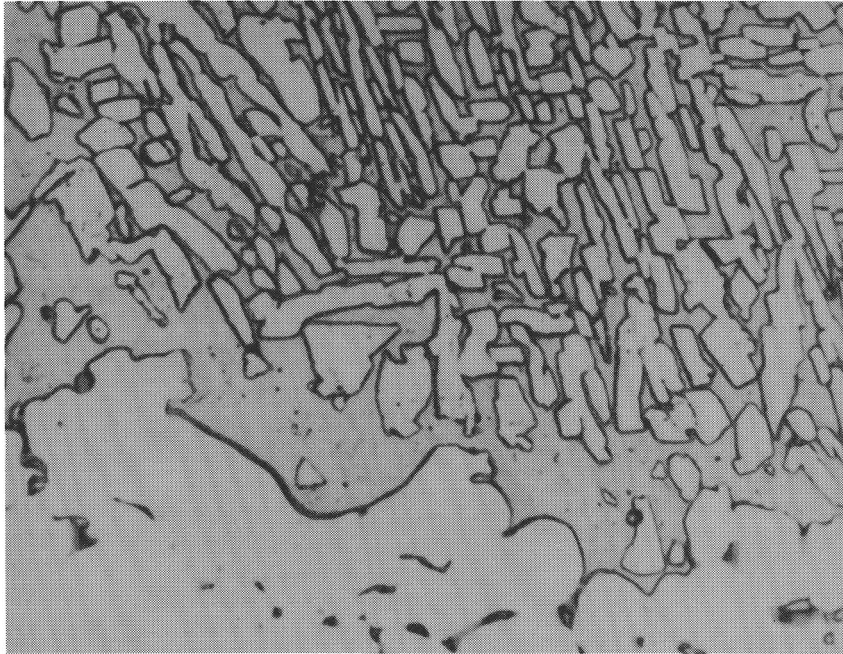


Figure 37. Molybdenum-Iron Alloy on the 1350°C Cathode Pin. (1300x), nital etch.

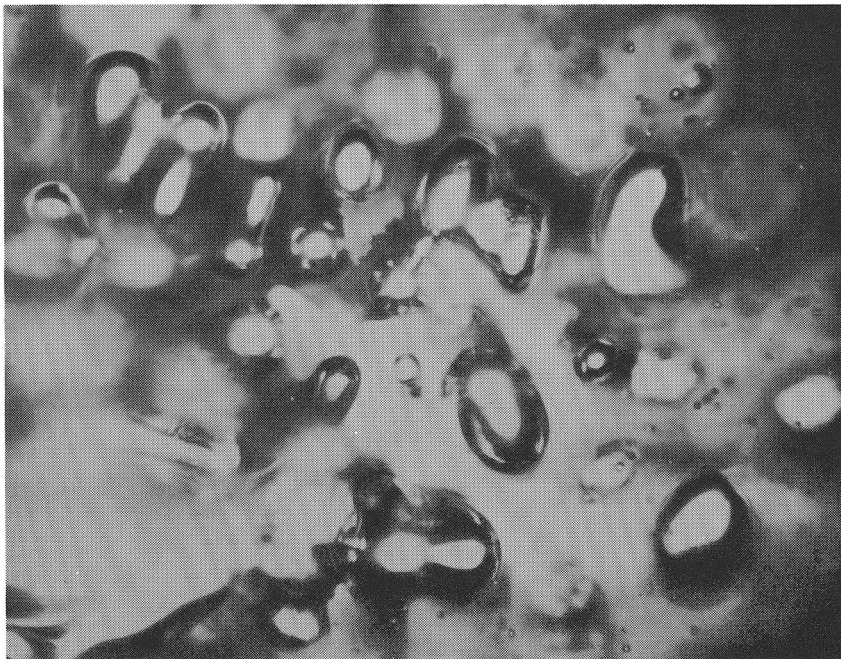


Figure 38. Surface of the 1350°C Cathode Pin Alloy, Seen by Looking Through the Slag. (600x).

4. Direct Molybdenum-Iron Reactions. The phase structure of the molybdenum-iron cathode alloys was further studied in two additional tests, in which iron powder was reacted with molybdenum wire. Conceivably, localized increases in temperature to 1440°C could be present even at the 1350°C test condition, given the relatively well insulating slag. The structure of the alloy was examined under two conditions using sample arrangements with high and low heat dissipation. Iron powder was packed around molybdenum wire for both the tests and the resulting samples were compared. Another test used powdered iron mixed directly with slag to insure iron alloying, while further reducing thermal losses.

a. Molybdenum in Iron Powder. The first test enhanced heat transfer by using a large pressed pellet of iron to contain a length of molybdenum wire. The pellet was held at 1400°C in flowing hydrogen to maximize heat dissipation. The second test minimized heat loss by surrounding the molybdenum with a minimum amount of iron. A 2 mm layer of iron powder was packed around the wire inside of an alumina tube. The alumina tube and a slow argon gas flow further minimized heat losses.

No differences in microstructure were found between the two tests. A section of the high heat dissipation sample is shown in Figures 39 and 40. Iron and molybdenum apparently cross-diffused and the molybdenum diffused into the iron in solid solution, except for a small amount that precipitated as an iron-molybdenum intermetallic on iron grain boundaries. The diffused molybdenum made the iron near the wire more resistant to the etchants than was the pure iron distant from the interface. The original surface of the molybdenum wire was located at the darker band of precipitated molybdenum-iron intermetallic, as noted in Figure 39 (Appendix D-64).

In the smaller sample, the molybdenum wire reacted more with the iron, resulting in a smaller final diameter. The molybdenum surface receded 127  $\mu\text{m}$  in the large sample and 178  $\mu\text{m}$  in the small.

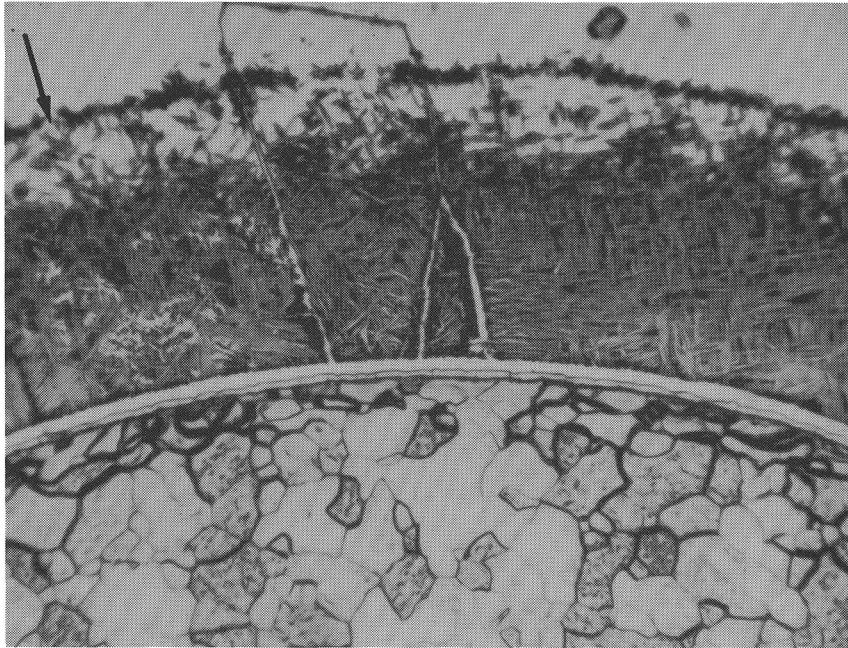


Figure 39. Molybdenum Wire in Iron Pack, Sintered 12 hours, High Heat Transfer Arrangement. (300x), nital and Murakami's Reagent etch. (Arrow Notes Original Molybdenum-Iron Interface.)

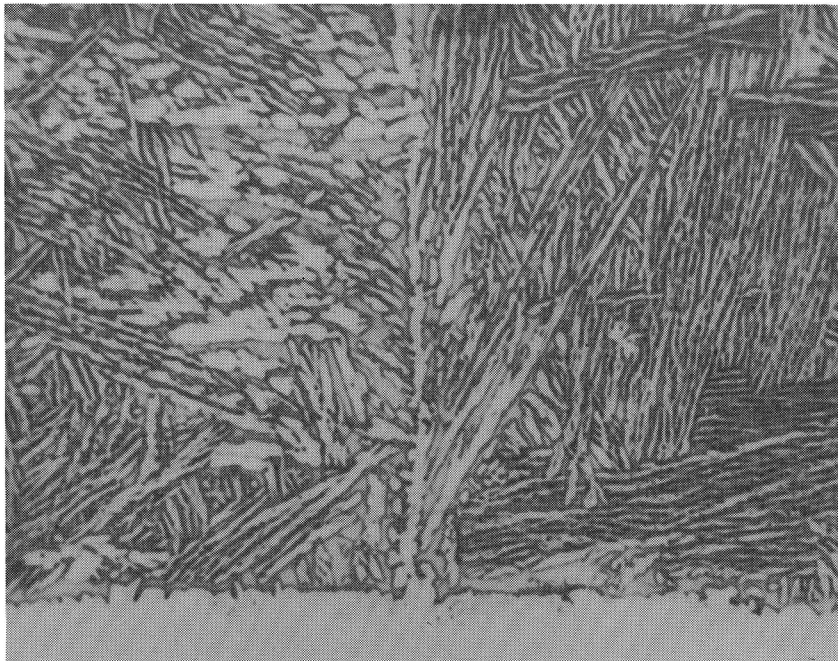


Figure 40. Molybdenum-Iron Alloy, Iron Pack Experiment, High Heat Transfer Arrangement. (1300x), nital etch.

The only uncontrolled variation was tighter compaction of the large sample.

In both cases, the dominant reaction product was the wide two-phase region containing accicular molybdenum-iron intermetallic. Two additional reaction layers formed next to the molybdenum surface, one over the other, as seen in Figure 39. Only one layer was evident in the cathode pin tests (Figure 31). As a whole, the microstructures are quite similar to those in the electrical current tests, despite the difference in diffusion time available (12 versus 3 hours) and the different cooling rates encountered when pulling the two different type tests from the furnace.

b. Molybdenum in Iron-Doped Slag. A third test used UMR-1 slag mixed with iron powder as the source of iron. The test ran 6 hours using nitrogen as an atmosphere. A section of this sample revealed the structure shown in Figures 41 and 42. A surface recession of 76  $\mu\text{m}$  was measured to the molybdenum surface. The iron reacted with the molybdenum much like it did in the iron contact experiments. Figure 42 shows areas of the molybdenum-iron intermetallic that are not so accicular as found in the contact experiments. Possibly, the slower cooling in the slag allowed more restructuring of the phases as they cooled and, indeed, Figure 42 appears more like Figures 34 and 37 from the cathode pin experiments than does Figure 40 from the iron contact tests.

The shape of the iron coating on the wire suggests that iron particles coalesce easily in the slag, though iron does not melt until 1539°C. Some similarity to the structure of Figure 38, the 1350°C cathode pin alloy, is noted.



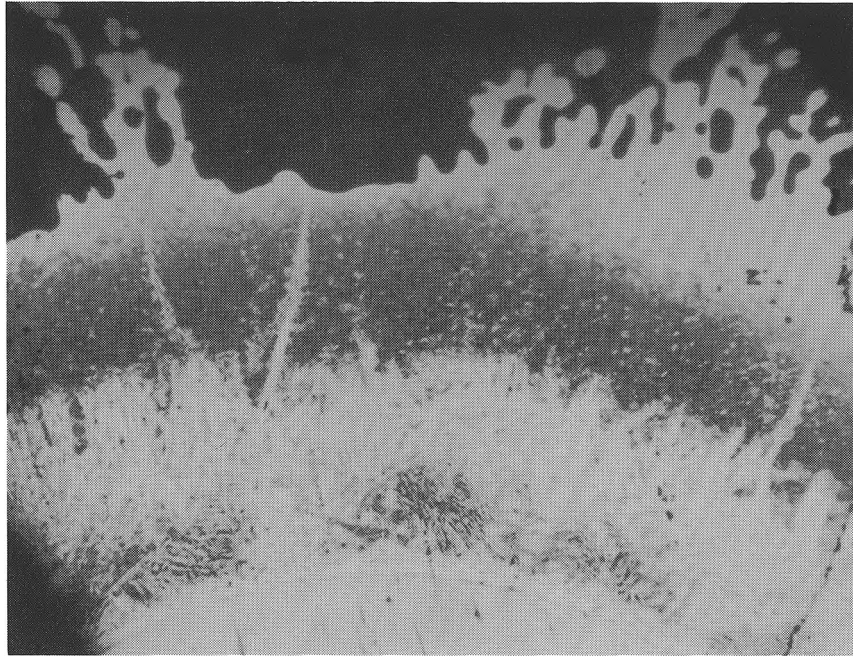


Figure 41. Slag-Metal Interface, UMR-1 Slag with Added Iron Powder. (300x), nital etch.

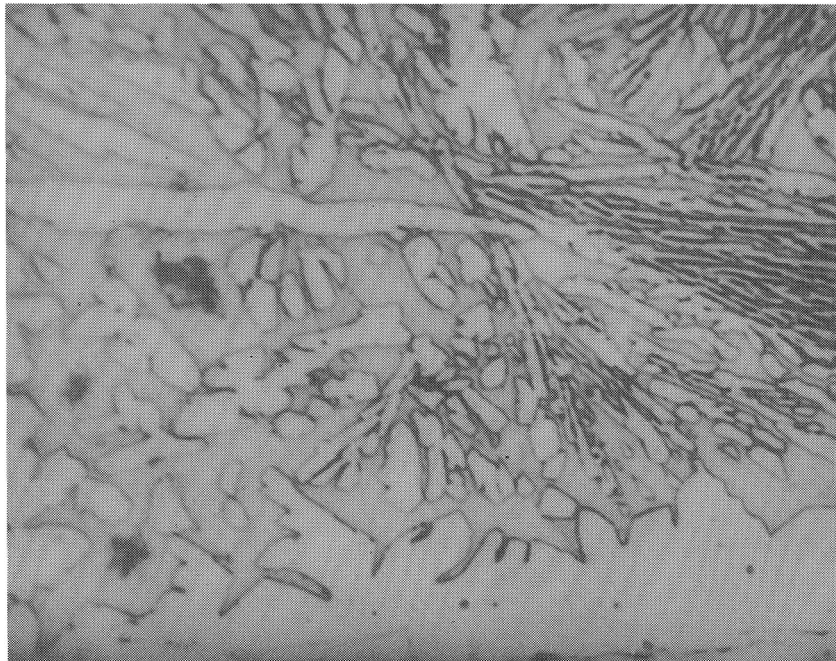


Figure 42. Molybdenum-Alloy Interface, UMR-1 Slag with Added Iron Powder. (1300x), nital etch.

## V. DISCUSSION OF RESULTS

Test results are explained in terms of thermodynamic and kinetic criteria. Detailed activity-composition relationships are not available for this system, so the reactions are interpreted using the equilibria equations qualitatively.

Many reactions occurred simultaneously, making interpretation difficult. Iron, molybdenum, and oxygen species interacted and equilibrium was never reached. In many cases, the measured concentration profiles of iron and molybdenum were very steep and values measured at standardized distances from the reaction interfaces were quite different from values 2  $\mu\text{m}$  separated. For that reason the data from the microprobe traces are included as reference in Appendix C.

Discussions concentrate on reactions at the molybdenum-slag interface. The results are explained in terms of oxidation/reduction reactions and some possible rate-controlled steps are suggested. Some information from addition experiments is presented as needed to better explain specific aspects of the results.

### A. STATIC IMMERSION TESTS

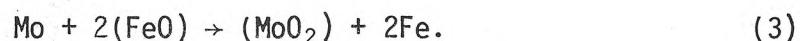
The static tests identified reactions in the molybdenum-slag system. The results are used as a point of reference for interpreting other experiments.

1. Static Immersion In Union Electric Slag. The corrosion of molybdenum is shown to be a function of oxygen potential. The corrosion involves oxidation of the molybdenum surface and adsorption of the oxide into the slag. Iron is reduced from the slag and alloys with molybdenum to an extent dependent again upon the oxidation potential. The concentration of molybdenum dioxide dissolved in the slag did not exceed 4.7% (3.5% molybdenum) in the static tests.

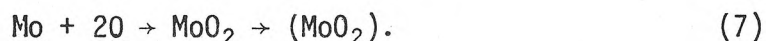
a. Molybdenum Oxidation and Corrosion. Referring to Table II, the amount of surface recession increased with increasing

oxygen potential. Molybdenum dioxide was present as a separate phase at the interface, the prevalence of this reaction layer increasing with increased oxygen pressure. In contact with slag, molybdenum oxidized even at applied oxygen potentials for which molybdenum in contact with gas is stable.

The oxidation of molybdenum in slag depended upon the activity of iron oxides in the slag, in turn controlled by the oxygen potential of the covering gas. At the lower oxygen potentials tested, isolated pockets of molybdenum dioxide were found on the interface and molybdenum remained in contact with slag. The undissolved dioxide was due either to molybdenum dioxide saturation of the slag, or to slow oxide dissolution kinetics. This was investigated and is discussed later. Molybdenum-slag contact occurred in the oxygen potential range  $10^{-11.6}$  to  $10^{-9.1}$  atm, with the equilibrium between molybdenum and slag expressed primarily by the reaction:



At higher applied oxygen potentials the molybdenum is completely covered with molybdenum dioxide when the molybdenum oxidation rate outpaces dissolution of the dioxide into the slag. Equation (3) may no longer be valid once the molybdenum is isolated from the slag. Instead the reaction may become:



Dissolution of the dioxide into the slag occurs until saturation is reached. In this situation, the transfer of species through the dioxide layer must be considered as additional reaction steps. The mechanism may be complex, involving variations in the molybdenum oxidation state, or indirectly involving iron oxides present in the oxide layer.

The morphology of the molybdenum dioxide layers is evident from the photomicrographs. To some degree, comparison between short preliminary tests and longer immersion tests indicate the dioxide forms early in the test and remains more constant in

thickness thereafter. The duplex structure found in UE-4 and Mo<sub>γ</sub>-2 tests cannot be explained. The structure may be significant to the oxidation mechanism, or it may simply be a preferred dioxide grain orientation.

A maximum concentration of 3.5% molybdenum dissolved into the slag in the UE-4 test, while only 0.55% dissolved in the UE-1 test, showing the strong decrease in dioxide concentration under lower oxygen potential conditions. The concentrations may be determined by equilibria, by Equation (3) at low oxygen potential, or by kinetic or solubility criteria, as suggested in Equation (7).

On occasion, small gas bubbles were found attached to the molybdenum surfaces at the conclusion of the test. Aggravated surface erosion occurred beneath the bubbles, appearing as concave depressions or as pitting (Appendix D-65,67). The effect was studied briefly. The molybdenum wire was replaced by platinum in one test and the bubbles again appeared, ruling out reaction related origins. The bubbles are thought to be gases trapped in the slag during melting of the powder. Once on the molybdenum surface, the bubbles cause pitting, perhaps explained in terms of surface areas. A small molybdenum area was exposed to a much larger slag area along the inner surface of the bubble. The oxidation could proceed by rapid absorption of vaporous molybdenum trioxides into the slag.

During the 9 hour test at  $10^{-8.6}$  atm oxygen potential, the platinum had a weight gain of 2.2%, thought to be absorbed iron. This may prove an effective tool to determine the iron activity of the slag without disrupting the molybdenum-slag equilibrium.

b. Molybdenum-Iron Alloying. In conjunction with the oxidation of molybdenum, iron reduced from the slag and alloyed with molybdenum, as is evident in Table II. The concentration of iron was very dependent upon the applied oxygen potential.

At the lower potentials, more iron alloyed with molybdenum, consistent with the equilibrium of Equation (3). Since the reactions remained dynamic, as the alloying proceeded the molybdenum

activity was lowered by dilution with iron. Iron diffusing into the molybdenum tended to compensate for metal volume lost from molybdenum oxidation.

As oxygen potential increased, the iron alloying was reduced in response to Equations (3), (4), and (7). In addition, the iron concentration was lowered by increased erosion of the molybdenum surface. The rate of dissolution offsets the rate of iron diffusion into the molybdenum.

Several samples showed a band of enlarged grains at the wire surface. The grains were evident only in samples with little surface erosion, but not all samples showed similar enlargement and no definite trends were noted. Recrystallization of cold worked grains originally present in the surface layer is one possibility,<sup>23</sup> but other unknown factors may be involved.

2. Static Immersion In Seeded Union Electric Slag. The addition of potassium sulfate seed caused a substantial shift in results from the UE static immersion tests, as Table II shows. Molybdenum erosion increased from 1.6 to 17 times that in unseeded testing, assuming a linear erosion rate, with the biggest increase in the lower oxygen potential tests. The amount of iron alloying also changed dramatically, increasing to about 5 times the unseeded value at  $10^{-10.9}$  atm oxygen pressure and decreasing to 0.08 times the unseeded value at  $10^{-2.8}$  atm. The slag solubility for molybdenum dioxide had much the same values as in plain UE slag tests. The fused-in-air seeded slag was far more corrosive than the mixed seed and slag, as expected from Equation (2), since the slag contained greater amounts of ferric oxide.

When the seed-slag mixtures were first heated, much sulfurous material evolved from the melt, apparently as the result of reaction between the slag oxides and potassium sulfate. In a separate test, pure potassium sulfate remained stable when heated in the same gases. Because of the sulfur oxides lost, the slag composition and iron oxidation state were changed. In other observations, the appearance of the slag after testing suggested the viscosity

decreased with seeding. The work of Capps suggests the slag viscosity increases with potassium content, but decreases with the addition of sulfur.<sup>15</sup>

An iron-rich metallic precipitate formed in the seeded slag at  $10^{-10.9}$  atm oxygen potential, while none formed in the plain slag even at  $10^{-11.6}$  atm. It is possible the activity coefficient of iron in the slag changed significantly due to the presence of potassium or sulfur. Based on the results of the rotated carbon rod test, where iron also precipitated in the slag and similar concentrations of iron were present in the molybdenum, the microstructures were expected to be similar. They were not. The differences are discussed with the carbon rod test.

3. Static Immersion in UMR Synthetic Slags. The brief tests studied erosion in higher iron content slag. Large surface recessions occurred, compared to the UE slag tests. The UMR-1 slag caused 9 times as much erosion and the higher iron UMR-2 slag caused 57 times as much at an applied oxygen potential of  $10^{-6.8}$  atm. The increased erosion is directly related to the increased iron content.

There are several related factors involved. First, preparation of the UMR slag in contact with air caused higher internal oxygen potentials, just as happened with the seeded slag prepared in air. The higher iron content also allows greater oxygen mobility, according to a concept of oxygen transfer through the slag by exchange between iron ions. The rapid oxygen transport minimized oxygen depletion of the slag near the molybdenum. Also, the higher iron/silica ratio results in a higher ferric/ferrous ratio, contributing to the increased erosion.<sup>17</sup>

The slag behavior changed with increased iron content. The slag crept badly for the UMR-2 slag, the effect decreased with UMR-1, and was almost non-existent with UE slag. The synthetic slags also attacked the alumina crucibles more rapidly. The greatest erosion occurs at the slag line, due to surface tension effects.

## B. STIRRED SLAG TESTS

The three types of stirred tests covered specific conditions for better understanding of the reactions occurring. The molybdenum dioxide saturation tests establish solubility limits dependent on oxygen activity and slag composition. The rotated molybdenum wire tests show slag movement affects erosion rates. The rotated carbon rod experiment shows the effects of a strong reducing agent: iron reduction, alloying, and minimum erosion of the molybdenum.

1. Molybdenum Dioxide Saturation of Union Electric Slag. In the previous experiments, molybdenum is shown to react with iron oxide in the slag. Molybdenum thus exerts a slight oxygen gettering effect on the slag. To determine the molybdenum dioxide saturation free of any gettering of oxygen by molybdenum, slag and dioxide were mixed. No iron oxide would then be reduced by molybdenum species.

The UE slag did not readily react with the dioxide, as seen in the results of MoO<sub>2</sub>-1 in Table III. Very little of the finely ground dioxide dissolved. However, seeded UE slag dissolved the dioxide much more readily. The sample, MoO<sub>2</sub>-4, clearly reached saturation throughout.

Stirring the plain UE slag samples overcame the slow molybdenum dioxide dissolution such that saturation was reached, as in the MoO<sub>2</sub>-2 test. In the MoO<sub>2</sub>-3 test, all excess molybdenum dioxide was consumed, as expected by the high molybdenum trioxide partial pressures at 10<sup>-2.8</sup> atm oxygen partial pressure (Figure 2). As the dioxide was stirred to the slag surface, it reacted to form trioxides, which vaporized.

The concentration of molybdenum dioxide soluble in slag increased with increasing oxygen potential. The seeding of slag did not appear to have a strong affect on dioxide concentration, although it greatly increased the rate of dissolution.

2. Rotated Molybdenum Wire. The wire movement enlarged the volume of slag in direct contact with molybdenum. This is

reflected in results from both tests, Table IV, when compared to the static immersion data, given in Table II.

a. Mo<sub>r</sub>-1. At an applied oxygen potential of  $10^{-9.1}$  atm, the rotation test generated lower molybdenum dioxide concentrations alongside the molybdenum than found in the static tests. The dispersion of slag containing dissolved dioxide reduced the dioxide concentration, indicating again that the corrosion reaction does not occur rapidly. The molybdenum dioxide concentration near the wire ranged from 20% to 40% lower than in the static test.

The concentration of dissolved molybdenum dioxide decreased deep in the slag, possibly because less oxygen was transported from the slag gas-surface. The higher concentration of iron in the molybdenum at the bottom section also appeared to confirm lower oxygen potentials at the bottom. However, the lower section also had molybdenum dioxide particles on the interface, while the upper section did not. This is possibly explained by slight differences in molybdenum dioxide solubility due to the slightly different oxygen potentials suspected.

Overall, the erosion and appearance of the Mo<sub>r</sub>-1 sample was quite like that of UE-3, the comparable static test. Rotation did not change the conditions significantly at  $10^{-9.1}$  atm oxygen potential.

b. Mo<sub>r</sub>-2. At  $10^{-2.8}$  atm oxygen pressure, the molybdenum erosion differed immensely from upper to lower sections. The dioxide layer was much thicker deep in the slag, as it had been in the Mo<sub>r</sub>-1 test, but the molybdenum dioxide concentration at the upper section was slightly lower than at the bottom section, reverse that of Mo<sub>r</sub>-1. Extremely severe molybdenum corrosion occurred at the top section. Increased volatilization of molybdenum trioxides and ample oxygen potential combined to erode the wire.

The thick, uneven dioxide layer at the lower section did not stop oxidation of the molybdenum surface, since oxidation must have occurred after formation of the initial dioxide layer. The



duplex structure in the oxide layer was very prominent, supporting the possibility the projecting oxide fingers were areas of lower oxygen content.

3. Rotated Carbon Rod. In the coal slag, carbon is a reducing agent likely to be present. Tests on the as-received Union Electric slag showed 1.0% carbon in the flyash and a trace amount in the bottom slag. The MHD system may also have some amount of carryover, or the carbon might be added intentionally to reduce electrode oxidation.

In the experiment, summarized in Table IV, very little molybdenum dioxide was present in the slag and iron alloyed with the molybdenum to a greater extent than in previous tests. Comparison with the static immersion and other stirred slag tests showed the measured  $C_{Mo \rightarrow S}^{10 Mo/S}$  was lowest in the presence of carbon.

The dominant reaction was reduction of iron from the slag. The iron is thought to reduce out near the carbon rod surface, forming small beads in the slag. Though very little dioxide entered the slag, greater amounts of molybdenum were present in the metallic beads, indicating the bead compositions were moving towards the same equilibrium, expressed in Equation (3), as was established at the molybdenum-slag interface. The microprobe analysis of the beads for molybdenum and iron did not add up to 100%. The missing fraction may be carbon.

The composition of the wire surface stabilized at about 5% iron. The molybdenum underwent swelling due to the alloying. At 1400°C, molybdenum saturates with about 7% iron, according to the phase diagram, Figure 3. The lack of a second phase in the surface microstructure is consistent with this information. The light etching band at the surface, Figure 23, may be a quench effect or the effect of slight carbon penetration. The carbon diffusion concept is supported by lack of a similar band in the seeded slag test mentioned earlier.

The small dendrites found growing from the molybdenum surface were likely an iron-molybdenum alloy. Similar dendrite growth is

noted by Borm and Pask for iron in glass containing cobalt.<sup>27</sup> The effect is attributed to a localized galvanic cell reaction between an iron-cobalt alloy and their ions in solution in the glass.

### C. CORRELATION OF STATIC AND STIRRED TESTS

Iron and molybdenum concentration data from the static and stirred tests are plotted against applied oxygen potential in Figures 43 and 44. The data is that reported in Tables II, III, and IV, generally 10  $\mu\text{m}$  from the interfaces. These graphs clearly show the regions where different equilibria are controlling.

An explanation of the reactions using molybdenum-slag equilibrium is suitable at the lower oxygen pressures tested,  $10^{-11.6}$  to  $10^{-9.1}$  atm. The ferrous oxide slag component is an integral part of the corrosion reaction and reactions proceed until the molybdenum dioxide concentration in the slag is in equilibrium. Further reaction is governed by diffusion of iron into the molybdenum and molybdenum dioxide into the slag.

When the molybdenum dioxide layer does isolate the molybdenum and the slag from each other, it is because the saturation limit for the slag has been reached. The molybdenum dioxide layer becomes a barrier to further molybdenum oxidation, but substantial amounts of oxidation still continue by diffusion or exchange reactions.

The data from UE-2 (at  $10^{-10.9}$  atm oxygen potential) stands out in Figure 43 as being misplaced. If shifted to the right, the concentrations of both iron and molybdenum fit the curves at the same point, around  $10^{-8.5}$  atm oxygen potential. It is thought control of the atmosphere could have been lost during the test.

### D. ELECTRICAL CURRENT STUDIES

Electrochemical cells involving molten oxide electrolytes are complex, so a thorough study is beyond the scope of this work. The electrochemical cell used simply identifies and characterizes the reaction types in the molybdenum-slag system. A major reaction was electrolysis of the slag. Current flow decomposed the ferrous oxide, causing iron to be reduced at the cathode and as a result the slag composition changed.

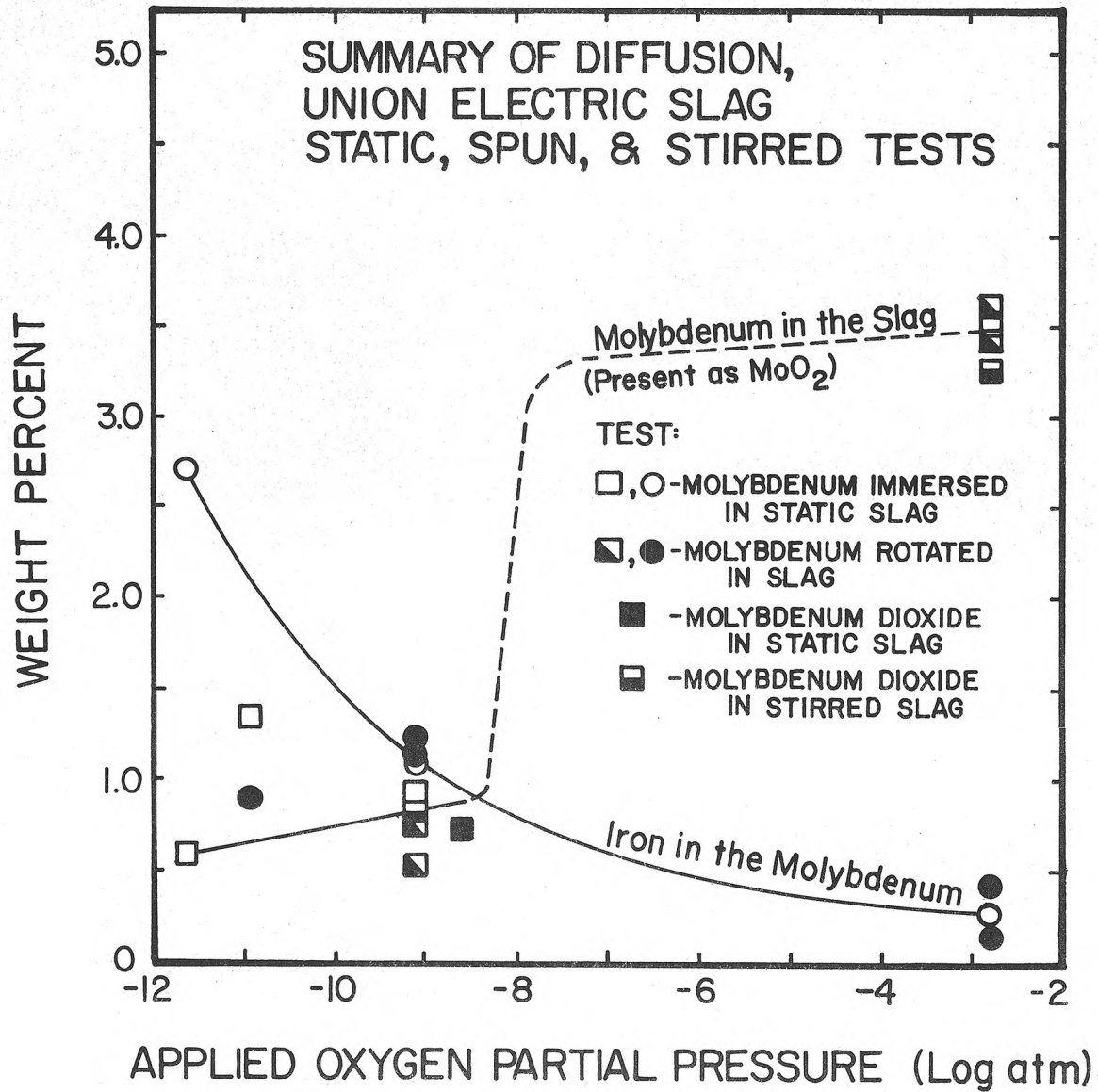


Figure 43. Summary of Microprobe Concentrations for Selected Points: Static Immersion, Rotated Wire, and Molybdenum Dioxide Saturation Tests in UE Slag.

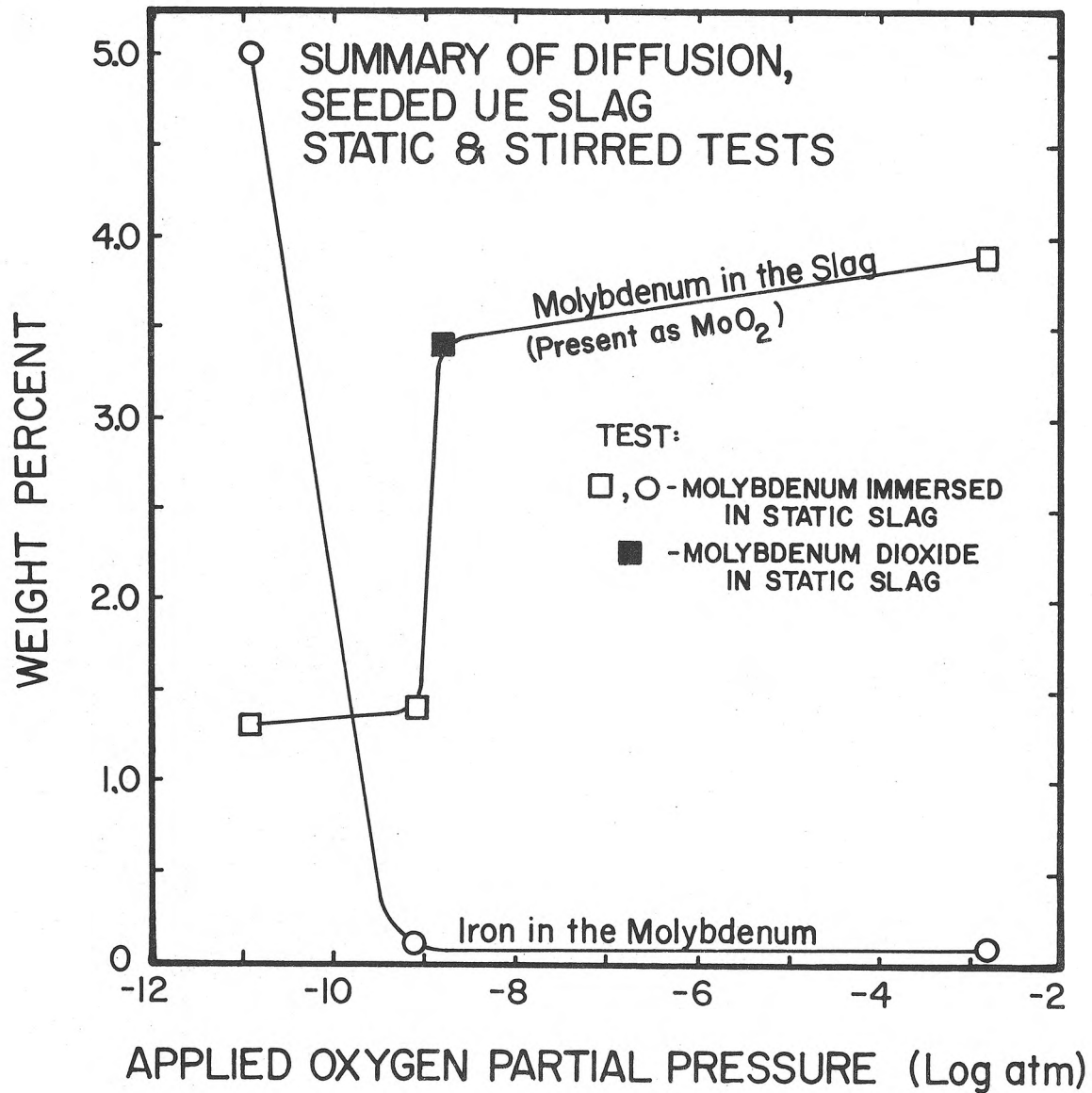


Figure 44. Summary of Microprobe Concentrations for Selected Points: Static Immersion and Molybdenum Dioxide Saturation Tests in Seeded UE Slag.

A small cathode/anode area ratio allowed greater current flow than did a large ratio, presumably because of polarization at the anode. Significantly more slag electrolysis occurred with the larger anode. The current flowing with a large anode area was 3.75 times that with a small area.

A reaction at the cathode released a gas from the slag. The nature of the gas is not known, but it is thought oxygen or molybdenum trioxide may be released because of slow diffusion of oxygen from cathode to anode as ferrous oxide reduced, resulting in high oxygen potential in the vicinity of the cathode. The released bubbles partially covered the cathode, reducing the effective electrode area.

During the later part of the cathode pin/anode ring tests, the current increased and decreased in surges. Part of the effect may be due to the formation of gases, but more must be involved. The current flow decreased (increasing resistance) when the slag was stirred, so some current transport mechanism must be disrupted. Possibly, the current moved along metallic and molybdenum dioxide debris.

Cadoff et al. used a similar slag in similar tests on ceramic electrode materials.<sup>19</sup> At higher current density (1 amp/cm<sup>2</sup>), the same slag electrolysis and cathode bubble formation are found. The voltage drop for the higher current flow was greater than the 1.5 V drop used in this study. This study confirms electrolysis at the lower potential, reinforcing the need to consider slag electrolysis in choosing suitable materials for the semi-hot, slagging channel.

As expected with the metallic electrodes, the corrosion is greatest at the anode, but reduction of iron at the cathode is also detrimental to the molybdenum. The results of the electrical current testing are collected in Table V.

1. Anode Reactions. At the anode, the only reaction was oxidation. The impressed voltage corroded the metal rapidly and the localized high oxygen potential raised the molybdenum dioxide solubility of the slag above that of any other test condition.

Large amounts of molybdenum dioxide formed on the surface and in the slag. Corrosion was more pronounced at the anode pin, where the current density was nearly 3 times greater. For each coulomb of charge, twice as much molybdenum corroded at the anode ring than at the anode pin. The current corroded more efficiently at the lower current density.

The concentration of iron found in the anodes followed in much the same manner as in the immersion tests, indicating the slag still exerted some alloying potential on the anodes. The concentration data for molybdenum and iron could not be plotted in Figure 43, since the oxygen potential at the interface was unknown. For the anode ring, both the iron and molybdenum concentrations match values predicted for an oxygen potential of  $10^{-7.6}$  atm.

Referring to the microprobe concentration profiles for the electrode tests, Figures 26 and 33, it appears the iron content of the slag was lower near the anode. This is thought to be an artifact of the analysis technique. The effect is discussed briefly in Appendix B. The iron concentration is thought to be nearly constant across the slag from anode to cathode.

2. Cathode Reactions. The iron reduced at the cathode formed small drops or globules on the molybdenum surface. Extensive alloying produced a variety of alloy phases. Where alloys of up to 70% iron formed, the material had poor mechanical strength and either slumped to the bottom of the wire, or formed dendrites that easily broke loose of the surface. The former occurred at 1400°C, the latter at 1350°C.

Less alloying occurred in the lower current density at the cathode ring, where the maximum concentration of iron was 33%. The  $\frac{C_{Mo}^{10}}{C_{Mo} \rightarrow S}$  was not exceptionally low, being 4 times the concentration found in the carbon rod test, even though much more iron was reduced.

A detailed description of the phases and alloying reactions is not attempted. The complex structures could be sensitive to cooling rates and may involve phases not present at the elevated temperatures.

3. Direct Molybdenum-Iron Reactions. The reactions found in the direct contact experiments do not differ significantly from those found at the cathodes. The most important variation is between the rate of reaction of the different tests. In the cathode pin test, 1400°C, the surface alloyed with iron for the first 270  $\mu\text{m}$  in only 3 hours, while in direct contact with iron for 12 hours, the alloy went only 127 to 178  $\mu\text{m}$  deep. In the direct contact experiments, molybdenum had the opportunity to diffuse into surrounding iron, something that could not happen in the current tests. The greater corrosion of the molybdenum in current flow suggests the current does more to cause alloying than to simply reduce iron.

The reaction and recession found in the iron powder doped slag experiment are very similar to the iron pack experiments. The molybdenum surface receded 76  $\mu\text{m}$  in 6 hours.

## VI. SUMMARY AND CONCLUSIONS

Corrosion of molybdenum by molten coal slag is characterized by oxidation to molybdenum dioxide or reduction of iron oxide and iron alloying of the molybdenum. The corrosion amount and type is strongly dependent upon oxygen potential and slag composition. Both influence steady state concentration levels of corrosion products: molybdenum dioxide dissolved in the slag and iron alloyed into the molybdenum. Increasing either the oxygen potential or the iron oxide content can cause a several-fold increase in corrosion.

In static conditions, accumulation of reaction products acts to slow further corrosion, whether the products are dissolved in the slag or present as separate phases. Slag movement strips away the protective products and reaction potential gradients, so at highly corrosive conditions the attack on molybdenum accelerates. Under the milder conditions of low oxygen potential, slag movement makes little difference in corrosion rates.

The tested slag had a rather low solubility for molybdenum dioxide, giving dissolved molybdenum concentrations below 3.9%. Values down to 1.1% molybdenum occurred at reduced oxygen potentials. The low solubility appears to be the most important agent slowing corrosion, allowing formation of semi-protective molybdenum dioxide coatings on molybdenum. Even with a dioxide layer present, corrosion continues at reduced rates, evidenced by coatings approaching 20  $\mu\text{m}$  thick. Seeding the slag had little effect on molybdenum dioxide solubility in the slag, though corrosion increased slightly. Significantly different corrosion product concentrations were measured in seeded slag, in general indicating greater sensitivity to slight changes in applied oxygen potential.

Innoculating the slag with carbon reduces corrosion, but increases the amount of iron alloying into molybdenum. The importance of this trade-off remains to be determined, though it is



clear excessive iron alloying reduces the maximum electrode working temperature. The flow of current also protects cathodic molybdenum from oxidation, but even more extensive iron alloying occurs, due to electrolysis of the slag. The reduced iron seriously attacks the molybdenum, forming iron-molybdenum alloys with little mechanical strength above 1350°C. Current flow causes extreme oxidation corrosion of anodic molybdenum, as all protective mechanisms appear to break down.

Molybdenum shows some promise as an electrode material, for the cathode, if the iron oxide content of the slag is low and the slag oxygen potential can be controlled. The stability of oxide reaction layers opens prospects of successfully inhibiting corrosion using alloying to form more stable oxide layers. Refractory molybdenum alloys with iron and silicon additions, major slag constituents, may reduce reaction potentials between the electrode and slag, producing successful lifetimes.

The type of testing described in this work identifies reactions and aids in accessing relative importance of these reactions with simple experiments. The relative corrosion resistance of potential metals, alloys, and oxides can be rapidly ascertained by performing a series of similar tests on the different candidates. The tests do not provide insight into effects of prolonged channel exposure or determine compatibility with other channel components. Channel tests best fill this need, while the corrosion tests serve as material screening techniques.

## BIBLIOGRAPHY

1. L. M. Raring: "Materials Engineering and Development for Coal Fired MHD Power Generators," Met. Trans., 1978, Vol. 9A, pp. 161-173.
2. B. R. Rossing: Private communication, Westinghouse Research Lab., Information compiled for ECAS report under sponsorship of NASA and ERDA.
3. M. Yoshimura and H. K. Bowen: Private communication, Department of Materials Science and Engineering, MIT.
4. L. Northcott: Molybdenum, Academic Press, New York, 1956, p. 7.
5. J. B. Heywood and G. J. Womack, Editors: Open Cycle MHD Power Generation, Pergamon Press, Oxford, England, 1969.
6. J. B. Wachtman, Jr., S. J. Schneider, and A. D. Franklin: "Role of Ceramics in Energy Systems," ERDA/NSF Workshop - Ceramics for Energy Applications, Battelle Memorial Institute, Columbus, Ohio, 1975.
7. H. K. Bowen and B. R. Rossing: "Materials Problems in Open Cycle Magnetohydrodynamics," Critical Materials Problems in Energy Production, Edited by C. Stein, Academic Press, Inc., New York, 1976, pp. 311-334.
8. R. J. Rosa: Magnetohydrodynamic Energy Conversion, McGraw-Hill, New York, 1968, pp. 1-10, 158-175.
9. J. F. Louis, et al.: "Open Cycle Coal Burning MHD Power Generation, an Assessment and a Plan for Action," Office of Coal Research, Department of the Interior, June, 1971.
10. G. Rudins: "US and USSR MHD Electrode Materials Development," R-1656-ERDA, December, 1974.
11. B. R. Rossing and H. K. Bowen, "Materials for Open Cycle Magnetohydrodynamic (MHD) Channels," Critical Materials Problems in Energy Production, Edited by C. Stein, Academic Press, Inc., New York, 1976, pp. 335-356.
12. H. K. Bowen, et al.: "Chemical Stability and Degradation of MHD Electrodes," Proceedings of the 14th Symposium on the Engineering Aspects of Magnetohydrodynamics, April, 1974, pp. IV.1.1-IV.1.14.
13. J. L. Bates: "Properties of Molten Coal Slags Relating to Open Cycle MHD, Final Progress Report to NSF (RANN)," Battelle Pacific Northwest Laboratories, BNWL-B-466, December, 1975.

14. J. L. Bates: "Electrical Conductivity of Molten Coal Slags Containing Potassium Seed," Proceedings of the 16th Symposium on the Engineering Aspects of Magnetohydrodynamics, May, 1977, pp. VIII.5.32-VIII.5.36.
15. W. Capps: "Coal Slag Properties Related to MHD," Conference on High Temperature Sciences Related to Open-Cycle, Coal-Fired MHD Systems, Argonne National Laboratory, ANL-77-21, April, 1977, pp. 190-195.
16. W. Capps, "Some Properties of Coal Slags of Importance to MHD," Proceedings of the 16th Symposium on the Engineering Aspects of Magnetohydrodynamics, May, 1977, pp. VIII.3.21-VIII.3.25.
17. The Making, Shaping and Treating of Steel, 9th Edition, Edited by H. E. McGannon, United States Steel, 1971, pp. 281-374.
18. M. Timucin and A. E. Morris: "Phase Equilibria and Thermodynamic Studies in the System  $\text{CaO-FeO-Fe}_2\text{O}_3\text{-SiO}_2$ ," Met. Trans., 1970, Vol. 1, pp. 3193-3201.
19. S. Petty, A. Demirjian, and A. Solbes: "Electrode Phenomena in Slagging MHD Channels," Proceedings of the 16th Symposium on the Engineering Aspects of Magnetohydrodynamics, May, 1977, pp. VIII.1.1-VIII.1.12.
20. L. H. Cadoff, H. D. Smith, and B. R. Rossing: "The Evaluation of Electrode Materials of Slag Coated MHD Channels," Proceedings of the 16th Symposium on the Engineering Aspects of Magnetohydrodynamics, May, 1977, IV.8.47-IV.8.54.
21. L. W. Crawford, C. K. Peterson, J. B. Dicks, and M. S. Beaton: "Generator Wall Slag Coating and Material Corrosion Experiments," Proceedings of the 16th Symposium on the Engineering Aspects of Magnetohydrodynamics, May, 1977, IV.5.29-IV.5.34.
22. Metals Handbook, 8th Edition, 1961, Vol. 1, American Society for Metals, Metals Park, Ohio, pp. 1215-1217.
23. E. M. Savitskii and G. S. Burkhanov: Physical Metallurgy of Refractory Metals and Alloys, Trans. from Russian, Consultants Bureau, New York, 1970, pp. 119-133.
24. E. A. Gulbransen: "Thermochemistry and the Oxidation of Refractory Metals," Corrosion, January, 1970, Vol. 26, No. 1, pp. 19-28.
25. J. K. Thorne, J. M. Dahl, and L. H. Van Vlack: "Partition Coefficient of Molybdenum in the Fe-Mo-Si-O System," Met. Trans., Vol. 1, August, 1970, pp. 2125-2132.

26. L. N. Rusakov, I. A. Novokhatskii, L. M. Levev, A. S. Dubrovin, and A. A. Savinskaya: "Essperiment v Tekhn. Minerlog. i Petrogr.," po Materialam Soveshch., 7th, Lvov 1964, 1966, pp. 246-50.
27. M. P. Borom and J. A. Pask: "Role of "Adherence Oxides" in the Development of Chemical Bonding at Glass-Metal Interfaces," J. Am. Ceram. Soc., Vol. 49, No. 1, 1966, pp. 1-6.
28. G. Economos and W. D. Kingery, "Metal-Ceramic Interactions: II, Metal-Oxide Interfacial Reactions at Elevated Temperatures," J. Am. Ceram. Soc., Vol. 36, No. 12, pp. 403-409.
29. Metal-Slag Gas Reactions and Processes, Edited by Z. A. Foroulis and W. W. Smeltzer, The Electrochemical Society, Inc., 1975.
30. R. Hultgren, P. D. Desai, D. T. Hawkins, M. Gleiser, and K. K. Kelley: Selected Values of the Thermodynamic Properties of Binary Alloys, American Society for Metals, 1973.
31. V. D. Chaskar: "The Solubility of Lead in Iron Sulfide and Oxysulfide Mattes at 1100°C and 1200°C," M.S. Thesis, Department of Metallurgical Engineering, University of Missouri-Rolla, 1976.
32. L. S. Birks: Electron Probe Microanalysis, Interscience Publishers, 1976.
33. S. J. B. Reed, Electron Microprobe Analysis, Cambridge University Press, 1975.
34. K. Keil: "Applications of the Electron Microprobe in Geology," Microprobe Analysis, Edited by C. A. Andersen, John Wiley & Sons, 1973, pp. 189-203.

## VITA

Kenton Brian Wright was born on June 19, 1953, in Columbia, Missouri. He received his primary and secondary education in Overland Park, Kansas. He received a Bachelor of Science in Metallurgical Engineering from the University of Missouri-Rolla in May, 1975.

He enrolled in the Graduate School of the University of Missouri-Rolla in August, 1975. During the period August, 1975 to December, 1977, he held a USOE Domestic Mining, Mineral, and Mineral Fuel Conservation Fellowship.

He is a member of Alpha Sigma Mu, the Metallurgical Society of AIME, and the American Society of Metals. He is employed with the Aluminum Company of America, Warrick Operations, Newburgh, Indiana.

APPENDIX A  
MATERIAL PREPARATION

1. PREPARATION OF MOLYBDENUM DIOXIDE

Molybdenum and molybdenum trioxide react to form molybdenum dioxide:



Sixteen grams of the dioxide were prepared by weighing the stoichiometric amounts of each powder and thoroughly mixing these together. The mixture was then sealed into an evacuated fused silica capsule and heated slowly to 900°C. Too rapid heating caused excessive amounts of molybdenum trioxide to volatilize from the charge and condense on the silica container. After 24 hours, the sample was cooled and ground to -100 mesh.

The oxygen content of the oxide product was analyzed gravimetrically. A weighed amount of powder was placed in a weighed porcelain boat, loaded into a furnace fitted with a Vycor tube, and slowly heated to 800°C in flowing hydrogen. After 10 hours of reduction, the boat was cooled (still under hydrogen) and reweighed. The molar ratio of oxygen to molybdenum was 1.99:1.

The molybdenum dioxide was analyzed structurally using a powdered sample run on a General Electric XRD 700 Diffractometer. Comparison of the results to data from the ASTM Diffraction File (Hanawalt Cards) showed no lines corresponding to molybdenum trioxide. Only the strongest line of metallic molybdenum was above background levels. The remaining lines matched the pattern for molybdenum dioxide.

2. TREATMENT OF UNION ELECTRIC SLAG

A homogeneous melt of Union Electric slag was prepared by fusing 10 kg of the as-received slag in an iron crucible. The iron crucible served as a susceptor for induction heating and was contained within a ceramic crucible. Refractory wool filled the space between the two crucibles and Alundum Cement sealed the top

edges together. Nitrogen purged oxygen from around the outside of the iron crucible to minimize oxidation of the iron. As the original slag charge melted and gas evolution subsided, additional slag was added. Thermal gradients stirred the melt and occasional mixing with an iron rod further blended the slag. The remelted slag was held at 1300°C for 5 hours, during which it equilibrated with the iron container. The slag was poured off into iron molds to cool, then was reduced to pass -35 mesh using a jaw crusher and roll mill.

## APPENDIX B

### TECHNIQUES OF ANALYSIS

#### 1. MOLYBDENUM-SLAG SAMPLE PREPARATION

The desired part of the sample was extracted by cutting with a thin rim diamond blade. A 1¼ inch mount of plastic resin protected the brittle samples and provided an accurate alignment in the microprobe sample current.

Surface preparation began with grinding on a wet 240 grit silicon carbide paper and progressed through 600 grit. Successive polishing with #9 and #1 diamond paste using a methanol wash on microcloth-covered lapping wheels provided a flat surface.

Samples were etched in modified Murakami's reagent (15 g potassium ferricyanide, 2 g sodium hydroxide, and 100 ml water) by wiping 5 to 10 seconds with a saturated cotton swab. A light polish with 0.1 micron alumina on a damp cloth between successive repeat etchings became necessary in some cases to obtain a clean etch. The same procedures were followed for etching in nital (5% nitric acid in methanol).

For the dual etch, nital was used first to bring out alloy phases, then Murakami's reagent followed to etch the molybdenum. Any light polishing needed to clean up the molybdenum surface did not interfere with the nital etch. Care must be taken to rinse all nital thoroughly away before using the Murakami's reagent, so hydrogen cyanide cannot form.

#### 2. MICROPROBE CALIBRATIONS

The methods used to set up microprobe standards are given below. Calculated corrections were used for molybdenum-iron alloys and comparison standards were used for slag phase calibration.

a. Molybdenum-Iron Alloys. Following the method of Birks, correction curves are calculated for the relative intensity of molybdenum in molybdenum-iron alloys. Several phenomena are considered. Fe  $K_{\alpha}$  radiation has sufficient energy to excite the



Mo  $L_\alpha$  wavelength, so a matrix enhancement factor is used to correct for this. Emitted Mo  $L_\alpha$  radiation is reabsorbed by the alloy, so matrix absorption terms for absorption by molybdenum and iron are used. Because of the spread in atomic number between iron and molybdenum, an atomic number correction is added.

For an assumed composition of 70% molybdenum and 30% iron, using data from Appendices 1-6 in Birks, the calculation proceeds as given below.

With the information:

$$W_{\text{Mo}} = 70\%, W_{\text{Fe}} = 30\% \text{ (assumed weight fractions),}$$

$$\mu_{\text{MoFe}} = 270 \text{ (mass absorption coefficient of Mo for Fe characteristic radiation),}$$

$$\mu_{\text{FeMo}} = 1160 \text{ (mass absorption coefficient of Fe for Fe characteristic radiation),}$$

$$\mu_{\text{MoMo}} = \mu'_{100\text{Mo}} = 720, \mu_{\text{FeFe}} = 76 \text{ (mass self-absorption coefficients),}$$

the total mass absorption coefficient,  $\mu'_{\text{Mo}}$ , is calculated as:

$$\mu' = (\mu_{\text{MoMo}} \cdot W_{\text{Mo}}) + (\mu_{\text{FeMo}} \cdot W_{\text{Fe}}) = 852. \quad (9)$$

By similar calculation,  $\mu'_{\text{Fe}} = 212$ .

Then with the values:

$$V = 15 \text{ k.e.v. (the operating beam potential),}$$

$$V_{\text{oMo}} = 2.87 \text{ k.e.v. (the Mo } L_\alpha \text{ threshold excitation potential),}$$

$$V_{\text{oFe}} = 7.1 \text{ k.e.v. (the Fe } K_\alpha \text{ excitation threshold),}$$

$$E_{\text{MoFe}} = 0.012 \text{ (the excitation efficiency),}$$

$$k = 0.6 \text{ (a constant),}$$

the total enhancement coefficient,  $K_F$ , is calculated as:

$$K_F = k E_{\text{MoFe}} W_{\text{Fe}} \left( \frac{\mu_{\text{MoFe}}}{\mu'_{\text{Fe}}} \right) \frac{(V - V_{\text{oFe}})^2}{(V - V_{\text{oMo}})^2} = 0.012. \quad (10)$$

Finally with:

$\psi = 30^\circ$  (the detector take-off angle),

$p_{Mo} = 0.94$  (correction for atomic number),

$F_{Mo} = 71.4$  (intensity function from Birks, using a graph of  $p_{Mo} \text{csc}\mu'_{Mo}$  versus  $F_{Mo}$ ),

$F_{100Mo} = 74$  (intensity function for pure Mo, using a graph of  $\text{csc}\mu'_{100Mo}$  versus  $F_{100Mo}$ ),

the relative intensity expected at the assumed composition is then calculated as:

$$\frac{I_{Mo}}{I_{100Mo}} = \frac{F_{Mo} \cdot W_{Mo} \cdot (1 + K_F)}{F_{100Mo}} = 0.684. \quad (11)$$

The above correction shows that a relative intensity reading of 0.684 would be expected to indicate 70% molybdenum present in the alloy. Similar computations at other assumed compositions give the complete calibration curve shown in Figure 45. For values of relative intensity above 0.60, a linear equation,

$$0.94 I_{Mo}/I_{100Mo} + 0.06 = W_{Mo} \quad (12)$$

was substituted.

For iron concentrations in the alloy system, only corrections for matrix absorption were necessary. The results of these calculations are also shown in Figure 45. The equation,

$$1.083 I_{Fe}/I_{100Fe} = W_{Fe} \quad (13)$$

was used for iron relative intensities below 0.10.

b. Slag Phase. For molybdenum measurements in the slag, a linear correlation between relative intensity and concentration was found. The equation of this line is:

$$1.106 I_{Mo}/I_{100Mo} = W_{Mo}. \quad (14)$$

The iron concentration in the slag was roughly estimated by a direct comparison of relative intensities in the blank slag standard and in the samples.

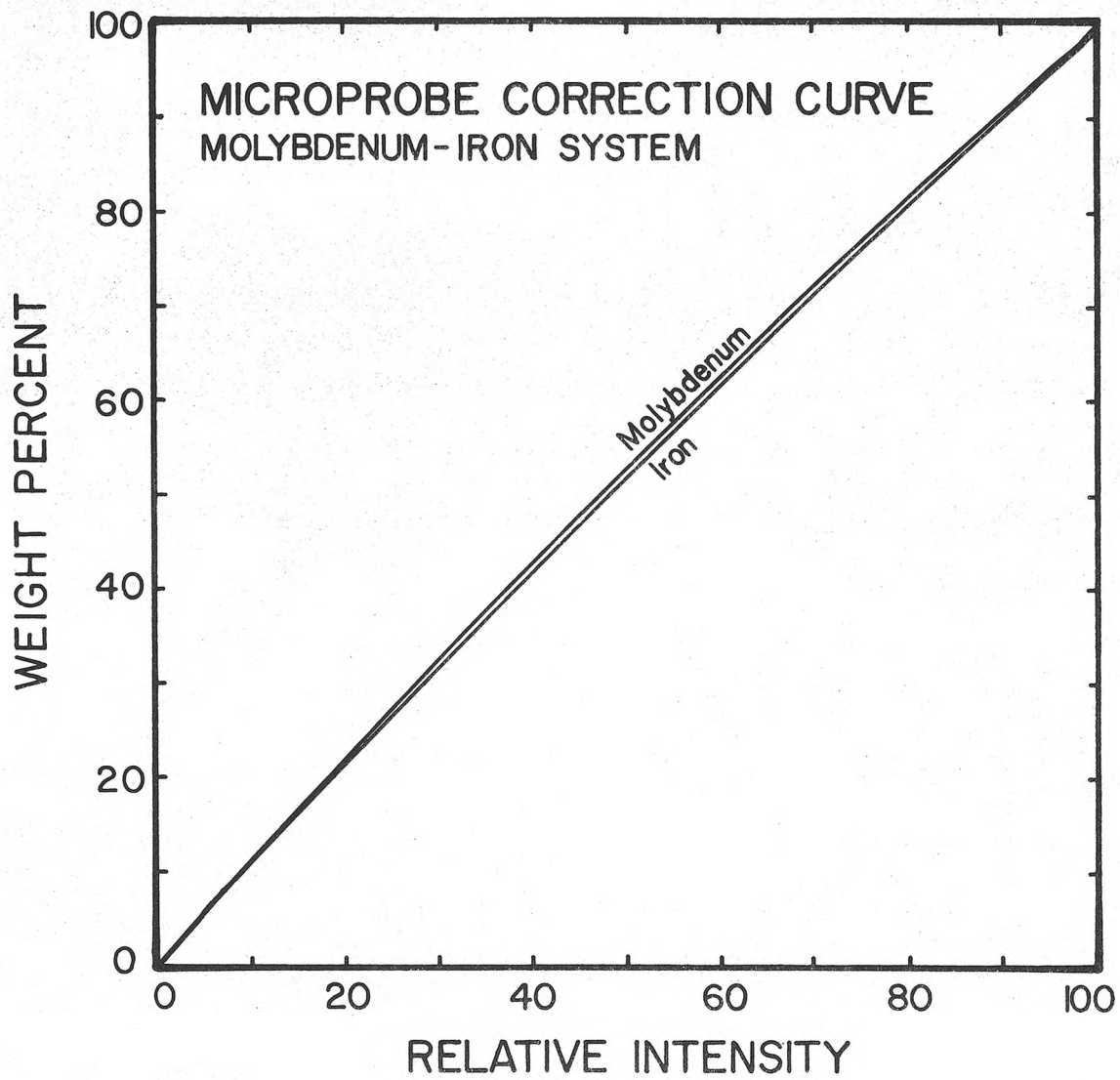


Figure 45. Calculated Correction Curves for Molybdenum-Iron Alloys, Relating Relative Intensity with Composition for Microprobe Calibration.

The molybdenum dioxide comparison standards used in slag phase calibration were prepared either by adding molybdenum dioxide to potassium sulfate seeded slags or by stirring molybdenum dioxide powder within a plain slag melt with a platinum loop attached to a rotating ceramic rod. Long periods of time (over 20 hours) and very fine molybdenum dioxide powder (-400 mesh) were required for satisfactory homogeneity. The first method was used for the 1.06% molybdenum standard and the second was used for the 3.23% standard. Both techniques gave homogeneous samples.

These samples were analyzed for molybdenum by atomic absorption techniques. The samples were first ground to -200 mesh and dissolved in hot nitric acid, to which hydrofluoric acid was added dropwise until all residue had reacted. After cooling and careful dilution to the necessary concentration (5 to 30 ppm molybdenum), the samples were tested in a nitrous oxide/acetylene flame.

The atomic absorption unit was calibrated by constructing a curve of absorption versus concentration using solutions containing known concentrations of molybdenum. Acid-dissolved slag solution was added to the standards to duplicate the matrix of the samples. Standards lacking the addition caused the measured sample concentrations to be 30% below actual values. The reason this occurred was not pursued, but it was noted that the amount of slag solution added was not critical. All procedures were checked by dissolving known mixtures of slag and molybdenum dioxide and running the normal dilutions and analysis. As a final check, the microprobe standards were analyzed by a commercial assayer, who obtained the same values, to two significant places, for both standards.

The iron concentration in the slag was not considered an important variable, since the amount of slag is much greater than the amount of molybdenum. The slag composition could not change significantly by reaction with the molybdenum unless massive reduction of iron oxide occurred. For the purpose of constructing microprobe concentration profiles, the calibration of iron in slag was established by equating the iron count detected for a molybdenum-free slag blank to 13.5% iron, the original composition of the slag.

The correction curve is assumed linear and is assumed to intercept the origin.

Deviations from 13.5% iron were found, but a rough calculation shows the deviation is proportional to the amount of molybdenum dioxide in the slag sample. The measured intensity of iron is apparently reduced by matrix effects of molybdenum. The effect was left uncorrected, since no rigorous calibration was necessary. In the electrical current tests, where substantial amounts of iron reduced from the slag, depressed values of iron concentration were noted across the slag and very low values were found near the anodes. Partially, the matrix effect explains the low values, but for any further testing the use of accurate standards for iron might be justified.

### 3. CARBON DIOXIDE GAS ANALYSIS

A modified Orsat apparatus determined the carbon dioxide content of carbon monoxide-carbon dioxide gas mixtures. A known volume (59 cc) of the gas to be analyzed was introduced into a gas buret, and then repeatedly contacted with sodium hydroxide solution. The change in volume, measured by solution height in the buret, indicated the amount of carbon dioxide selectively absorbed by the solution. The apparatus used for the analysis is shown in Figure 46.

In practice, the buret was flushed with a large volume of the gas to be analyzed and then was isolated from the atmosphere. With caustic solution admitted, the tube was turned over several times until no more volume change was noted. The buret was elevated such that its solution level was equal to that in the reservoir while the volume change was measured. Despite moisture pickup from the solution, any slight absorption of carbon monoxide by the solution, and deviations of the gas from ideal behavior were neglected, analysis of gas mixtures containing known amounts of carbon dioxide gave results which agreed within 1% of the true composition.

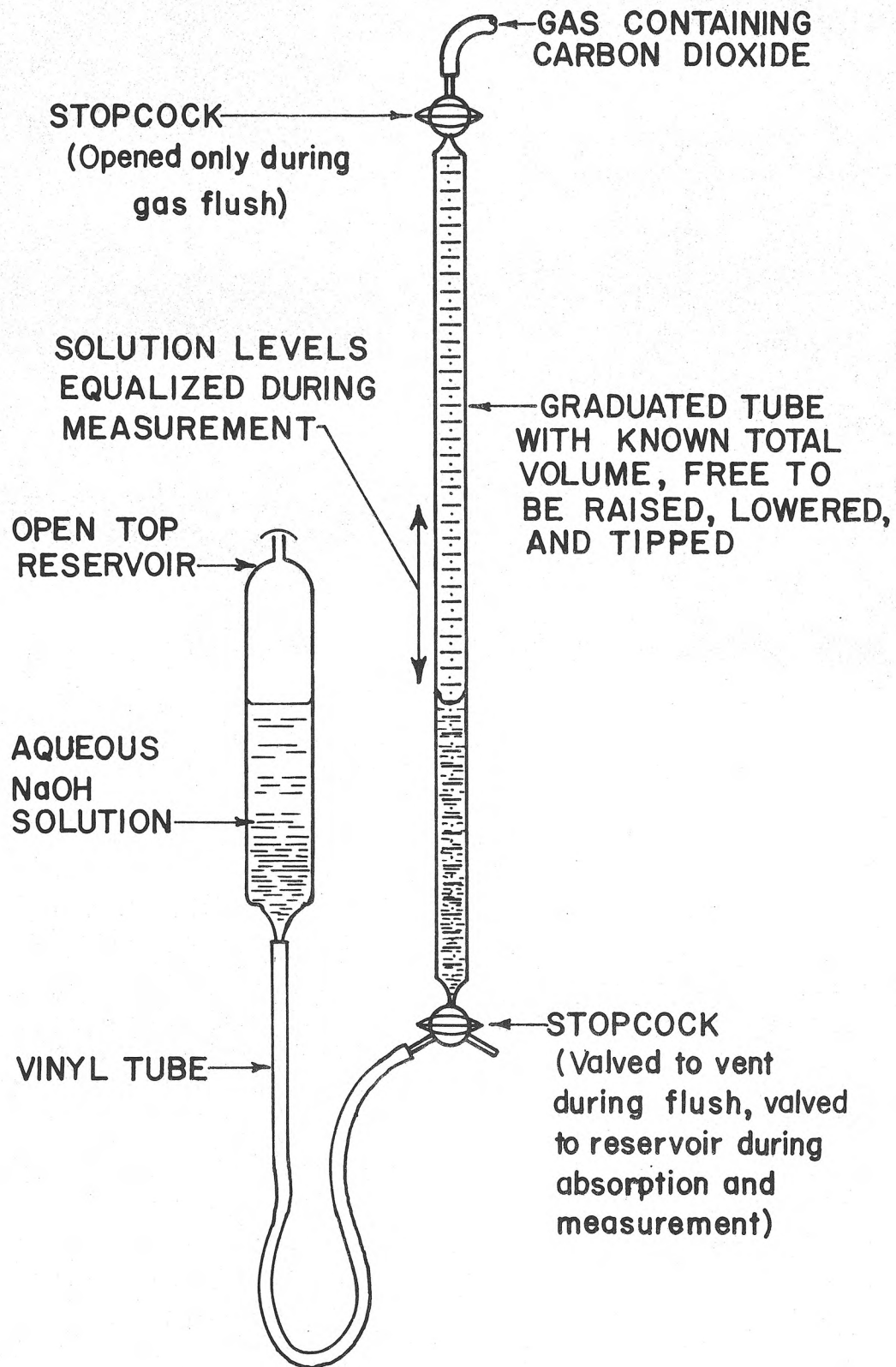


Figure 46. Carbon Dioxide Analyzer Used for Gas Analysis of Furnace Atmosphere.

#### 4. CARBON ANALYSIS OF SLAGS

The technique employed combustion of carbon in pure oxygen, followed by absorption and weighing of carbon dioxide in Ascarite. An oxidizing flux, lead oxide, was added to lower the slag melting temperature and to expose all carbon to oxidizing conditions. Precautions were taken to eliminate any carbonaceous material from the combustion boat, any carbon dioxide from the entering oxygen, and any carbonates from the lead oxide flux. Before the exit gas contacted Ascarite, it passed through manganese dioxide to remove any sulfur oxides possibly evolved from the slag, and through silica gel to remove any water vapor. The equipment is shown in Figure 47.

In the procedure, about 3 g of slag and an equal amount of lead oxide, weighed and mixed, were placed in a combustion boat and sealed into the furnace. All air was flushed from the system and the Ascarite bulb was weighed for tare. The boat was pushed into the 900°C hot zone under a steady flow of oxygen. The flow continued, with interruptions for weighing the Ascarite bulb, until a constant weight was obtained.

The accuracy of the procedure was checked by analysis of a synthetic slag containing a known amount of added carbon powder, equivalent to 1.7 weight percent carbon in the sample. The resultant value of 1.69% accounted for 99.4% of the added carbon.

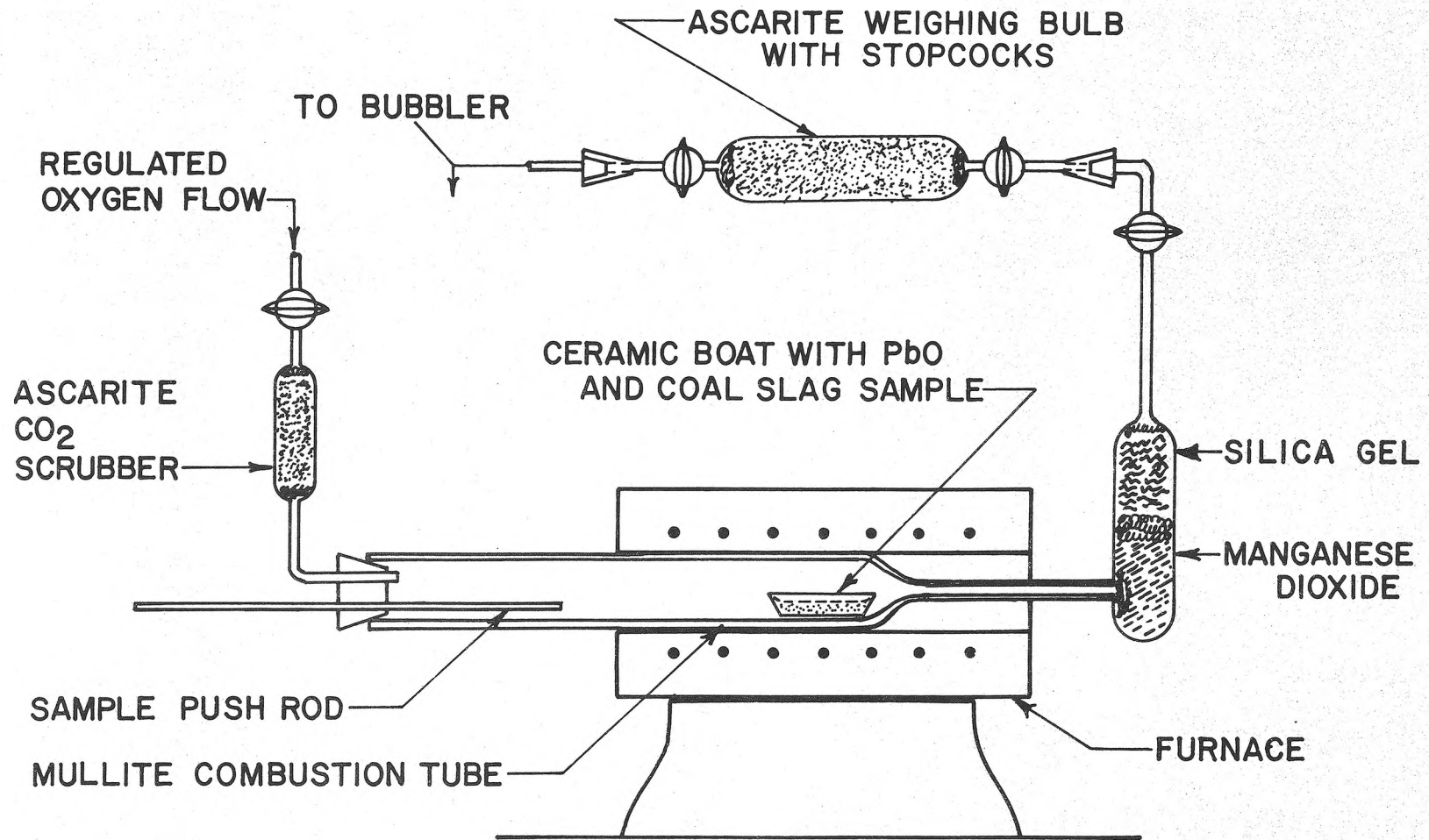


Figure 47. Apparatus Used to Analyze Coal Slags for Carbon.



APPENDIX C  
COMPILATION OF DATA TABLES

Appendix C contains data for microprobe composition profiles in Tables VI through IX. For simplicity, the interface position is rounded to the nearest 2  $\mu\text{m}$ . For more accuracy, a correction based on the aluminum counts was used to exactly locate the interface between the slag and other phases. The correction is included in the tables, a negative value denoting a shift towards the slag for the interface and a positive value denoting a shift towards the molybdenum.

Appendix C also contains data for the electrical current measured at various times throughout the electrode tests in Table X.

TABLE VI. MICROPROBE CONCENTRATION DATA FOR STATIC IMMERSION TESTS USING UNION ELECTRIC SLAG.

Distance From Interface ( $\mu\text{m}$ )	Sample Identification								
	UE-1		UE-2		UE-3		UE-4		
	%Mo	%Fe	%Mo	%Fe	%Mo	%Fe	%Mo	%Fe	
Molybdenum	50								
	48			98.0	0.18				
	46			99.3	0.21				
	44			100.5	0.23				
	42			100.0	0.30				
	40			99.9	0.36				
	38			99.9	0.53				
	36			98.4	0.56				
	34			98.7	0.45				
	32			99.5	0.42				
	30			99.3	0.50				
	28			98.4	0.60			99.4	0.09
	26			99.3	0.61			100.7	0.17
	24			98.0	0.59			99.8	0.20
	22			99.8	0.59			100.9	0.24
	20			100.0	0.59			100.5	0.24
	18	97.4	2.26	100.5	0.63			100.4	0.26
	16	98.0	2.34	100.0	0.70			100.6	0.29
	14	97.5	2.41	100.0	0.75	99.2	1.04	100.6	0.36
	12	97.7	2.46	98.7	0.88	99.7	1.10	101.2	0.41
10	97.1	2.52	98.9	0.93	99.0	1.14	101.1	0.44	
8	97.2	2.64	98.9	1.09	99.6	1.17	96.5	0.45	
6	96.4	2.87	98.8	1.08	99.9	1.30	79.4	0.33	
4	96.9	2.99	98.8	1.34	99.0	1.41	71.3	0.21	
2	96.2	3.24	89	2.6	96.6	2.02	68.6	0.64	
Interface	0	72.9	4.54	30	10.1	33	12.3	39.3	5.7
Slag	2	4.55	12.5	1.37	12.6	1.10	12.4	4.48	9.9
	4	0.59	12.5	1.33	13.0	0.94	12.4	3.22	10.2
	6	0.56	12.4	1.29	12.9	1.00	12.4	3.33	10.2
	8	0.57	12.5	1.29	12.8	0.86	12.3	3.35	10.2
	10	0.54	12.5	1.24	12.8	0.96	12.5	3.47	10.2
	12	0.55	12.4	1.27	12.9	0.95	12.6	3.29	10.4
	14			1.22	13.0	0.96	12.6	3.49	10.3
	16			1.28	13.0			3.41	10.3
	18			1.26	13.0				
	20			1.30	12.8				
30			1.20	12.9					
40			1.18	1.29					
Correction		-0.9 $\mu\text{m}$		+0.5 $\mu\text{m}$		-0.3 $\mu\text{m}$		0.0	

TABLE VII. MICROPROBE CONCENTRATION DATA FOR STATIC IMMERSION TESTS USING SEEDED UNION ELECTRIC SLAG

Distance From Interface ( $\mu\text{m}$ )	Sample Identification						
	UE <sub>S</sub> -1		UE <sub>S</sub> -2		UE <sub>S</sub> -3		
	%Mo	%Fe	%Mo	%Fe	%Mo	%Fe	
Molybdenum	26				99.5	0.00	
	24				99.6	0.04	
	22	96.7	3.63	102.2	0.16	99.7	0.02
	20	96.6	3.63	99.7	0.06	100.1	0.00
	18	96.5	3.83	99.5	0.06	99.9	0.03
	16	95.3	4.21	99.4	0.04	99.9	0.09
	14	95.6	4.63	99.2	0.07	100.5	0.11
	12	95.6	4.65	99.2	0.09	100.1	0.10
	10	95.3	5.00	99.2	0.08	100.6	0.10
	8	94.7	5.39	99.7	0.12	95.7	0.20
	6	94.5	5.82	99.6	0.17	93.5	0.27
	4	93.9	6.27	100.0	0.22	80.6	0.27
	2	71.3	7.03	100.0	0.36	63.8	0.24
Interface	0	24.2	10.3	95.8	0.74	41.7	2.88
Slag	2	1.48	11.4	2.30	10.3	4.05	8.9
	4	6.40	13.3	1.28	10.6	3.53	9.1
	6	18.3	17.6	1.40	10.7	3.66	9.0
	8	9.12	14.3	1.39	10.7	3.91	9.1
	10	1.27	11.4	1.42	10.9	3.92	9.2
	12	15.0	11.1	1.42	11.0	3.95	9.1
	14	49.3	10.0	1.60	11.1	3.98	9.2
	16	55.4	9.7	1.38	10.9	3.98	9.1
	18	25.4	10.8	1.35	10.8	3.92	9.2
	20	5.52	11.6			3.79	9.2
	22	1.68	11.5			3.86	9.1
	24	1.29	11.5				
	26	1.14	11.3				
28	1.11	11.4					
30	1.04	11.3					
Correction		+0.9 $\mu\text{m}$		-0.1 $\mu\text{m}$		-0.2 $\mu\text{m}$	

TABLE VIII. MICROPROBE CONCENTRATION DATA FOR STIRRED SLAG TESTS (ROTATED MOLYBDENUM ROD AND ROTATED CARBON ROD).

Distance From Interface ( $\mu\text{m}$ )	Sample Identification									
	$\text{Mo}_r\text{-1T}$		$\text{Mo}_r\text{-1B}$		$\text{Mo}_r\text{-2T}$		$\text{Mo}_r\text{-2B}$		UE + C	
	%Mo	%Fe	%Mo	%Fe	%Mo	%Fe	%Mo	%Fe	%Mo	%Fe
74									100.1	0.05
64									100.0	0.08
54									100.2	0.09
44									98.6	1.97
42									98.7	2.23
40									99.8	2.57
38			98.3	0.62					97.9	2.87
36			97.1	0.72					97.5	3.24
34			97.1	0.82					97.4	3.57
32			97.3	0.94					96.2	3.88
Molybdenum 30			96.8	1.18					96.3	4.17
28			97.5	1.12					96.3	4.52
26			98.0	0.96					96.0	4.80
24			98.3	0.81					95.4	5.00
22			96.9	0.86					95.4	5.11
20	99.8	0.25	97.5	0.91					95.9	5.12
18			97.8	0.93			97.7	0.14	96.4	4.65
16	99.1	0.72	97.6	1.00	100.0	0.09	98.3	0.17	95.4	4.79
14			97.6	1.05	100.9	0.13	97.4	0.25	95.6	4.99
12	98.3	1.00	97.4	1.14	100.7	0.15	98.3	0.33	94.9	5.09
10			97.7	1.21	101.4	0.18	97.8	0.42	96.1	5.05
8	98.4	1.24	96.7	1.32	100.6	0.23	98.5	0.48	96.1	5.10
6			98.0	1.49	98.7	0.32	97.6	0.72	95.7	4.73
4	98.9	1.49	97.2	1.61	69.2	0.24	96.2	0.95	95.7	5.74
2			96.8	1.90	67.0	0.54	73	0.27	94.0	6.42
Interface 0	50.2	7.5	40.7	11.1	4.90	10.0	60	1.96	58.7	7.95
2			1.52	13.1	3.02	10.2	5.04	10.0	2.00	12.4
4	0.76	12.0	0.63	13.3	3.30	10.2	2.95	10.3	0.07	12.5
6			0.64	14.4	3.33	10.2	3.16	10.4	0.09	12.7
8	0.79	12.2	0.61	14.1	3.37	10.2	3.46	10.3	0.06	12.5
10			0.60	13.6	3.40	10.4	3.61	10.2	0.02	12.7
12	0.76	12.2	0.60	13.6	3.32	10.4	3.59	10.2		
14			0.50	13.5	3.25	10.4	3.70	10.2		
16	0.80	12.3	0.63	13.5	3.27	10.5	3.85	10.3		
18			0.56	13.4	3.36	10.5				
20	0.81	12.2	0.58	13.4	3.25	10.6			0.03	12.6
22			0.53	13.5						
24	0.80	12.2	0.51	13.6						
26										
28	0.75	12.3								
30									0.07	12.6
32	0.76	12.4								
40									0.03	12.8
Correction	-0.2 $\mu\text{m}$		-0.3 $\mu\text{m}$		+0.7 $\mu\text{m}$		-0.6 $\mu\text{m}$		-0.4 $\mu\text{m}$	

TABLE IX. MICROPROBE CONCENTRATION DATA FOR ELECTRICAL CURRENT TESTS IN UNION ELECTRIC SLAG.

Distance From Interface ( $\mu\text{m}$ )	Sample Identification								
	Anode Pin		Cathode Ring		Cathode Pin		Anode Ring		
	%Mo	%Fe	%Mo	%Fe	%Mo	%Fe	%Mo	%Fe	
Molybdenum	272				98.5	0.27			
	270				98.5	0.25			
	268				98.5	0.23			
	266				98.4	0.28			
	264				98.9	0.32			
	262				98.8	0.41			
	260				96.9	1.81			
	258				94.6	3.80			
	256				94.0	4.80			
	254				64.6	35.0			
	252				49.9	49.0			
	250				48.0	51.2			
	248				48.2	51.9			
	246				49.1	45.7			
	244				25.5	71.0			
	242				22.2	76.2			
	26			92.9	5.59				
	24			93.4	5.82			98.5	0.02
	22			93.0	6.06			98.5	0.02
	20			93.0	6.37			98.1	0.24
	18			93.1	6.57			98.3	0.59
	16	100.1	0.04	92.2	6.85			98.1	0.69
	14	99.8	0.05	92.2	7.16			97.8	0.75
	12	99.6	0.07	92.6	7.28			98.2	0.80
10	100.2	0.10	92.2	7.54	28.6	73.0	98.0	0.87	
8	100.1	0.11	91.0	8.28	43.9	57.7	97.2	0.99	
6	100.2	0.12	67.1	32.2	47.0	54.8	97.8	1.07	
4	99.8	0.18	66.4	33.1	30.3	71.0	67.1	0.49	
2	79.8	0.12	66.0	33.2	48.5	50.7	69.9	0.25	
Interface	0	54.3	0.19	56.4	29	0.55	13.2	37.4	4.79
Slag	2	7.40	1.6	2.57	13.6	2.00	13.0	1.87	8.5
	4	2.20	1.35	0.39	13.6	0.42	12.3	1.62	8.8
	6	5.19	3.17	0.29	13.3	0.31	12.2		
	8	2.90	3.11	0.27	13.3	0.29	12.0		
	10	2.00	2.59	0.32	13.2	0.91	11.8		
	12	3.21	4.83	0.25	13.2	2.17	11.4	2.14	9.0
	14	15.8	4.43	0.28	13.2	0.77	11.6		
	16	17.8	4.23	0.21	13.0	0.32	11.4		
	18	3.14	5.37	0.24	13.1				
	20	4.61	5.60	0.20	13.1			2.79	9.1
	22	15.7	5.00	0.25	13.0				
	24	33.5	3.71	0.29	13.0				
	26	4.35	4.27	0.85	13.4				
	28	3.72	5.48	0.89	13.3			2.94	9.3
	30	3.41	2.20	0.26	13.1				
	32	2.61	3.65	0.56	11.3				
	34	3.61	5.42	0.29	13.2				
	36	2.87	4.35					3.30	9.2
	46	4.95	6.71	0.49	13.2			3.32	9.4
	56	9.6	6.30	0.21	13.2			3.54	9.8
66	4.76	6.99	0.23	13.1					
76	4.04	7.19	0.19	13.2			3.32	9.3	
86	4.97	7.79	0.21	13.3					
126	3.51	8.71	0.22	13.0			3.30	9.5	
166	2.86	9.67	0.18	12.8					
206	1.63	11.7	0.27	12.9					
Correction		-0.8 $\mu\text{m}$		-0.5 $\mu\text{m}$		+1.0 $\mu\text{m}$		0.0	

TABLE X. CURRENT FLOW IN ELECTRICAL CURRENT STUDIES

Time (min)	Current (milliamps)		
	Anode Pin Cathode Ring 1400°C	Cathode Pin Anode Ring 1400°C	Cathode Pin Anode Ring 1350°C
0.0	60	73	48
0.5	40		
1	27.5	70	
2	25	70	47
4	22	70	44
6	20	70	42
8	19.2	70	41
10	18.3	70	39
15	17.8	70	39
20	18.0	70	48
25	18.2		52
30	18.8	75	58
35	18.5		61
40	18.2		61
45	18.0	75	62
60	17.9		66
75	17.8	70	69
90	17.5		80
105	16.5	80	61
120	20.0	110	130
135	16.5	280	180
150	17.5	165	280
165	17.0	300	340
180	17.0	275	200

APPENDIX D  
ADDITIONAL PHOTOMICROGRAPHS

The section contains a number of photographs as a record of results. In addition, several photomicrographs showing unusual features are included. Each photograph is accompanied by a short discussion explaining aspects of the results.

Figure 48

The amount of grain growth found at the molybdenum wire surface varied somewhat between samples. This section from UE-1 shows less growth than most. Substantial iron alloying occurred at the  $10^{-11.6}$  atm oxygen pressure, but the section does not show this in any metallographic changes. The amount of iron present is less than solid solubility limits.

Figure 49

Although the data from UE-2 does not follow the trends established by the other tests, the oxide formation at the interface is typical of the type found in oxygen potentials of  $10^{-9}$  atm and below.

Figure 50

The surface grain growth of this sample, UE-2 is more pronounced than for UE-1, Figure 48. No reason is known.

Figure 51

The molybdenum dioxide reaction product from the UE-3 sample appears little different from that of UE-2.



Figure 48. Molybdenum Surface, UE-1. (125x), Murakami's Reagent.

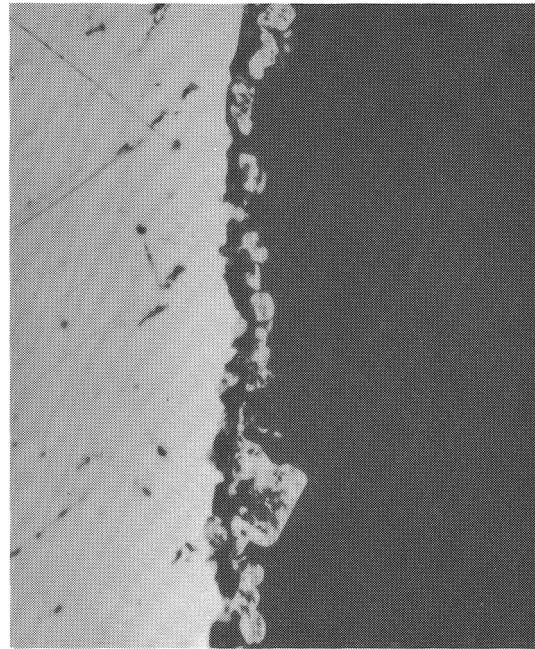


Figure 49. Slag-Metal Interface, UE-2. (1500x), unetched.

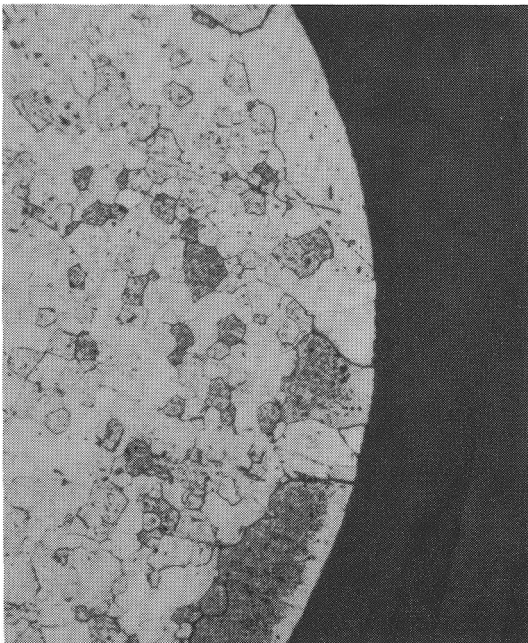


Figure 50. Molybdenum Surface, UE-2. (125x), Murakami's Reagent.

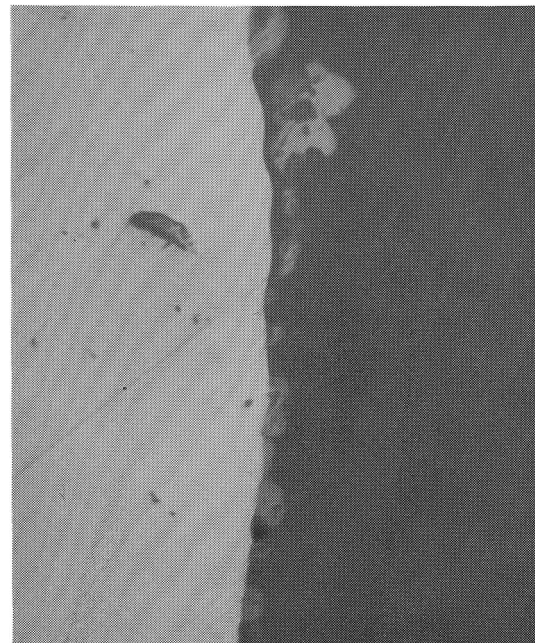


Figure 51. Slag-Metal Interface, UE-3. (1500x), unetched.



Figure 52

The polarized light examination of UE-4 showed that under certain analyzer orientations the distinction between the projecting oxides and the matrix almost disappeared. This micrograph illustrates that phenomena. It further shows the different crystals making up the matrix oxide and the relative position between the matrix and projecting oxides.

Figure 53

Seeded UE slag eroded the molybdenum more rapidly and left a different type of oxide layer than did the plain UE slag. The broken coating of oxide and the dispersed debris in the slag in this micrograph are typical of the seeded tests.

Figure 54

For the UE<sub>s</sub>-2 sample, little reaction was apparent at the interface, as seen in Figure 53, but within the molybdenum a defined area of grain growth is evident. The sharp division between equiaxed and recrystallized grains is not detected by microprobe analysis to be any change in composition. The form taken here is different than that in Figures 48 and 50 and again no explanation is apparent in the variables measured. The effect is tentatively attributed to the sensitivity of molybdenum towards impurities and cold work effects discussed briefly in the Literature Review.

Figure 55

The top section of the rotated molybdenum rod from the test at an applied oxygen pressure of  $10^{-9.1}$  atm shows no reaction products. Some products were found at the bottom section (Figure 16). The difference between top and bottom is likely due to more oxygen present near the slag surface, as explained in the Discussion of Results.

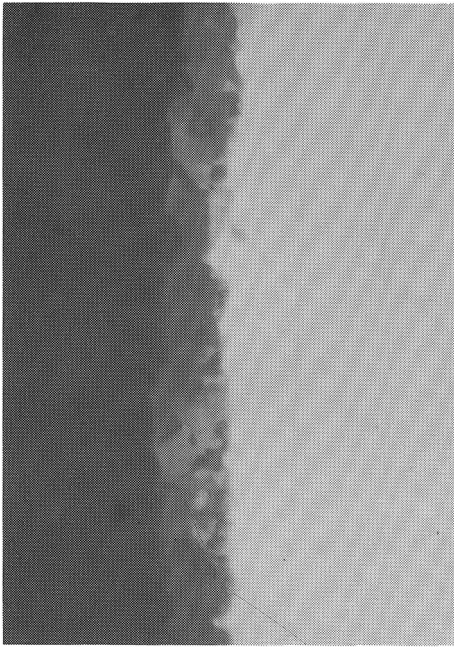


Figure 52. Slag-Metal Interface, UE-4, Under Polarized Light. (1500x), unetched.

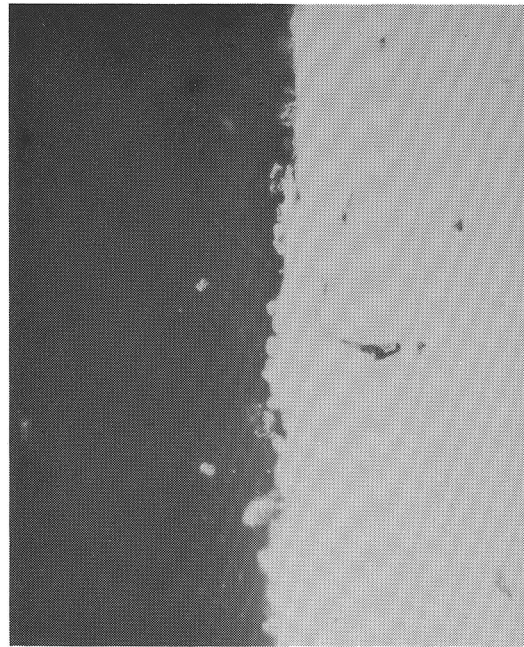


Figure 53. Slag-Metal Interface, UE<sub>S</sub>-2. (1500x), unetched.

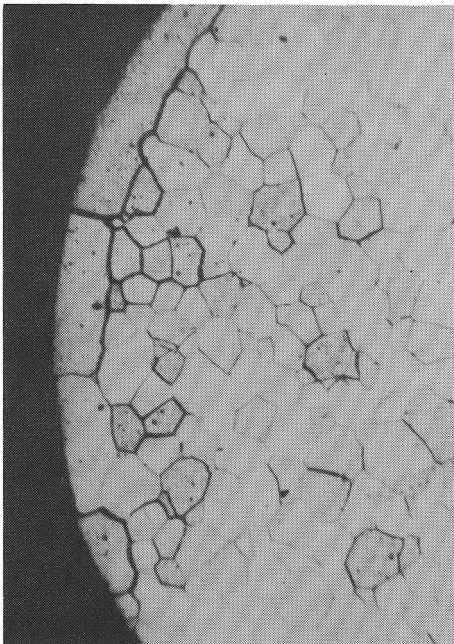


Figure 54. Molybdenum Section, UE<sub>S</sub>-2. (125x), Murakami's Reagent.

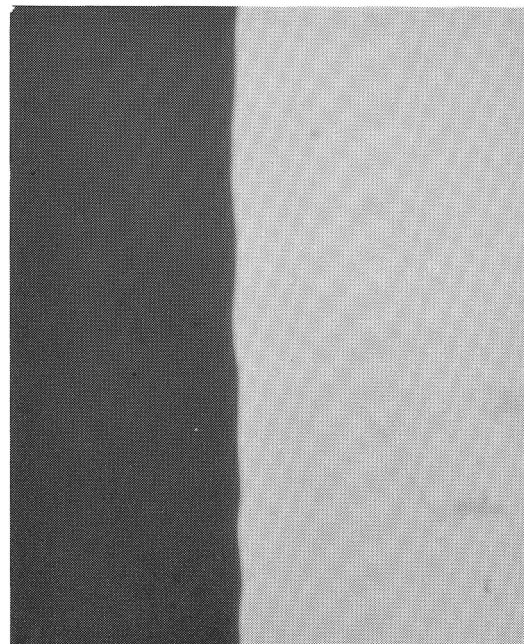


Figure 55. Slag-Metal Interface, Mo<sub>γ</sub>-1T. (1300x), unetched.

Figure 56

Some of the precipitate and debris found in the slag between electrodes in the electrical current tests are shown. These appear to be oxide material by the crystalline forms seen, most likely molybdenum dioxide.

Figure 57

The cathode ring surface contained 33% iron. The details of the alloy in this band are somewhat more evident in this figure, showing the very fine structure that forms into clusters of intermetallic-rich and iron-rich alloy. The structure is much too fine for microprobe analyses of the different phases.

Figure 58

The surface exposed by the section through the cathode pin drop (Figure 30) is shown. The higher side of the drop is towards the right. Much larger clusters of intermetallic within the iron-rich matrix make up the bulk of the drop structure. The intermetallic layer coating the molybdenum wire shows clearly.

Figure 59

In the 1350°C cathode pin/anode ring electrical current test, the alloy formed as mossy deposits on the wire surface. When the sample was jostled during removal from the furnace, the dendrites broke loose from the wire. A polished section through the slag shows several of these dendrites.



Figure 56. Precipitate and Debris in Slag Between Electrodes, Electrical Current Tests. (1300x), unetched.

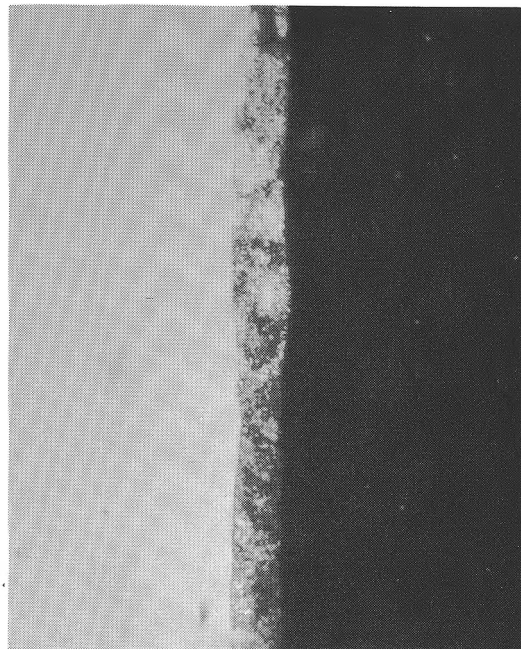


Figure 57. Slag-Metal Interface, Cathode Ring, 1400°C. (550x), nital etch.

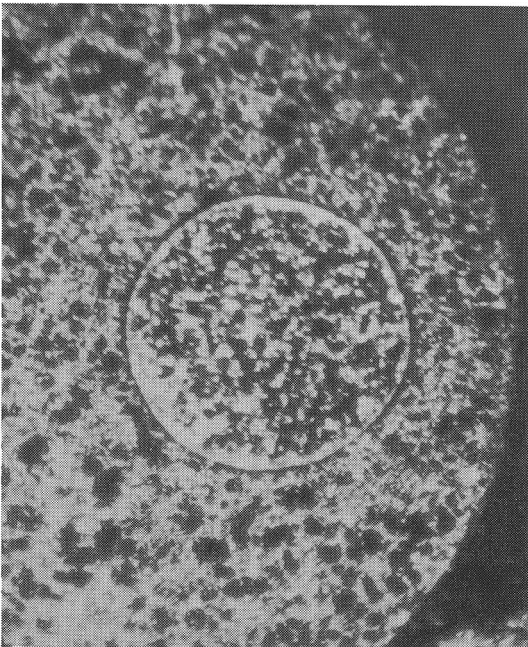


Figure 58. Droplet Section, Cathode Pin, 1400°C. (32x), nital and Murakami's Reagent.

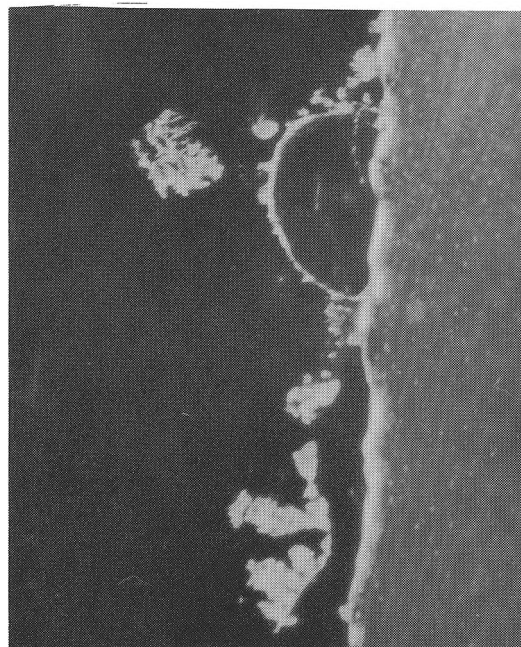


Figure 59. Mossy Deposit From Cathode Pin, Cathode Pin/Anode Ring, 1350°C. (18x), unetched.

Figure 60

The photomicrograph shows a section of the cathode pin taken from a vertical section of the pin. Both the alloy on the surface and the loose alloy nearby indicate the alloy dendrites had little physical strength at 1350°C.

Figure 61

A somewhat different impression of the alloy structure on the 1350°C cathode pin is given by this micrograph, the intermetallic phases being less square-edged than in Figure 37. This structure appears much like parts of Figure 34, the 1400°C cathode pin.

Figure 62

The cathode alloy surface has a very nodular appearance when viewed with oil immersion lenses. The short focal range of the optical microscope made photographing the surface very difficult. The slag was removed from the alloy surface chemically and the surface was examined by SEM. The nodular appearance is confirmed, but debris obscures the very smooth surface visible in Figure 38.

Figure 63

Again in reference to Figure 38, the very shiny, smooth surface of the nodules is not present in all areas. One such area is shown here, a series of indentations on the surface. The effect is not thought important and is not explained.

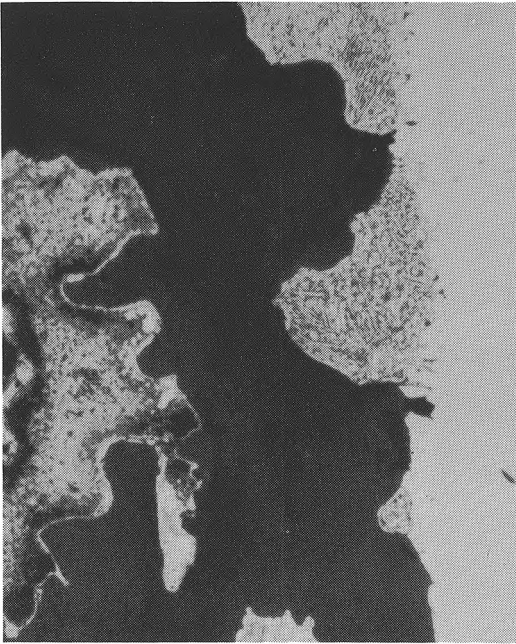


Figure 60. Slag-Metal Interface, Cathode Pin, 1350°C. (270x), nital etch.

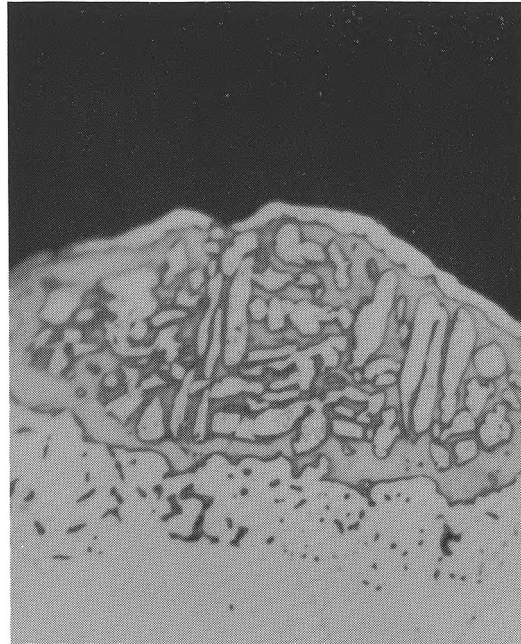


Figure 61. Slag-Metal Interface, Cathode Pin, 1350°C. (830x), nital etch.

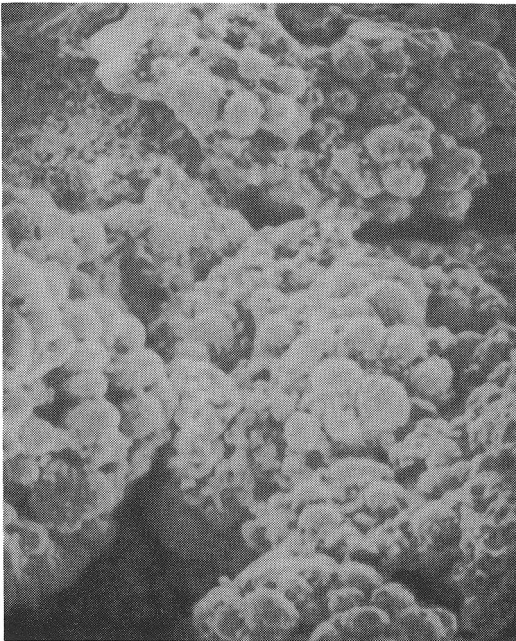


Figure 62. SEM Photomicrograph of Mossy Alloy Surface Seen as Removed From the Slag by LiH + LiOH Leach. (500x).

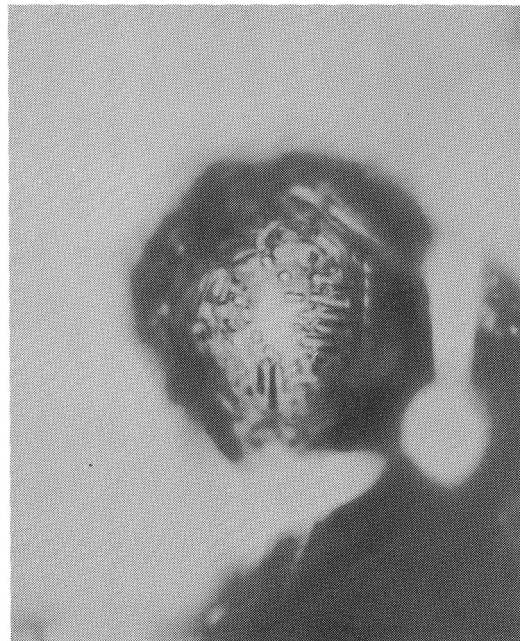


Figure 63. Alloy Surface as Seen Looking Through the Slag, Cathode Pin, 1350°C. (2800x).

Figure 64

The resulting iron-molybdenum structure in the direct contact experiments is shown. The molybdenum surface receded as molybdenum diffused several millimeters into the surrounding iron, evident by increased etch resistance of that iron. The iron grains in contact with the molybdenum grew as the molybdenum receded, evident from the radial pattern of iron grain boundaries within the region of molybdenum recession. Within these iron grains, and along the grain boundaries further from the molybdenum, a second phase precipitated (probably on cooling). The structure differs from that of alloys in the molybdenum-slag tests, likely due to different cooling rates. The dark bubbles along the original molybdenum surface are macroporosity.

Figure 65

In trial tests, the molybdenum surface was often found to be pitted, or covered with shallow depressions. One such pit was found on this sample. The wire had several gas bubbles on the surface in other areas. These covered other slight depressions. The effect is described in the Discussion of Results.

Figure 66

A SEM photomicrograph shows the edge of a molybdenum wire broken across the wire. The molybdenum fractured intergranularly in a brittle manner. A molybdenum dioxide layer is visible at the wire edge.

Figure 67

A second SEM photomicrograph shows the molybdenum metal surface in the lower portion, with a slightly dimpled surface. Behind is the molybdenum dioxide layer and a bubble on the oxide surface, which appears to have a molybdenum dioxide crystal protruding into it.

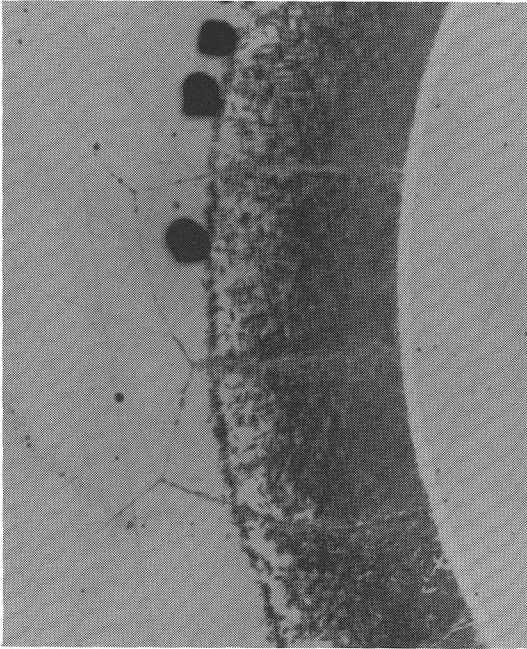


Figure 64. Molybdenum-Iron Interface, Iron Pack Experiment. (160x), nital etch.



Figure 65. Slag-Metal Interface Showing Pitting Corrosion, A Four-Hour Test in UE Slag,  $p_{O_2}=10^{-7}$  atm. (1000x), unetched.



Figure 66. SEM Photomicrograph of Molybdenum-Slag Interface Showing Oxide Reaction Layer. (1500x).



Figure 67. SEM Photomicrograph of Interface Showing Oxide Layer and Texture of Underlying Molybdenum Surface. (1000x).